

Cross-regulatory interactions of trichome patterning genes in
***Arabidopsis thaliana* and related species**

In a u g u r a l - D i s s e r t a t i o n

zur

Erlangung des Doktorgrades

der Mathematisch-Naturwissenschaftlichen Fakultät

der Universität zu Köln

vorgelegt von

Jessica Pietsch

aus Aachen

Köln, 2022

Berichterstatter/in: Prof. Dr. Martin Hülskamp

Prof. Dr. Ute Höcker

Prüfungsvorsitzender: Prof. Dr. Siegfried Roth

Tag der mündlichen Prüfung: 14.04.2022

Everything is interaction and reciprocal.

Alexander von Humboldt

Table of contents

List of figures	IV
List of tables	VI
List of abbreviations	VII
Zusammenfassung	XI
Abstract	XIII
1. Introduction	1
1.1. Trichome morphogenesis in <i>Arabidopsis thaliana</i>	1
1.2. Gene regulatory network in trichome patterning	2
1.3. Measuring protein stability via “self-cleaving” peptides	4
1.4. <i>Arabis alpina</i> and <i>Cardamine hirsuta</i> - two related Brassicaceae	5
1.5. Aim of this work	8
2. Material & Methods	10
2.1. Material	10
2.1.1. Bacterial strains	10
2.1.2. General vectors	10
2.1.3. Constructs and stably transformed lines.....	11
2.1.4. Wildtype and mutant plant lines for transcription analysis	12
2.1.5. Antibiotics	13
2.1.6. Oligonucleotides	13
2.1.7. Software.....	13
2.2. Molecular techniques	14
2.2.1. Generation of chemically competent <i>E. coli</i> and <i>A. tumefaciens</i> cells.....	14
2.2.2. Heat-shock transformation of competent <i>E. coli</i> or <i>A. tumefaciens</i> cells.....	14
2.2.3. Plasmid DNA isolation.....	15
2.2.4. Restriction digest	15
2.2.5. Gel electrophoresis	15
2.2.6. Cloning	15

2.2.7. Genomic DNA isolation	16
2.2.8. PCR.....	17
2.2.9. Generation of constructs	17
2.2.10. Genotyping	18
2.2.11. PCR-based site-directed mutagenesis.....	19
2.2.12. qPCR.....	19
2.2.13. Sequencing	23
2.3. Plant techniques.....	23
2.3.1. Propagation of <i>A. thaliana</i> and <i>N. benthamiana</i>	23
2.3.2. Seed sterilization	23
2.3.3. Generation of stably transformed Arabidopsis lines	24
2.3.4. Tobacco infiltration	24
2.3.5. Particle bombardment.....	24
2.3.6. Blue light treatment	25
2.3.7. Leaf dissection.....	25
2.3.8. Transformation of dark-grown Arabidopsis cell culture	25
2.3.9. β -Glucuronidase (GUS) assay	25
2.4. Protein techniques	26
2.4.1. Western blot.....	26
2.5. Microscopic techniques.....	27
2.5.1. Stereo and fluorescence microscopy	27
2.5.2. Confocal laser scanning microscopy	27
2.6. <i>In silico</i> techniques.....	28
2.6.1. Compiling <i>GLI</i> synteny	28
2.6.2. Calculation of protein stability in ratiometric approach.....	28
2.6.3. Calculation of fluctuation	28
2.6.4. Calculation of promoter expression.....	29
3. Results	30
3.1. Gene fluctuation in <i>A. thaliana</i>	30
3.1.1. Protein expression fluctuates over time.....	31
3.1.2. Extrinsic noise is the primary source of fluctuation in root tips and hypocotyls.....	33

3.2.	Protein stability of trichome patterning genes.....	34
3.2.1.	Proof of concept	34
3.2.2.	bHLH proteins are capable to stabilize MYB proteins	36
3.2.3.	Dosage-dependent stabilization of TRY by MYC1	39
3.3.	<i>MYC1</i> - an outstanding trichome patterning gene	40
3.3.1.	Comparison of MYC1 splicing variants.....	41
3.3.2.	<i>pMYC1</i> _{1970 bp} is equally applicable as <i>pMYC1</i> _{2581 bp}	42
3.3.3.	Endogenous MYC1 is expressed in nucleus and cytoplasm	45
3.3.4.	<i>MYC1</i> influences trichome patterning	47
3.4.	Expression of patterning genes in trichomes and epidermis cells.....	49
3.4.1.	Expression can be neglected in undifferentiated epidermal cells.....	50
3.4.2.	Results of <i>pGL2</i> / <i>pCPC</i> / <i>pTRY</i> / <i>pETC1</i> / <i>pETC2</i> in Col-0.....	51
3.5.	Cross-regulatory interactions of <i>Arabidopsis thaliana</i> and its mutants	53
3.5.1.	Comparison of trichome density in <i>A. thaliana</i> wildtype and various patterning mutants	53
3.5.2.	Transcriptional expression of trichome patterning genes in <i>A. thaliana</i>	56
3.6.	Trichome patterning in different Brassicaceae.....	71
3.6.1.	Comparison of trichome density in Brassicaceae.....	72
3.6.2.	Patterning gene expression in different Brassicaceae	73
3.6.3.	Comparison of gene expression in <i>Atgl2</i> and <i>Aagl2</i> mutants.....	77
3.6.4.	Synteny of <i>GLI</i> in related Brassicaceae.....	79
3.6.5.	Expression of MYB homologs in multiple tissues.....	80
4.	Discussion	82
5.	Appendix	93
6.	Bibliography	113
	Danksagung	129
	Declaration of academic integrity	131

List of figures

Figure 1: Single steps of trichome morphogenesis.....	2
Figure 2: Models of trichome patterning.....	4
Figure 3: Morphological comparison of three different mature Brassicaceae leaves.....	7
Figure 4: Analysis of temporal fluctuation in stable <i>Arabidopsis p35S:NLS-KikGR</i> lines.....	32
Figure 5: Extrinsic and intrinsic noise in root tip and hypocotyl in <i>p35S:2xNLS-YFP p35S:2xNLS-CFP</i> plants.....	33
Figure 6: Blue light inducible degradation of LOV2-ODC.....	36
Figure 7: MYB proteins stabilized by bHLH proteins.....	38
Figure 8: Concentration-dependent stabilization of TRY by MYC1.....	40
Figure 9: Comparison of MYC1 splicing variants.....	42
Figure 10: Comparative study of <i>pMYC1_{1970 bp}</i> and <i>pMYC1_{2581 bp}</i>	44
Figure 11: CLSM images of <i>Arabidopsis</i> plants stably transformed with <i>pMYC1_{1970 bp}:YFP-MYC1</i> in different backgrounds.....	46
Figure 12: The influence of <i>MYC1</i> on trichome patterning.....	48
Figure 13: <i>pTRY:GUS</i> expression in trichomes and undifferentiated epidermal cells in dependence of staining duration.....	50
Figure 14: Expression of patterning promoters in different trichome developmental stages.....	52
Figure 15: Trichome density in <i>A. thaliana</i> wildtype and various patterning mutants.....	54
Figure 16: Trichome phenotypes of <i>A. thaliana</i> Col-0 wildtype and 21 patterning mutants.....	55
Figure 17: Interaction scheme of the trichome patterning network.....	57
Figure 18: Dissection scheme of <i>Arabidopsis</i> plants.....	57
Figure 19: Transcriptional patterning gene expression in <i>A. thaliana</i> Col-0 wildtype.....	59
Figure 20: Transcriptional expression analysis of the activators in <i>A. thaliana</i> mutants.....	61

Figure 21: Transcriptional expression analysis of inhibitor mutants in <i>A. thaliana</i>	63
Figure 22: Transcriptional expression analysis of prominent double mutants in <i>A. thaliana</i>	67
Figure 23: Transcriptional expression analysis of subordinated double mutants in <i>A. thaliana</i>	69
Figure 24: Cross-regulatory interaction scheme of the core components.	71
Figure 25: Schematic illustration of trichome counting areas on rosette leaves.	73
Figure 26: Comparative patterning gene expression in three Brassicaceae.	75
Figure 27: Comparative patterning gene expression combining functional units.....	77
Figure 28: Comparison of gene expressions in <i>Atgl2</i> and <i>Aagl2</i>	78
Figure 29: Synteny of <i>GL1</i> , <i>MYB23</i> , and <i>WER</i> in <i>A. thaliana</i> , <i>A. alpina</i> , and <i>C. hirsuta</i>	79
Figure 30: Quantitative expression analysis of three MYB homologs in different species and tissues.....	81
Figure S1: Graphs of <i>Arabidopsis thaliana</i> qPCR primer efficiency tests.....	97
Figure S2: Graphs of <i>Arabis alpina</i> qPCR primer efficiency tests.	98
Figure S3: Graphs of <i>Cardamine hirsuta</i> qPCR primer efficiency tests.	99
Figure S4: Analysis of temporal fluctuation in stable <i>Arabidopsis p35S:NLS-</i> <i>KikGR</i> lines.	100
Figure S5: Comparison of P2A and F2A cleavage efficiency.....	101
Figure S6: Blue light inducible degradation of LOV2-ODC.....	102
Figure S7: MYB proteins stabilized by bHLH proteins.	104
Figure S8: Cleavage efficiency of a dual P2A construct.	105
Figure S9: <i>pMYC1_{1970 bp}:GUS</i> staining in <i>A. thaliana</i>	106
Figure S10: Summary of all relative expression values of <i>Arabidopsis</i> patterning genes in various trichome mutants.	110
Figure S11: Summary of 2-fold cut-off relative expression values of <i>Arabidopsis</i> patterning genes in various trichome mutants.....	111
Figure S12: Cross-regulatory interaction scheme of all trichome patterning genes.	112

List of tables

Table 1: List of used bacterial strains.	10
Table 2: Vectors used for desired expression constructs.	10
Table 3: Constructs and stably transformed <i>A. thaliana</i> lines used for experimental work.	11
Table 4: <i>Arabidopsis thaliana</i> , <i>Arabis alpina</i> , and <i>Cardamine hirsuta</i> plant lines used for the transcriptional expression analysis.	12
Table 5: List of antibiotics used for this study.	13
Table 6: Software and its applications used in this study.	13
Table 7: Composition of BP and LR reaction.	16
Table 8: Default PCR composition and program.	17
Table 9: PCR composition and program using a ready-to-use mix.	18
Table 10: PCR composition and program for site-directed mutagenesis.	19
Table 11: Composition of qPCR reaction and program.	22
Table 12: Excitation lines and detection ranges.	27
Table 13: The influence of <i>MYC1</i> on intercalation in different leaf developmental stages.	49
Table 14: Leaf area, trichome number, and density of three Brassicaceae.	73
Table S1: Oligonucleotide sequences used for construct generation.	93
Table S2: Oligonucleotide sequences for <i>A. thaliana</i> used for qPCR experiments.	94
Table S3: Oligonucleotide sequences for <i>A. alpina</i> used for qPCR experiments.	95
Table S4: Oligonucleotide sequences for <i>C. hirsuta</i> used for qPCR experiments.	96
Table S5: Leaf area, trichome number, and density in <i>A. thaliana</i> wildtype and various patterning mutants.	107
Table S6: Summary of all gene expression fold changes of Arabidopsis patterning genes in various trichome mutants.	108
Table S7: Summary of 2-fold cut-off gene expressions changes of Arabidopsis patterning genes in various trichome mutants.	109

List of abbreviations

<i>A. tumefaciens</i>	<i>Agrobacterium tumefaciens</i>
<i>Aa</i>	<i>Arabidopsis alpina</i>
AC	active complex
AcOH	acetic acid
ANOVA	analysis of variance
AP	alkaline phosphatase
approx.	approximately
APS	ammonium persulfate
<i>At</i>	<i>Arabidopsis thaliana</i>
bHLH	basic Helix-Loop-Helix
BLAST	Basic Local Alignment Search Tool
bp	base pairs
CaCl ₂	calcium chloride
ccdB	control of cell death with the corresponding bacterial B protein
cDNA	complementary DNA
CDS	coding sequence
CFP	cyan fluorescent protein
<i>Ch</i>	<i>Cardamine hirsuta</i>
CLSM	confocal laser scanning microscopy
cm	centimeter
Col-0	Columbia-0
<i>CPC</i>	<i>CAPRICE</i>
Cq	quantification cycle
ddH ₂ O	double distilled water
DNA	deoxyribonucleic acid
dNTPs	deoxyribonucleotides
DTT	dithiothreitol
<i>E. coli</i>	<i>Escherichia coli</i>
e.g.	<i>exempli gratia</i> , latin for "for example"
E2A	2A sequence from equine rhinitis A virus
EDTA	ethylenediaminetetraacetic acid
EF	elongation factor
<i>EGL3</i>	<i>ENHANCER OF GLABRA3</i>
et al.	<i>et alii</i> , latin for "and others"
<i>ETC1</i>	<i>ENHANCER OF TRIPTYCHON AND CAPRICE1</i>
<i>ETC2</i>	<i>ENHANCER OF TRIPTYCHON AND CAPRICE2</i>
<i>ETC3</i>	<i>ENHANCER OF TRIPTYCHON AND CAPRICE3</i>
EtOH	ethanol
F2A	2A sequence from foot-and-mouth disease virus
<i>g</i>	g-force
g	grams

List of abbreviations

<i>GAPDH</i>	<i>GLYCERALDEHYDE-3-PHOSPHATE DEHYDROGENASE</i>
GFP	green fluorescent protein
<i>GL1</i>	<i>GLABRA1</i>
<i>GL2</i>	<i>GLABRA2</i>
<i>GL3</i>	<i>GLABRA3</i>
GUS	glucuronidase
h	hour(s)
HA	human influenza hemagglutinin
HCl	hydrogen chloride
Hg	inch of mercury
Hz	Hertz
i.e.	<i>id est</i> , latin for "in other words"
IC	inactive complex
ID	identification
IgG	Immunoglobulin G
IRES	internal ribosome entry sites
KAc	potassium acetate
kb	kilo base pairs
KCl	potassium chloride
kDa	kilodaltons
KH ₂ PO ₄	potassium dihydrogenphosphate
KikGR	Kikume Green Red
KOH	potassium hydroxide
l	liter
LAS	Leica Application Suite
LB	lysogeny broth
<i>Ler</i>	Landsberg <i>erecta</i>
log ₁₀	decadic logarithm
LOV	light oxygen voltage
LUMIER	luminescence-based mammalian interactome mapping
m	meter; monomeric
M	molar
MBW	complex of MYB, bHLH, and WD40 proteins
MES	2-(N-morpholino)ethanesulfonic acid
mg	milligrams
MgSO ₄	magnesium sulfate
min	minute(s)
ml	milliliter
mM	millimolar
mm	millimeter
MnCl ₂	manganese(II) chloride
MOPS	3-(N-morpholino)propanesulfonic acid
mRNA	messenger RNA
MS	Murashige and Skoog

List of abbreviations

MYB	myeloblastosis
MYC	myelocytomatosis
<i>n</i>	number
<i>N. benthamiana</i>	<i>Nicotiana benthamiana</i>
Na ₂ HPO ₄	disodium hydrogen phosphate
NaCl	sodium chloride
NaOCl	sodium hypochlorite
NaOH	sodium hydroxide
NaPO ₄	sodium phosphate
NLS	nuclear localization signal
nm	nanometer
OD	optical density
ODC	ornithine decarboxylase
Ox	Oxford
<i>p</i>	probability value; promoter
P2A	2A sequence from porcine teschovirus-1
Pa	pascal
Paj	Pajares
PBS	phosphate buffer saline
PBS-T	phosphate buffer saline with Tween
PCR	polymerase chain reaction
PH	pleckstrin homology
<i>PP2A</i>	<i>PROTEIN PHOSPHATASE 2</i>
psi	pound-force per square inch
PVDF	polyvinylidene difluoride
<i>r</i>	correlation coefficient
<i>RAN3</i>	<i>RAS-RELATED NUCLEAR PROTEIN3</i>
RbCl ₂	rubidium chloride
RFP	red fluorescent protein
RNA	ribonucleic acid
rpm	rounds per minute
rRNA	ribosomal RNA
RT-qPCR	quantitative Real-Time PCR
SDS	sodium dodecyl sulfate
SDS-PAGE	sodium dodecyl sulfate polyacrylamide gel electrophoresis
sec	second(s)
T2A	2A sequence from thossea asigna virus
TAIR	The Arabidopsis Information Resource
<i>TCL1</i>	<i>TRICHOMELESS1</i>
<i>TCL2</i>	<i>TRICHOMELESS2</i>
T-DNA	transfer DNA
TEMED	tetramethylethylenediamine
<i>TIP41</i>	<i>TYPE 2A PHOSPHATASE ACTIVATOR41</i>
TRI	TRIzol

List of abbreviations

Tris	tris(hydroxymethyl)aminomethane
<i>TRY</i>	<i>TRIPTYCHON</i>
TSS	transcription start site
<i>TTG1</i>	<i>TRANSPARENT TESTA GLABRA1</i>
<i>TTG2</i>	<i>TRANSPARENT TESTA GLABRA2</i>
<i>UBQ10</i>	<i>UBIQUITIN10</i>
UTR	untranslated region
vs.	versus
w/o	without
WD40	tryptophan-aspartic acid repeat domain
<i>WER</i>	<i>WEREWOLF</i>
WRKY	tryptophan-arginine-lysine-tyrosine domain
WS	Wassilewskija
YEB	yeast extract beef
YFP	yellow fluorescent protein
α	alpha, anti
β	beta
μg	micrograms
μl	microliter
μm	micrometer
μM	micromolar
μmol	micromol
ψ	psi
$^{\circ}\text{C}$	degree Celsius
<i>35S CaMV</i>	<i>35S</i> promoter of the Cauliflower mosaic virus

Zusammenfassung

Die Pflanzenentwicklung ist durch eine Vielzahl von Regulationsprozessen charakterisiert. Allerdings ist bisher nur eine Minderheit von Gennetzwerken verstanden, was die Notwendigkeit verstärkt, wechselwirkende Signalwege detaillierter aufzuklären. Das konservierte *TTG1*-Netzwerk reguliert fünf verschiedene Merkmale in *Arabidopsis thaliana* und kontrolliert ein breites Spektrum regulatorischer Prozesse während der gesamten Pflanzenentwicklung, einschließlich der Trichommusterung. Dies wird durch das Zusammenspiel von Trichomen-fördernden und -hemmenden Faktoren erreicht, die als Aktivatoren und Inhibitoren bezeichnet werden.

Das regelmäßig verteilte Trichommuster beginnt in einem Feld identischer Zellen. Genfluktuationen stören die Homogenität und *de novo* Musterungsprozesse werden initiiert. In dieser Studie wurden Fluktuationen von Proteinexpressionen aufgeklärt, die die allerersten durchgeführten Experimente in Pflanzengeweben beschreiben. Es wurde demonstriert, dass Proteine im Laufe der Zeit fluktuieren und extrinsisches Rauschen die Hauptquelle für Genfluktuationen in verschiedenen *Arabidopsis*-Gewebe darstellt.

Nachdem die ersten relativen Unterschiede zwischen Trichomaktivatoren und -inhibitoren die Musterbildung in Gang gesetzt haben, reguliert eine komplexe Maschinerie die Trichompositionierung und -entwicklung. Hier wurde die Quantifizierung der transkriptionellen Expressionen aller *TTG1*-abhängigen Trichom-musterungsgene in *Arabidopsis* durchgeführt, erweitert durch vergleichende Analysen in zwei verwandten Spezies.

Die systematische Untersuchung von 15 differentiell regulierten Musterungsgenen in *Arabidopsis Col-0* Wildtyp und 21 mutierten Hintergründen hob die Kernkomponenten des konservierten *TTG1*-Netzwerks hervor und enthüllte den Einfluss der Genhomologie. Die umfangreiche Studie wies darauf hin, dass die prominenten Musterungsaktivatoren *GL3/EGL3* und *GL1/MYB23* als funktionelle Einheiten betrachtet werden können, und identifizierte eine gegenseitige positive Rückkopplungsschleife zwischen ihnen, die zur Selbstverstärkung der Musterungsaktivatoren bei der Initiierung eines Trichomzellschicksals beiträgt. Überraschenderweise zeigte sich, dass der Homöodomänen-Transkriptionsfaktor *GL2* viel stärker mit anderen Musterungsgenen verwoben ist als bisher angenommen, was ihn als reines Downstream-Gen des Systems negiert.

Ein vergleichender Ansatz in den verwandten Brassicaceae *A. alpina* und *C. hirsuta* ermöglichte erste evolutionäre Einblicke in das konservierte *TTG1*-Netzwerk, da er ähnliche und abweichende Funktionen zwischen allen drei Arten hervorhebt. Am auffälligsten ist, dass *GLI* - ein essentieller Faktor des Aktivator-Komplexes in *Arabidopsis* - nur eine schwache biologische Relevanz in Cardamine aufweist und die Daten stark auf eine funktionelle Kompensation durch *ChWER* hindeuten.

Für ein regelmäßig verteiltes Trichommuster ist nicht nur die Genregulation entscheidend, sondern auch die Stabilität der translatierten Proteine. Hier wurde eine signifikante Stabilisierung von MYB-Proteinen durch bHLH-Proteine aufgedeckt, die dosisabhängig sogar noch zunahm. Diese Studie liefert den Machbarkeitsnachweis, dass - unter Verwendung des viralen 2A-Spaltungssystems - der adoptierte ratiometrische Ansatz anwendbar ist, um die Proteinstabilität durch die äquimolare Translation von bis zu drei Proteinen aus einem offenen Leseraster *in planta* zu quantifizieren.

Darüber hinaus hat sich *MYC1* als außergewöhnlicher Vertreter der Musterungsene herausgestellt. Einerseits und im Gegensatz zu einer früheren Studie wurde festgestellt, dass *pMYC1* überall in der Blattspreite exprimiert wird. Zusätzlich deckte die Quantifizierung eine Expressionsabnahme mit fortschreitender Trichomentwicklung auf. Andererseits unterschied sich das regulatorische Schema von *MYC1* von anderen Aktivatoren und es war unwahrscheinlich, dass es durch homologe Gene kompensiert wurde, was die abweichende Rolle dieses Aktivators hervorhebt.

Abstract

Plant development is characterized by a multitude of regulatory processes. However, only a minority of gene networks is yet understood, strengthening the need to elucidate cross-interacting pathways in more detail. Regulating five different traits in *Arabidopsis thaliana*, the conserved *TTG1* network controls a wide range of regulatory processes throughout plant development, including trichome patterning. This is achieved by the interplay of trichome promoting and repressing factors, called activators and inhibitors.

The regularly distributed trichome pattern begins in a field of identical cells. Gene fluctuations disrupt the homogeneity and *de novo* patterning processes are initiated. In this study, fluctuations of protein expressions were elucidated, describing the first-ever conducted experiments in plant tissues. It was demonstrated that proteins fluctuate over time and extrinsic noise represents the primary source of gene fluctuation in different *Arabidopsis* tissues.

After the first relative differences between trichome activators and inhibitors set the pattern formation in motion, a complex machinery regulates trichome positioning and development. Here, the quantification of the transcriptional expressions of all *TTG1*-dependent trichome patterning genes in *Arabidopsis* was performed, extended by comparative analyses in two related species.

The systematical investigation of 15 differentially regulated patterning genes in *Arabidopsis* Col-0 wildtype and 21 mutant backgrounds highlighted the core components of the conserved *TTG1* network and revealed the impact of gene homology. The vast study pointed out that the prominent patterning activators *GL3/EGL3* and *GL1/MYB23* can be considered functional units and identified a mutual positive feedback loop between them, contributing to the self-enhancement of the patterning activators when initiating a trichome cell fate. Surprisingly, it was revealed that the homeodomain transcription factor *GL2* is much more interwoven with other patterning genes than previously thought, negating it as a pure downstream gene of the system.

A comparative approach in the related Brassicaceae *A. alpina* and *C. hirsuta* enabled first evolutionary insights into the conserved *TTG1* network as it highlights similar and divergent functions between all three species. Most strikingly, *GL1* - an essential factor of the activator complex in *Arabidopsis* - exhibits only a weak

biological relevance in Cardamine, and the data strongly suggested a functional compensation by *ChWER*.

For a regularly distributed trichome pattern, not only gene regulation is crucial but also the stability of the translated proteins. Here, a significant stabilization of MYB proteins by bHLH proteins was revealed, which even increased in a dosage-dependent manner. This study provides the proof of concept that the adopted ratiometric approach - using the viral 2A cleavage system - is applicable to quantify protein stability *in planta* by the equimolar translation of up to three proteins from one open reading frame.

Furthermore, *MYC1* has turned out to be an exceptional representative of the patterning genes. On the one hand and contradictory to a previous study, *pMYC1* was found to be ubiquitously expressed throughout the leaf blade. In addition, the quantification revealed an expression decrease with progressing trichome development. On the other hand, the regulatory scheme of *MYC1* differed from other activators and was unlikely to be compensated by homologous genes, highlighting the divergent role of this activator.

1. Introduction

A multitude of biological processes underlies cross-regulatory networks (Hong et al., 2021). However, only a small fraction of all annotated pathways and biological processes is unraveled in *Arabidopsis thaliana* (Arabidopsis; Deng et al., 2017). Therefore, a great need exists to study the internal crosstalk, to comprehend the challenges a plant faces during its development, from randomness to determinism.

1.1. Trichome morphogenesis in *Arabidopsis thaliana*

The Brassicaceae *Arabidopsis thaliana* is a valuable model system due to its small and completely sequenced genome, comprising of five chromosomes, its short generation cycle, as well as the feasibility of transient and stable transformation (Passardi et al., 2007; Clough & Bent, 1998; Ueki et al., 2009; Sessa et al., 1998). Hence, gene regulatory networks and cell-cell communication pathways can be excellently studied to deepen our understanding of plant biology. This includes, among others, molecular, physiological, and biochemical mechanisms during morphological evolution, nutrient acquisition, or adaptation to local environmental conditions (Alonso-Blanco et al., 2009; Erwin & Davidson, 2009; Fabiańska et al., 2019).

In molecular and developmental biology, trichomes are the focus of research because they are dispensable for plant growth and their manipulation has little to no influence on the plant's development (Wagner et al., 2004). Mutants are still fertile and viable (Koorneef et al., 1983), and their macroscopic size enables effortless screening (Zhang & Oppenheimer, 2004).

In *Arabidopsis* wildtype accessions, trichomes are single-celled, non-glandular, three-branched epidermal outgrowths, which are regularly distributed on the rosette and cauline leaves, as well as on the stem and sepals. Their counterpart on roots, the root hairs, develops only on one of two parallel-running cell files, termed H-file. They are formed above the cleft of two cortical cells (Dolan et al., 1994; Hülskamp et al., 1994; Ishida et al., 2008).

Trichome morphogenesis is characterized by clearly defined developmental stages (Figure 1). Initially, the designated trichome raises as a bulge from a unique field of epidermal cells perpendicularly to the leaf surface. A stalk develops, and two consecutive branching events occur. The expanded, tip-pointed, and mature trichome develops papillae on the incrustated cell wall surface (Folkers et al., 1997; Rerie et al.,

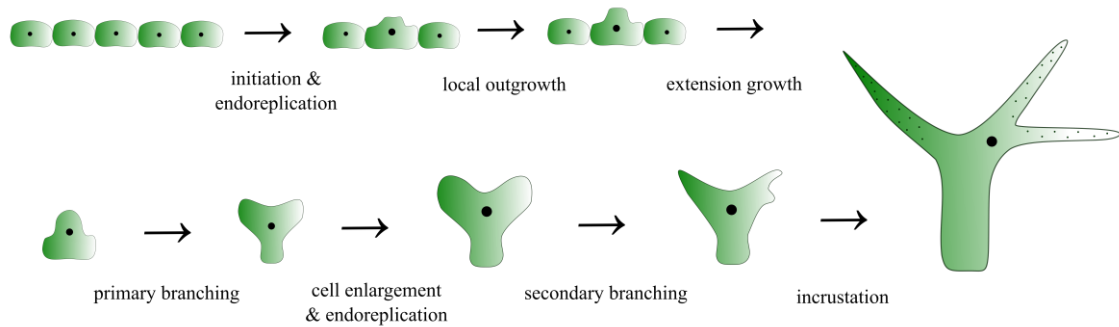


Figure 1: Single steps of trichome morphogenesis. Black dots indicate nuclei corresponding to DNA content. Illustration based on Hülskamp et al., 1994.

1994; Szymanski et al., 2000). Cell enlargement is accompanied by several endoreplication cycles, resulting in a total DNA content of 32C (Hülskamp et al., 1994).

Although the trichome pattern on the leaf blade may give the impression of being either randomly distributed or determined by cell lineage, it is generated *de novo*, without any preexisting information (Pesch et al., 2014; Schellmann & Hülskamp, 2005; Schnittger et al., 1999). Randomness was rejected by the analysis of the average distance between nearest neighbors as well as the minimal distance between trichomes (Greese et al., 2012; 2014), and dependence based on cell lineage was excluded via genetic mosaic experiments (Larkin et al., 1996; Schnittger et al., 1999). Instead, differences in gene expression between cells, so-called fluctuations or noise, are likely the source of positional trichome spacing. These fluctuations effectuate the regularly distributed trichome formation in a growing field of cells (Meinhardt & Gierer, 1974; Turing, 1952).

The trichome initiation is restricted to the initiation zone at the leaf base. Thus, the general directionality of the different trichome developmental stages is stretched along the distal-proximal axis with the oldest trichome at the leaf tip and the youngest trichomes at the base (Schnittger et al., 1999). Mitotic cell divisions of undifferentiated epidermal cells increases the distances between trichomes (Hülskamp et al., 1994; Jaegle, 2014). The resulting spaces may function to produce so-called intercalating trichomes between already developed ones, outside of the initiation zone. Intercalation is, however, not found in every *Arabidopsis* accession or mutant (Jaegle, 2014).

1.2. Gene regulatory network in trichome patterning

Trichome formation underlies a complex, multi-gene molecular mechanism. Proteins of a handful of families must play in concert to achieve the regular trichome patterning on

leaf blades of *Arabidopsis* wildtype plants. These proteins can be roughly classified into trichome promoting and repressing factors (activators and inhibitors; Balkunde et al., 2010; Digiuni et al., 2008; Pesch & Hülskamp, 2009), as well as a downstream gene, which is required in later stages of trichome formation (Pesch & Hülskamp, 2004; Rerie et al., 1994).

The R2R3 MYB protein *GLABRA1* (GL1; Oppenheimer et al., 1991), the basic Helix-Loop-Helix (bHLH) protein *GLABRA3* (GL3; Bernhardt et al., 2003; Hülskamp et al., 1994; Koornneef et al., 1982; Payne et al., 2000), and the WD40 transcription factor *TRANSPARENT TESTA GLABRA1* (TTG1; Koornneef, 1981; Walker et al., 1999) form the so-called MBW complex (Ramsay & Glover, 2005; Xu et al., 2015; Zhang & Schrader, 2017). The protein encoded by *ENHANCER OF GLABRA3* (*EGL3*; bHLH; Zhang et al., 2003) shares regulatory functions and acts partially redundant to GL3 (Bernhardt et al., 2003). MYC1, a bHLH protein closely related to GL3/EGL3, is involved in the regulation of trichome patterning and considered as promoting factor (Morohashi & Grotewold, 2009; Symonds et al., 2011; Urao et al., 1996). In the root system, *WEREWOLF* (*WER*), another representative of the R2R3 MYB class, replaces GL1 in the MBW complex (Lee & Schiefelbein, 1999).

The trimeric MBW complex is likely self-enhancing by an autocatalytic loop and activates R3 MYBs, the class of proteins which comprises all inhibitors. Thereby, the activators activate their own repressors. So far, seven inhibitors are known. The most prominent are *CAPRICE* (*CPC*; Wada et al., 1997) and *TRIPTYCHON* (*TRY*; Hülskamp et al., 1994; Schellmann et al., 2002), followed by *ENHANCER OF TRIPTYCHON AND CAPRICE1, 2 and 3* (*ETC1/2/3*; Wada et al., 1997; Esch et al., 2004; Kirik et al., 2004a, b; Simon et al., 2007). Less importance is awarded to *TRICHOMELESS1* and 2 (*TCL1/2*; Wang et al., 2007; Gan et al., 2011).

After a trichome cell fate is irreversibly determined, *GLABRA2* (*GL2*; Hülskamp et al., 1994; Maarten Koornneef et al., 1982; Rerie et al., 1994), a homeodomain transcription factor, starts to act. *TRANSPARENT TESTA GLABRA2* (*TTG2*), encoding a plant-specific WRKY transcription factor, is supposed to share overlapping functions with *GL2*, but it is also involved in trichome development (Johnson et al., 2002).

Currently, two mechanisms for trichome patterning are postulated: The activator-inhibitor and the activator-depletion model (Figure 2). In the activator-inhibitor model, self-enhancing activator complex consisting of GL1, TTG1, and GL3/EGL3 creates a positive feedback loop. It promotes trichome initiation and the

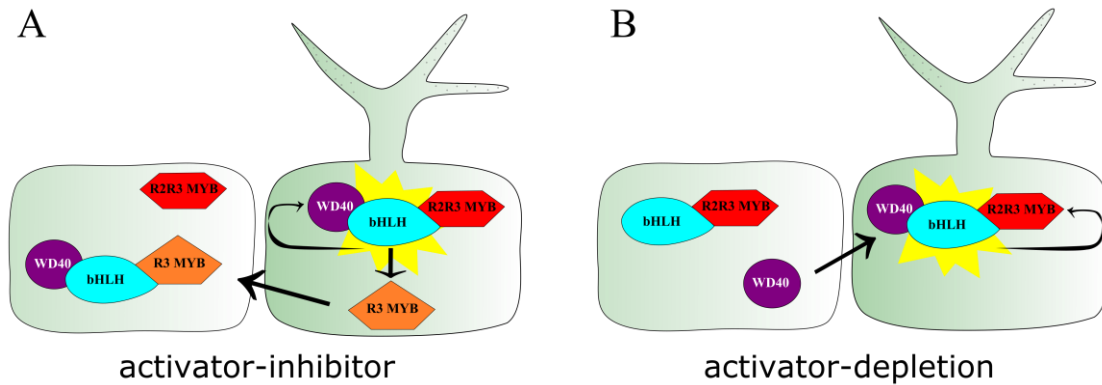


Figure 2: Models of trichome patterning. **A)** In the activator-inhibitor model, the activator complex (WD40, bHLH, and R2R3 MYB; yellow star) initiates the trichome cell fate by a positive feedback loop, and promotes the activation of R3 MYB proteins (right cell). R3 MYB proteins move to neighboring cells, where they compete with R2R3 MYB proteins for the binding to bHLH proteins, avoiding the trichome fate (left cell). **B)** According to the activator-depletion model, mobile WD40 proteins are trapped by bHLH proteins in the designated trichome cell. When bound to R2R3 MYB proteins, the activator complex is formed and trichome development initiated (right cell). The lack of WD40 in the adjacent cell avoids a trichome cell fate (left cell). Illustration based on Pesch et al., 2009.

activation of inhibitors such as CPC or TRY, which in turn repress the activators. According to the theory of pattern formation, inhibitors can move (or at least faster than activators, if they are also mobile) to neighboring cells, where they compete with R2R3 MYB proteins for binding to the bHLH transcription factor (Turing, 1952; Meinhardt & Gierer, 1974). The replacement of inhibitors renders the complex inactive and represses the trichome cell fate via lateral inhibition (Hülkamp, 2004; Pesch & Hülkamp, 2004; Figure 2A).

In the activator-depletion model, mobile TTG1 is trapped in the nucleus of the designated trichome cell by GL3, and together with GL1, the trimeric activator complex is formed. Via local self-enhancement, an inner threshold is exceeded, and trichomes are initiated. Depleting TTG1 in the surrounding cells prevents a trichome fate of these cells by lateral inhibition (Bouyer et al., 2008; Pesch & Hülkamp, 2009; Figure 2B).

1.3. Measuring protein stability via “self-cleaving” peptides

Many biological processes, including trichome patterning, are controlled by the interplay of the individual components of a regulatory network. A crucial factor for proper trichome development is the presence of the involved proteins within the cell. Their availability depends on protein synthesis, stability, and degradation. Initially, pulse-chase assays or cycloheximide treatments were conducted to investigate protein turnover. However, these experiments are often challenging (Yewdell et al., 2011). Conventional strategies to combine multiple genes, such as crossings or transformations, are elaborative and influenced by, e.g., gene silencing or the position of

integration (Halpin et al., 2001). A popular strategy to measure protein turnover utilizes internal ribosome entry sites (IRES) by translating two fluorescent proteins from one mRNA. One of the fluorophores presents the protein of interest and the other serves as a reference. The ratio of both determines the protein abundance (Yen et al., 2008). The downside of this method is the often occurring decreased expression of the second gene, resulting in misleading protein stabilities (Mizuguchi et al., 2000).

To overcome these issues, the viral 2A system was adopted to evaluate protein stabilities *in planta*. This approach allows the polycistronic translation of mRNA in eukaryotes and resembles the measurements via IRES. However, the “self-cleaving” function of the 2A peptides enables a highly efficient stoichiometric co-expression of all introduced proteins and does not vary from cell to cell (Szymczak et al., 2004). The cleavage of the 18-22 amino acids comprising 2A peptides is considered to be based on ribosomal skipping. It is suggested that the ribosomes skip the glycyl-propyl bond within the 2A sequence during translation, leading to the equimolar expression of two (or more) proteins from one open reading frame (Donnelly et al., 2001a, b). First described was the 2A sequence of the foot-and-mouth disease virus (F2A; Ryan et al., 1991). Other peptides followed, such as the 2A sequences from the porcine teschovirus-1 (P2A), the equine rhinitis A virus (E2A), and the thosa asigna virus (T2A; Szymczak & Vignali, 2005). However, significant differences in their cleavage efficiency were found in mammalian cell lines, mice, and zebrafish (Kim et al., 2011).

In order to study the stabilities of trichome patterning proteins, gateway-compatible fluorescent polycistronic 2A constructs were designed and used for ratiometric measurements in different plant organisms. On the one hand, the impact of bHLH proteins on the stability of MYB proteins was tested in epidermal leek and tobacco cells. On the other hand, a dosage-dependent stabilization behavior was quantified.

1.4. *Arabis alpina* and *Cardamine hirsuta* - two related Brassicaceae

ARABIS

The Brassicaceae *Arabis alpina* arose as an evolutionary and developmental model organism for molecular variation due to its perennial generation time. The plant naturally populates montane, alpine, and arctic habitats (Koch et al., 2006; Wang et al., 2009), i.e. harsh environmental conditions which favor a perennial life cycle to survive and propagate successfully (Wang et al., 2009). To enter the reproductive phase,

prolonged exposure to low temperatures (vernalization) is an indispensable requirement for *A. alpina* accessions, including the commonly used wildtype accession Pajares (Paj; Wang et al., 2009). In the vegetative phase, *A. alpina* copes with its perennial life cycle by producing elongated internodes and developing axillary branches, whereas *A. thaliana* internodes do not expand, resulting in tight rosette leaves (Wang et al., 2011). Both species exhibit simple leaves with smooth margins of juvenile leaves and serrations on later developed leaves (Park et al., 2017).

A. alpina and *A. thaliana* diverged between 19-25 (Koch et al., 2001) or 26-40 (Beilstein et al., 2010; Koch et al., 2006) million years ago. Thus, divergent and redundant functions on the molecular level are expected. The diploid and completely sequenced genome, which is divided into eight chromosomes, as well as being self-fertile and transformable by *Agrobacteria*, makes *A. alpina* a suitable research organism (Wang et al., 2009; Willing et al., 2015). However, the duration of vernalization must be taken into account in the experimental planning.

The trichome morphology of *A. alpina* is comparable to *A. thaliana*. Also, trichome initiation seems restricted to the basal zone of the leaves in the perennial species. Mature trichomes are found at the leaf tip and intermediate stages in between. The pattern is regular, but trichome density is much higher in *A. alpina* (Figure 3). Taking a closer look, two classes of mature trichomes become visible: larger trichomes with occasionally occurring smaller ones in between (Chopra et al., 2014). It was shown that these smaller trichomes undergo fewer endoreplication cycles than the others (Chopra et al., 2019). Compared to *A. thaliana*, all leaves develop trichomes on the ad- and abaxial sides. Generally, the roots of both species are organized in alternating H- and N-files (hair and non-hair files), but in contrast to *A. thaliana*, *A. alpina* Paj shows 30% ectopic root hair formation on N-files (Chopra et al., 2014).

As closely related Brassicaceae, the *TTG1*-dependent pathway regulates trichome and root hair formation in both species, suggesting similar phenotypes. This is indeed the case for *ttg1* mutants as both species are glabrous (Chopra et al., 2014; Walker et al., 1999). Whereas only *Atgl3 Ategl3* double mutants exhibit glabrous leaves, this phenotype already appears in *Aagl3* mutants, indicating a more divergent function of the homologous genes *GL3* and *EGL3* in *A. alpina* (Chopra et al., 2019; Zhang et al., 2003).

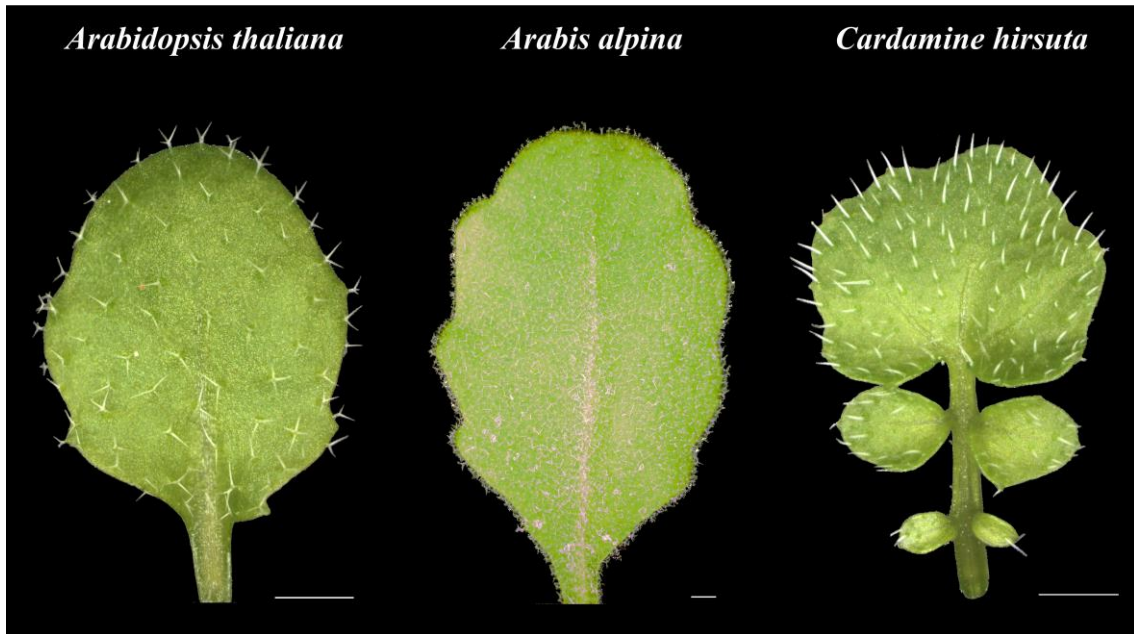


Figure 3: Morphological comparison of three different mature Brassicaceae leaves. Leaf four is exemplarily shown for *A. thaliana*, *A. alpina*, and *C. hirsuta*. Scale bars indicate 1 mm.

CARDAMINE

The annual Brassicaceae *Cardamine hirsuta* emerged as an up-coming model organism for developmental comparisons in the last decades. For this species, the Oxford (Ox) accession is used as a reference (Gan et al., 2016). The leaf shape of *C. hirsuta* is striking and differs categorically from its related species *A. thaliana* by forming compound leaves. They comprise a terminal leaflet on the leaf tip and lateral leaflets towards the basis. Typically, lateral leaflets appear from rosette leaf three, and their number increases with each additional leaf (Canales & Barkoulas, 2010; Cartolano et al., 2015). Besides that, *C. hirsuta* differs in other morphological traits such as plant habit, shoot branching, or floral morphogenesis from *A. thaliana* (Hay et al., 2014; Hay & Tsiantis, 2006, 2016; Pieper et al., 2016). In contrast to the latter, *C. hirsuta* possesses a variable number of petals between zero and four and develops more secondary branches, leading to a more abundant shoot architecture (Hay et al., 2014). Their divergence is estimated to occur 13-19 million years ago (Beilstein et al., 2008; 2010; Koch et al., 2001) and, similar to *A. alpina*, enables the identification of redundant as well as divergent functions between both species.

C. hirsuta is similarly accessible to forward and reverse genetic approaches. Molecularly, its small, diploid, and nowadays completely sequenced genome is divided into eight chromosomes. An 8-week generation cycle, providing abundant progeny via self-pollination, its small rosette size, and commonly standardized growth conditions

present further beneficial traits for large-scale experiments. Laboratory work is feasible due to simple genetic transformation by chemical or *Agrobacterium*-mediated mutagenesis (Hay et al., 2014).

While *C. hirsuta* trichomes on petals and sepals were already investigated molecularly (Pieper et al., 2016), leaf trichomes were so far only morphologically compared to *A. thaliana* (Hay et al., 2014; Hay & Tsiantis, 2016). *C. hirsuta* produces unicellular but unbranched trichomes on leaves (Figure 3) that are missing on the stem (Hay et al., 2014). To date, root hair formation in *C. hirsuta* has not reached the focus of research. However, different root anatomy was observed: In contrast to *A. thaliana*, two cortical layers and a mixed tissue consisting of cortical and endodermal identity develop in the root system (Di Ruocco et al., 2018).

1.5. Aim of this work

This study aims to deepen the knowledge of the underlying cross-regulatory mechanisms of fluent acting networks required to establish cell fate specifications and tissue patterns. The focus is on the regularly distributed trichome pattern on *A. thaliana* rosette leaves and related species.

Gene fluctuations are the basis of cell fate specification in *de novo* patterning processes. They are required to break the homogeneity of genetically identical cells and develop different tissues and organs (Hong et al., 2016; Raj & van Oudenaarden, 2008). Two experimental setups were performed to elucidate protein fluctuations in living plants. On the one hand, a photoconvertible protein was utilized to analyze gene fluctuations in *A. thaliana* rosette leaves temporally. On the other hand, the primary source of fluctuating gene expressions was revealed in different plant tissues using a dual reporter system in a spatial approach. These experiments contribute to bridging between random gene expressions and reproducible patterns.

Moreover, this work investigates the protein stability to execute and maintain the regularly distributed trichome pattern. After establishing the viral P2A “self-cleavage” system *in planta*, it was utilized to answer the questions of whether proteins influence each other’s stability and whether a dosage-dependent stabilizing effect can be measured. The obtained results may provide insights into the protein behavior and function of the trichome patterning machinery *in vivo*.

With the aid of quantitative Real-Time PCR (RT-qPCR; hereinafter referred to as qPCR), an extensive, systematical, and functional study of the cross-regulatory *TTG1*

network was conducted in *A. thaliana* wildtype and 21 patterning mutants. So far, individual studies have only focused on a subset of genes and are not combinable due to varying biological sample material. Here, all patterning genes were investigated simultaneously under the same conditions with comparable leaf material. Using this standardized approach, this study aimed to uncover the core components among the activators and inhibitors of trichome patterning, and analyzed the impact of gene homologs.

Related Brassicaceae represent ideal model organisms to study the conserved cross-interacting *TTG1* network because of their predicted redundant and divergent gene regulations. Due to their similar trichome pattern, *Arabis alpina* and *Cardamine hirsuta* were compared to *Arabidopsis thaliana* to investigate the patterning genes from an evolutionary and developmental perspective. More than 20 members of the network could be identified in *A. alpina* using the commonly available genome and transcriptome sequencing data (Willing et al., 2015) based on preliminary work and own investigations. In addition, most gene orthologs of the *TTG1* network could be identified based on sequence similarity and synteny with the Cardamine genome data (Gan et al., 2016). Although - or precisely because - there are only a few studies yet available on that topic, this offers the opportunity for a broad range of comparative studies between related Brassicaceae beyond descriptive research. Together, expression analyses of the network components were carried out to unravel the mechanism of trichome pattern formation and the influence of gene homologs in rosette leaves and other plant tissues.

Taken together, this study aimed to elucidate the cross-regulatory interactions of all trichome patterning genes of the *TTG1*-dependent system in *A. thaliana*, and gain evolutionary insights into the conserved network by a comparative approach in two related species.

2. Material & Methods

2.1. Material

2.1.1. Bacterial strains

Table 1: List of used bacterial strains.

Description	Property	Reference
<i>Agrobacterium tumefaciens</i> GV3101:pMP90RK	Rif-, Kan-resistance	Koncz & Schell, 1986
<i>Agrobacterium tumefaciens</i> RK	Rif-, Kan-resistance anti-silencing strain	Voinnet et al., 1999
<i>Escherichia coli</i> DH5 α	F- Φ 80 <i>lacZ</i> Δ M15 Δ (<i>lacZYA-argF</i>) U169 <i>recA1 endA1 hsdR17</i> (rK-, mK+) <i>phoA supE44 λ-thi-1 gyrA96 relA1</i>	Hanahan, 1983
<i>Escherichia coli</i> DB3.1	F- <i>gyrA462 endA1 glnV44 Δ(sr1-recA) mcrB mrr hsdS20(rB-, mB-) ara14 galK2 lacY1 proA2 rpsL20(Smr) xyl5 Δleu mtl1</i>	Bernard & Couturier, 1992; Miki et al., 1992

2.1.2. General vectors

Table 2: Vectors used for desired expression constructs.

Vector	Feature	Resistance	Reference
pDONR201	Entry vector for gateway cloning	Kanamycin	Invitrogen
pDONR207	Entry vector for gateway cloning	Gentamicin	Invitrogen
pENSG:CFP/YFP	Plant expression vector driven by <i>35S CaMV</i> promoter; N-terminal CFP or YFP tag	Carbenicillin	Feys et al., 2005
pAMPAT	Plant expression vector; driven by either <i>35S CaMV</i> or endogenous promoter	Carbenicillin	derived from GenBank ID AY436765

2.1.3. Constructs and stably transformed lines

Table 3: Constructs and stably transformed *A. thaliana* lines used for experimental work.

Construct	Experiment	Source
<i>pAMPAT:NLS-KikGR</i>	Fluctuation	R. Balkunde
<i>pENSG:2xNLS-YFP + pENSG:2xNLS-CFP</i>	Fluctuation	I. Schultheiß Araújo
<i>pENSG:YFP-CPC-P2A-RFP-NLS</i>	Protein stability	I. Schultheiß Araújo
<i>pENSG:YFP-GL1-P2A-RFP-NLS</i>	Protein stability	I. Schultheiß Araújo
<i>pENSG:YFP-TRY-P2A-RFP-NLS</i>	Protein stability	I. Schultheiß Araújo
<i>pENSG:YFP-CPC-P2A-2xNLS-mCherry</i>	Protein stability	I. Schultheiß Araújo
<i>pENSG:YFP-GL1-P2A-2xNLS-mCherry</i>	Protein stability	I. Schultheiß Araújo
<i>pENSG:YFP-TRY-P2A-2xNLS-mCherry</i>	Protein stability	I. Schultheiß Araújo
<i>pENSG:CFP-w/o</i>	Protein stability	M. Pesch
<i>pENSG:CFP-GL3</i>	Protein stability	M. Pesch
<i>pENSG:CFP-MYC1</i>	Protein stability	I. Schultheiß Araújo
<i>pAMPAT:mTurquoise2-TRY-P2A-YFP-P2A-mCherry</i>	Protein stability	I. Schultheiß Araújo
<i>pAMPAT:mTurquoise2-TRY-P2A-YFP-P2A-mCherry-MYC1</i>	Protein stability	I. Schultheiß Araújo
<i>pENSG:YFP-LOV2-P2A-RFP-NLS</i>	Protein stability	I. Schultheiß Araújo
<i>pENSG:YFP-LOV2-ODC-P2A-RFP-NLS</i>	Protein stability	I. Schultheiß Araújo
<i>pAMPAT:pMYC1_{1970bp}:ccdB</i>	<i>pMYC1</i> comparison	I. Schultheiß Araújo
<i>pAMPAT:pMYC1_{1970bp}:GUS</i>	<i>pMYC1</i> comparison	This study
<i>pAMPAT:pMYC1_{1970bp}:2xNLS-mCherry</i>	<i>pMYC1</i> comparison	This study
<i>pAMPAT:pMYC1_{2581bp}:ccdB</i>	<i>pMYC1</i> comparison	This study
<i>pAMPAT:pMYC1_{2581bp}:GUS</i>	<i>pMYC1</i> comparison	This study
<i>pAMPAT:pMYC1_{2581bp}:2xNLS-mCherry</i>	<i>pMYC1</i> comparison	This study
<i>pAMPAT:pMYC1_{1970bp}:YFP-MYC1 WS</i>	<i>pMYC1</i> expression	M. Pesch
<i>pAMPAT:pMYC1_{1970bp}:YFP-MYC1 ttg1</i>	<i>pMYC1</i> expression	M. Pesch
<i>pAMPAT:pMYC1_{1970bp}:YFP-MYC1 gl3 egl3</i>	<i>pMYC1</i> expression	M. Pesch
<i>pAMPAT:pMYC1_{1970bp}:YFP-MYC1 gl1</i>	<i>pMYC1</i> expression	M. Pesch
<i>pENSG:pCPC:2xNLS-2xCFP</i>	Promoter expression	This study
<i>pENSG:pETC1:2xNLS-2xCFP</i>	Promoter expression	This study
<i>pENSG:pETC2:2xNLS-2xCFP</i>	Promoter expression	This study
<i>pENSG:pGL2:2xNLS-2xCFP</i>	Promoter expression	I. Schultheiß Araújo
<i>pENSG:pTRY:2xNLS-2xCFP</i>	Promoter expression	I. Schultheiß Araújo

2.1.4. Wildtype and mutant plant lines for transcription analysis

Table 4: *Arabidopsis thaliana*, *Arabis alpina*, and *Cardamine hirsuta* plant lines used for the transcriptional expression analysis.

Line	Ecotype	Target ID	Source
Arabidopsis			
Col-0	Col-0	-	-
<i>cpc-2</i>	Col-0	AT2G46410	Kurata et al., 2005
<i>cpc-2 try</i>	Col-0	AT2G46410 / AT5G53200	L. Rishmawi
<i>egl3</i>	Col-0	AT1G63650	A. Friede
<i>etcl 2-7</i>	Col-0	AT1G01380	Kirik et al., 2004a
<i>etcl etc3</i>	Col-0	AT1G01380 / AT4G01060	Wester et al., 2009
<i>etc2</i>	Col-0	AT2G30420	A. Steffens
<i>etc3</i>	Col-0	AT4G01060	Simon et al., 2007
<i>etc3 try-JC</i>	Col-0	AT4G01060 / AT5G53200	Wester et al., 2009
<i>gl1</i>	Col-0	AT3G27920	I. Schultheiß Araújo
<i>gl1 myb23</i>	Col-0	AT3G27920 / AT5G40330	V. Kirik
<i>gl2</i>	Col-0	AT1G79840	L. Rishmawi
<i>gl3-3</i>	Col-0	AT5G41315	Jakoby et al., 2008
<i>gl3-3 egl3</i>	Col-0	AT5G41315 / AT1G63650	Wester et al., 2009
<i>myb23-1</i>	Col-0	AT5G40330	Kirik et al., 2005
<i>myc1-1</i>	Col-0	AT4G00480	Pesch et al., 2013
<i>myc1-1 egl3</i>	Col-0	AT4G00480 / AT1G63650	Pesch et al., 2013
<i>tcl1</i>	Col-0	AT2G30432	A. Steffens
<i>tcl2</i>	Col-0	AT2G30424	A. Steffens
<i>try-JC</i>	Col-0	AT5G53200	Larkin et al., 1999
<i>ttg1-21</i>	Col-0	AT5G24520	Appelhagen et al., 2014
<i>ttg2-3</i>	Col-0	AT2G37260	Ishida et al., 2007
Arabis			
Paj	Paj	-	M. Albani / G. Coupland
<i>gl2</i>	Paj	Aa_G239140	D. Chopra-Ufer
Cardamine			
Ox	Ox	-	M. Tsiantis

2.1.5. Antibiotics

Table 5: List of antibiotics used for this study.

Antibiotic	Manufacturer
50 mg/ml Carbenicillin	Duchefa
35 mg/ml Chloramphenicol	Duchefa
50 mg/ml Gentamicin	Duchefa
25 mg/ml Kanamycin	Roth
50 mg/ml Rifampicin	Duchefa
50 mg/ml Spectinomycin	Duchefa

2.1.6. Oligonucleotides

The sequences of all primers used for this study can be found in the appendix (Table S1; Table S2; Table S3; Table S4).

2.1.7. Software

Table 6: Software and its applications used in this study.

Software	Application
Microsoft Office 2007	Text and data processing; creation of bar diagrams
ImageJ 1.49v	Measurements of mean gray values and leaf area; trichome counting; montage of CLSM images
OriginPro 8.5G	Statistical analyses; creation of box plots and diagrams
RStudio 3.2.1	Calculation and creation of scatter and bar plots
CLC DNA Workbench 5.6.1	<i>In silico</i> cloning; sequence analyses; alignment constructions
LAS X 3.7.2	Evaluation of CLSM images
QuantStudio™ Design & Analysis Software	Evaluation of qPCR data
Inkscape 0.91	Creation of figures

2.2. Molecular techniques

2.2.1. Generation of chemically competent *E. coli* and *A. tumefaciens* cells

E. coli DH5 α or DB3.1 cells

A 10 ml ψ broth (2% peptone, 0.5% yeast extract, 0.4% MgSO₄, 10 mM KCl, dissolved in ddH₂O, adjusted to pH 7.6 (KOH), autoclaved for 20 min at 121°C, stored at 4°C) pre-culture with *E. coli* cells was incubated overnight at 37°C, and 220 rpm was used to inoculate a 200 ml ψ broth main culture. At OD₅₅₀ = 0.48, the culture was split into 50 ml and cooled down on ice for 15 min. Cells were centrifuged for 10 min at 4°C and 800g. The pellet was resuspended in 1 ml Tfb1 medium (100 mM RbCl₂, 50 mM MnCl₂, 30 mM KAc, 10 mM CaCl₂, 15% glycerol, dissolved in ddH₂O, adjusted to pH 5.8 (0.2% AcOH), sterile-filtered, stored at 4°C) and filled up to 15 ml. After incubation for 2 h on ice, the cells were centrifuged for 5 min at 4°C and 800g, and the pellet was resuspended in 2 ml Tfb2 medium (10 mM RbCl₂, 75 mM CaCl₂, 15% glycerol, 10 mM MOPS, dissolved in ddH₂O, adjusted to pH 7.0 (NaOH), sterile-filtered, stored at 4°C). Cells were aliquoted, shock-frozen in liquid nitrogen, and stored at -80°C.

A. tumefaciens GV3101:pMP90RK

A 5 ml *A. tumefaciens* overnight culture (YEB; 0.5% peptone, 0.5% beef extract, 0.1% yeast extract, 0.5% sucrose, 0.2 M MgSO₄, dissolved in ddH₂O, autoclaved for 20 min at 121°C, incubated with rifampicin (20 mg/l) overnight at 28°C and 220 rpm; for YEB plates: add 1.6% agar) was used to inoculate 500 ml main culture. When the OD₆₀₀ reached 0.5 to 0.6, the culture was split and centrifuged at 7000g for 5 min at 4°C. Each pellet was resuspended in 25 ml icecold NaCl (0.15 M) and incubated on ice for 15 min. Centrifugation was repeated, and all cells were resuspended in 5 ml icecold CaCl₂ (20 mM). Aliquots were frozen in liquid nitrogen and stored at -80°C.

2.2.2. Heat-shock transformation of competent *E. coli* or *A. tumefaciens* cells

Competent cells were thawed on ice, mixed with 1 μ l (*E. coli*) or 2 μ l (*A. tumefaciens*) of the desired plasmid (or entire BP / LR reaction), and heat-shocked at 42°C for 90 sec. The mixture was chilled on ice for 10 min before adding 300 μ l LB media (1% peptone, 0.5% yeast extract, 1% NaCl, dissolved in ddH₂O, autoclaved for 20 min at 121°C; for LB plates: add 1.6% agar) for *E. coli* or 500 μ l YEB media for *A. tumefaciens*. Mixtures

were incubated for 30 min at 37°C (*E. coli*) or 2 h at 28°C (*A. tumefaciens*) and 650 rpm and plated on LB or YEB plates containing the required antibiotics of the transformed plasmid as well as rifampicin (50 mg/ml) and kanamycin (25 mg/ml) for *A. tumefaciens*.

2.2.3. Plasmid DNA isolation

Plasmid DNA was isolated from 5 ml *E. coli* liquid overnight cultures (37°C and 220 rpm on selected medium) according to the high-copy microcentrifuge protocol of the GeneJET Plasmid Miniprep Kit (ThermoFisher Scientific).

2.2.4. Restriction digest

For plasmid verification, DNA digests with bacterial restriction enzymes were performed. These enzymes are endonucleases that specifically degrade DNA by their inner phosphodiester bond. Following restriction enzymes were used: BamHI, BlnI, BsrGI, ClaI, DpnI, PstI, Sall, SgsI, XbaI, XhoI (ThermoFisher Scientific).

2.2.5. Gel electrophoresis

DNA fragments from a restriction digest or PCR products were visualized by gel electrophoresis. Staining was performed either with ethidium bromide (Roth) or with Thiazole Orange (Sigma-Aldrich), and samples enriched with loading dye (50 mM EDTA (NaOH pH 8.0), 50% glycine, 1% xylene cyanol, 10 mM Tris (HCl pH 8.0), dissolved in ddH₂O, stored at room temperature) were separated by the applied voltage. For ethidium bromide, 1% agarose gels were mixed with 0.25 µg/ml of the reagent, and visualization was achieved using BioRad Universal Hood II equipped with the Quantity One software version 4.5.0. For Thiazole Orange, 0.14 µg/ml of the dye were added to a 1% agarose gel and documented with the INTAS Gel Jet Imager equipped with Intas GDS Touch 2 version 2.1.4. 100 bp or 1 kb (plus) ladder (ThermoFisher Scientific) were used as references.

2.2.6. Cloning

T4 DNA ligation

Classically, the sequence of interest is incorporated into a vector by T4 DNA ligation. Therefore, it was flanked by restriction sites and amplified by PCR. The respective

products or suitable vectors were digested to generate an insert with sticky ends. The desired expression vectors were linearized by the same restriction enzymes and dephosphorylated by FastAP (ThermoFisher Scientific). Linearized vector and insert were mixed in a 1:5 ratio, 0.5 μ l T4 DNA ligase, and 1 μ l T4 DNA ligase buffer (ThermoFisher Scientific) were added and filled up with ddH₂O to a total volume of 10 μ l. Ligation reactions were incubated overnight at 12°C, then transformed into competent *E. coli* cells.

Gateway cloning

Gateway cloning is a two-step system to generate various expression vectors based on a single entry vector. A sequence of interest, flanked by attB sites, is amplified via PCR and integrated into an entry vector (pDONR201 or pDONR207). Afterwards, the entry clone can be used for LR reactions, integrating the gene of interest into a destination vector. Table 7 summarizes BP and LR reactions.

Table 7: Composition of BP and LR reaction.

BP reaction		LR reaction	
pDONR	0.25 μ l	destination vector	0.25 μ l
PCR product	0.5 μ l	entry vector	0.5 μ l
BP clonase	0.5 μ l	LR clonase	0.5 μ l
ddH ₂ O	1.25 μ l	ddH ₂ O	1.25 μ l
Total volume	2.5 μ l	Total volume	2.5 μ l

2.2.7. Genomic DNA isolation

To perform PCRs on the genomic level, small leaves (<1 cm) of Arabidopsis wildtype and mutant lines frozen in liquid nitrogen were pulverized using a TissueLyser (Qiagen) at 30 Hz for 90 sec. 125 μ l extraction buffer (200 mM Tris (HCl pH 8.0), 250 mM NaCl, 25 mM EDTA (NaOH pH 8.0), 0.5% SDS, dissolved in ddH₂O, stored at room temperature) were added, and the tube was inverted three times. After adding 38.5 μ l sodium acetate, the tube was inverted and centrifuged for 2 min at 16,100g. 125 μ l of the supernatant were added to 125 μ l isopropyl, inverted, and centrifuged for 10 min. The pellet was washed with 500 μ l of 70% ethanol and washed for 2 min. After drying at room temperature for 30 min, the pellet was resuspended in 20 μ l ddH₂O.

2.2.8. PCR

Polymerase chain reactions (PCR) were utilized to amplify a specific DNA sequence. Reactions were performed based on Table 8. Primers were ordered by Sigma-Aldrich, buffer, dNTPs, and polymerase by ThermoFisher Scientific. PCR reactions took place in C1000 or S1000 thermocycler (BioRad).

Table 8: Default PCR composition and program.

PCR composition		PCR program		
DNA template	0.5 μ l	95°C	2 min] 35 x
forward primer (10 μ M)	2 μ l	95°C	45 sec	
reverse primer (10 μ M)	2 μ l	primer specific	30 sec	
High fidelity buffer (5x)	10 μ l	72°C	30 sec/kb	
dNTPs (10 mM)	1 μ l	72°C	5 min	
Phusion polymerase	1 μ l	12°C	∞	
ddH ₂ O	33.5 μ l			
Total volume	50 μ l			

2.2.9. Generation of constructs

pENSG:[promoter]:2xNLS:2xCFP

pENSG:pCPC:2xNLS-2xCFP and *pENSG:pETC1:2xNLS-2xCFP* were generated by amplification of SgsI-*pCPC*-BamHI-ClaI and SgsI-*pETC1*-BamHI-ClaI, respectively, from genomic Col-0 Arabidopsis DNA, which were then incorporated into the pJET1.2/blunt cloning vector (Promega). The *pCPC* sequence comprises -1102 to -2 bp before the start codon of *CPC* and the *pETC1* sequence -1921 to -1 bp upstream of *ETC1*. *pENSG:pETC2:2xNLS-2xCFP* was digested with SgsI and ClaI and used as backbone for the ligation with SgsI-*pCPC*-BamHI-ClaI or SgsI-*pETC1*-BamHI-ClaI, respectively, leading to the constructs *pENSG:pCPC-2xCFP* and *pENSG:pETC1-2xCFP*. These plasmids were digested with BamHI and PstI to eliminate the first CFP. Next, BamHI-2xNLS-CFP-PstI was amplified from a suitable template and recombined with *pENSG:pCPC-CFP* and *pENSG:pETC1-CFP*, leading to the desired constructs.

To generate *pENSG:pETC2:2xNLS-2xCFP*, SgsI-*pETC2*-XhoI was amplified from genomic Col-0 DNA by PCR and incorporated into the pJET1.2/blunt cloning vector. *pENSG:pTRY:2xNLS-2xCFP* was digested with SgsI and XhoI, and used as

backbone for recombination with the SgsI-*pETC2*-XhoI insert. The *pETC2* sequence comprises -1638 bp to -34 bp before its start codon.

pAMPAT:pMYC1-[x]

pAMPAT:pMYC1_{1970 bp}:GUS was cloned by insertion of *pGWB2:GUS* into *pAMPAT:pMYC1_{1970 bp}:ccdB* via LR reaction.

To generate *pAMPAT:pMYC1_{1970 bp}:2xNLS-mCherry*, attB1-2xNLS-mCherry-attB2 was amplified from a suitable template by PCR, cloned into pDONR207 by BP reaction and introduced into the *pAMPAT:pMYC1_{1970 bp}:ccdB* vector by LR reaction. A stop codon at the C-terminal part of the fluorescence marker was introduced via PCR-based site-directed mutagenesis.

For *pAMPAT:pMYC1_{2581 bp}:ccdB*, *pAMPAT:pMYC1_{1970 bp}:ccdB* was digested with SgsI and XhoI to generate *pAMPAT:SgsI-XhoI-ccdB*. *pMYC1_{2581 bp}* was amplified from genomic DNA by PCR, cloned into the pJET1.2/blunt cloning vector, amplified by PCR with primers containing SgsI or XhoI restriction sites, respectively, digested and ligated into *pAMPAT:SgsI-XhoI-ccdB*.

pAMPAT:pMYC1_{2581 bp}:GUS and *pAMPAT:pMYC1_{2581 bp}:2xNLS-mCherry* were generated by LR reactions of suitable templates into *pAMPAT:pMYC1_{2581 bp}:ccdB*.

2.2.10. Genotyping

Determination of the genotypic background of Arabidopsis T-DNA lines was carried out by PCR (Table 9). Primers were designed to amplify either an overlapping fragment of the T-DNA sequence and the gene of interest or the wildtype sequence.

Table 9: PCR composition and program using a ready-to-use mix.

PCR composition		PCR program		
DNA template	1 µl	95°C	2 min] 35 x
forward primer (10 µM)	0.4 µl	95°C	45 sec	
reverse primer (10 µM)	0.4 µl	primer specific	30 sec	
DreamTaq Green PCR Master Mix (2X)	12.5 µl	72°C	30 sec/kb	
ddH ₂ O	10.7 µl	72°C	5 min	
Total volume	25 µl	12°C	∞	

2.2.11. PCR-based site-directed mutagenesis

Site-directed mutagenesis was utilized to generate specific point mutations in a sequence of interest. PCR was performed as described in Table 10 using 30 nt long primers with the desired base exchange in the middle. Afterwards, the PCR reaction was digested with 1 μ l DpnI for 90 min at 37°C, followed by inactivation for 20 min at 80°C. 1 μ l of the reaction was used to transform competent *E. coli* cells.

Table 10: PCR composition and program for site-directed mutagenesis.

PCR composition		PCR program		
DNA template	0.5 μ l	95°C	3 min] 13 x
forward primer (10 μ M)	2 μ l	95°C	45 sec	
reverse primer (10 μ M)	2 μ l	42°C	45 sec	
High fidelity buffer with MgCl ₂ (10x)	5 μ l	72°C	110 sec] 26 x
dNTPs (10 mM)	1 μ l	95°C	45 sec	
High fidelity polymerase	0.5 μ l	60°C	45 sec	
ddH ₂ O	39 μ l	72°C	7 min	
Total volume	50 μ l	72°C	10 min	
		12°C	∞	

2.2.12. qPCR

This PCR-based technique was employed to monitor and quantify the amplification of targeted gene fragments using a non-specific double-strand intercalating fluorescent dye.

Primer establishment and validation

Primers for qPCR assays need to fulfill several criteria. To design preferably intron-spanning primers, GenScript Real-time PCR Primer Design (www.genscript.com) was used with an optimal melting temperature of 60 \pm 2°C and sequence-specific amplicons of ideally 150-200 bp. Sequence and primer specificity was checked via BLAST search, agarose gel electrophoresis, and a single peak in the qPCR melting curve. qPCR reactions were performed as described in Table 11. Amplification efficiency and correlation were determined based on serial cDNA dilution steps (1:10, 1:20, 1:40, 1:80, 1:160, 1:320).

Cq (quantification cycle) and log10 values of the dilution series were used to calculate the slope with the formula

$$\text{slope} = \frac{\sum(x-\bar{x})(y-\bar{y})}{\sum(x-\bar{x})^2},$$

which served to calculate the primer efficiency E using the formula

$$E = 100 \times (10^{(-\frac{1}{\text{slope}})} - 1).$$

The R^2 correlation of the Cq and the log10 values was calculated using the formula

$$\rho_{x,y} = \frac{\text{Cov}(X,Y)}{\sigma_x \times \sigma_y}.$$

Primer efficiencies of 100±20% for genes of interest and 100±10% for reference genes, as well as a linear standard curve with a correlation of ≥ 0.99 , were accepted. Graphs displaying all qPCR primer efficiencies of the three species can be found in the appendix (Figure S1; Figure S2; Figure S3). Sequences were taken from TAIR (www.arabidopsis.org), Genomic resources for *Arabidopsis thaliana* (www.arabidopsis.org), and *Cardamine hirsuta* genetic and genomic resource (<http://chi.mpipz.mpg.de>).

Sample preparation

Depending on the experiment, different types of plant material were harvested from plants either grown on soil or plates with MS medium (0.44% MS (Murashige and Skoog), dissolved in ddH₂O, autoclaved for 20 min at 121°C). For the intra- and interspecies comparisons (Chapter 3.5.2 and 3.6.2), 200-400 µm sized leaves with on-going trichome patterning were gathered by removing juvenile leaves (leaves one and two for *A. thaliana* and *A. alpina*, additionally leaf three for *C. hirsuta*) as well as roots, hypocotyl, cotyledons of plant seedlings. Material of up to 45 plants was collected per biological replicate. For the tissue comparison in *A. thaliana*, *A. alpina*, and *C. hirsuta* (Chapter 3.6.4), samples containing either 25 roots, 15 shoots, 15 seedlings, or 2 mature leaves (terminal leaflets for *C. hirsuta*) were harvested. Plant materials were frozen in liquid nitrogen and stored at -80°C until further processing. Sample integrity was confirmed by actin amplification.

RNA extraction

Prior harvested and frozen material was pulverized using a TissueLyser (Qiagen) at 30 Hz for 1 min. After immersion into liquid nitrogen, 300 µl cold Tri-Reagent (Ambion by Life Technologies) was added, and samples were homogenized at 30 Hz

for 2 min. 700 μ l Tri-Reagent was added, samples were vortexed for 15 sec and incubated for 3 min at room temperature. After adding 200 μ l chloroform and brief vortexing, samples were centrifuged at 3200g for 15 min at 4°C. The aqueous upper phase was transferred into a new tube, 550 μ l isopropanol were added and vortexed. After incubation for 10 min at room temperature, samples were centrifuged at 3200g for 20 min at 4°C. The supernatant was discarded, and the pellet was washed with 500 μ l of 70% ethanol by centrifugation for 5 min. Washing was repeated with 500 μ l of absolute ethanol. Pellet was drying for 30 min at 37°C before resuspension in 30 μ l ddH₂O. Samples were stored at -20°C until DNaseI digest. Therefore, 1 μ l DNaseI and 2 μ l 10x DNaseI buffer were added to the entire sample, incubated at 37°C for 1 h before 2.5 μ l EDTA (25 mM) were added for inactivation at 65°C for 10 min. RNA concentration and purity were measured photometrically. Additionally, RNA integrity was verified on a bleach gel. Therefore, a 1% agarose gel was supplied with 2% sodium hypochlorite (NaOCl) to a final concentration of 0.04% and enriched with ethidium bromide (0.25 μ g/ml). 2 μ l RNA samples were added to 8 μ l ddH₂O, and 2 μ l loading dye, and voltage was supplied for separation.

cDNA synthesis

To synthesize RNA into cDNA, 2.5 μ g RNA were used to perform the reaction with the RevertAid First Strand cDNA Synthesis Kit (ThermoFisher Scientific). Samples were additionally treated with 0.4 μ l RNase H (RNase HI, ThermoFischer Scientific) at 37°C for 20 min.

qPCR composition and program

Dye-based qPCRs were performed using the GoTaq qPCR Master mix system (Promega). cDNA was added to prepared master mixes into 96-well plates (0.2 ml, BIOplastics), which were covered with Opti-Seal Optical Disposable Adhesive (BIOplastics), and reactions were carried out in a QuantStudio™ 5 Real-Time PCR System (Applied Biosystems™), equipped with the QuantStudio™ Design and Analysis Software using the standard program of the system (Table 11).

Table 11: Composition of qPCR reaction and program. Asterisks (*) mark data collection points.

qPCR composition			qPCR program		
Master mix	GoTaq qPCR Master Mix (2x)	5 μ l	50°C	2 min] 40 x
	forward primer (10 μ M)	0.2 μ l	95°C	10 min	
	reverse primer (10 μ M)	0.2 μ l	95°C	15 sec	
	ddH ₂ O	3.6 μ l	60°C	1 min *	
	cDNA	1 μ l	95°C	15 sec	
	Total volume	10 μ l	60-95°C	1 min *	

Analysis qPCR data

A two-sided Grubbs' test ($\alpha = 0.05$) was performed to identify outliers in the raw data. Normalization of the data was conducted according to the geNorm manual (Vandesompele; 2002), describing gene expressions relatively to each other. Special considerations were given to normalization factors and the individual primer efficiencies. Here, no generalized gene duplication per cycle ($I + I$) was assumed, but the individual amplification rate ($I + efficiency$) was used for further calculations. The expression data of each species was normalized against two different reference genes. Using normalizations factors and not the Cq values, allows interspecies comparison even with different reference genes for each organism.

Since log-normal distribution is not symmetric, empirical mean and standard deviation estimates are biased. Therefore, the data were log-transformed with respect to the base $I + efficiency$, and the standard formulas (Kirkwood; 1979) were adjusted accordingly. Hence, the Maximum Likelihood estimates for the mean and the bias corrected standard deviation are given by

$$E[X] = \frac{1}{n} \sum_{i=1}^n X_i \quad (\text{empirical mean})$$

and

$$SD[X] = E[X] * CV[X] \quad (\text{corrected standard deviation}),$$

where the empirical standard deviation is given by

$$\sigma^2 = \frac{1}{n-1} \sum_{i=1}^n (X_i - E[X])^2$$

and the coefficient of variation is given by

$$CV[X] = \sqrt{(1 + efficiency)^{\sigma^2} - 1}.$$

To compare tissues within one species, Cq values were normalized to the overall minimal Cq value. This resulted in larger differences within the replicates, which were enhanced by subsequent logarithmic calculation of the relative expression. To correct this, means were calculated by using the formula

$$\mu = \ln \left(\bar{x} / \sqrt{1 + \frac{\hat{\sigma}^2}{\bar{x}^2}} \right)$$

and the standard deviation is given by

$$\sigma^2 = \ln \left(1 + \frac{\hat{\sigma}^2}{\bar{x}^2} \right).$$

2.2.13. Sequencing

Sanger sequencing was carried out by GATC Biotech/Eurofins Genomics.

2.3. Plant techniques

2.3.1. Propagation of *A. thaliana* and *N. benthamiana*

Unless otherwise stated, all Arabidopsis lines and Nicotiana plants were grown on soil under greenhouse conditions with photoperiodic cycles of 16 h light and 8 h darkness.

2.3.2. Seed sterilization

Sodium hypochlorite

Seeds were covered with 1 ml 100% EtOH. After 5 min incubation with occasional inverting, the supernatant was discarded, and 1 ml 4% NaOCl + 0.1% Triton (Roth) was added. After 25 min incubation with occasional inverting, the liquid was replaced by ddH₂O to facilitate seed distribution on MS plates.

Chlorine gas

Seeds were transferred into a 2 ml reaction tube and put with an open lid to a desiccator. 7.61 ml NaOCl (12%) and 2.5 ml HCl (37%) were added to a beaker, placed next to the seed tubes, and the desiccator was quickly closed. Chlorine gas emerges and sterilizes the seeds in 3 h.

2.3.3. Generation of stably transformed Arabidopsis lines

200 ml YEB medium were inoculated with *Agrobacterium tumefaciens* carrying the desired construct. After two days of incubation at 28°C at 220 rpm, 10 g sucrose and 50 µl Silwet-L77 were added. For double transformation, 100 ml of each construct were mixed beforehand. Arabidopsis plants in full bloom were dipped into the suspension for 10 sec and recovered horizontally for one day before they finished their life cycle under greenhouse conditions. Seeds of the progeny were selected by BASTA (Aventis)/Glyphosate (Realchemie) treatment.

2.3.4. Tobacco infiltration

20 ml YEB medium were inoculated with *Agrobacterium tumefaciens* containing the desired construct and incubated overnight at 28°C and 220 rpm. After pelletizing for 10 min at 3200g cells were resuspended in 3 ml 1x Agro-Mix (For 10x Agro-Mix: 100 mM MgCl₂, 100 mM MES, dissolved in ddH₂O, adjusted to pH 5.6, autoclaved for 20 min at 121°C, stored at room temperature; for fresh 1x Agro-Mix: 9% 10x Agromix, 1% acetosyringone (3 mg/l in 100% EtOH), 90% ddH₂O). All constructs were adjusted to an OD₆₀₀ between 0.7-0.8. Samples were mixed in the desired combination in a 1:1 ratio and incubated at room temperature for 2-6 h. Subsequently, the abaxial sides of at least two leaves of *Nicotiana benthamiana* plants were infiltrated per combination.

2.3.5. Particle bombardment

400 ng DNA, 5 µl gold (30 mg/ml), 10 µl CaCl₂ (2.5 M), and 4 µl spermidine (0.1 M) were mixed and incubated for 10 min at room temperature. Samples were washed by 10-sec centrifugation steps at 9.300g and resuspended with 100 µl 70% ethanol, 50 µl 100% ethanol, and 12 µl 100% ethanol. DNA-coated gold was transferred onto a macrocarrier. After evaporation, the macrocarrier and rupture disc (650 psi) were placed into the Biolistic Particle Delivery System (PDS-1000/He, BioRad). Bombardments were performed on epidermal leek cells with a vacuum of 26 Hg (inch of mercury, equivalent to 3.38 Pa at 0°C). For transient transformation of Arabidopsis rosette leaves, DNA, gold, CaCl₂ and spermidine amounts were doubled, and 900 psi rupture discs were used. Samples were incubated in darkness at room temperature overnight until further investigation.

2.3.6. Blue light treatment

Tobacco leaves of *N. benthamiana* transiently expressing *p35S:YFP-LOV2-ODC-P2A-RFP-HA-NLS* or *p35S:YFP-LOV2-P2A-RFP-HA-NLS* were placed on agar plates and halfway covered with aluminum foil. Leaves were exposed to blue light (450-495 nm; 30 $\mu\text{mol m}^{-2} \text{s}^{-1}$) for 4 h and imaged by CLSM afterwards.

2.3.7. Leaf dissection

200-400 μm sized leaves with on-going trichome patterning need to be dissected from the whole plant, to enable imaging. Therefore, seedlings with two visible true leaves were selected, and cotyledons and the first two leaves were removed with a cannula. Leaves three to five were carefully dissected and put on a slide with a drop of 1% agarose. They were coated with a drop of 50% glycerin and a cover slip.

2.3.8. Transformation of dark-grown Arabidopsis cell culture

15 ml overnight culture of *Agrobacterium tumefaciens* carrying the desired construct were pelletized by centrifugation for 15 min at 3200g and resuspended in 5 ml AT medium (0.44% MS (Murashige and Skoog), 1.5% sucrose, 0.2% Gamborg B5 vitamin solution (Sigma-Aldrich), 0.025% 2,4-D, dissolved in ddH₂O, adjusted to pH 5.8 (KOH), autoclaved for 20 min at 121°C, stored at 4°C). When a cell culture was transformed with more than one construct, the samples were adjusted to the lowest OD₆₀₀ to achieve an equimolar ratio. 200 ml of cell culture were transformed with 100 μl agrobacteria. Flasks were closed and incubated in darkness for 5 days at 100 rpm before harvesting.

2.3.9. β -Glucuronidase (GUS) assay

To analyze a promoter expression in plant tissues, the GUS reporter system was applied. Therefore, leaves or entire plants were transferred into reaction tubes and covered with GUS staining solution (50 mM NaPO₄ (pH 7.2), 2 mM K-FerroCyanid, 2 mM K-FerriCyanid, 0.2% Triton X-100, 2 mM X-Gluc, dissolved in ddH₂O, stored at 4°C in darkness). Incubation took place between 0.5 h and 24 h at 37°C. The solution was replaced by 70% ethanol to remove the chlorophyll, followed by decreasing ethanol steps to restore the hydrostatic pressure.

2.4. Protein techniques

2.4.1. Western blot

This semi-dry immunoblotting technique was applied to detect target proteins from plant extracts by a specific antibody staining.

Protein extraction

- Tobacco: Three days after infiltration, fluorescent tobacco leaves were harvested and immediately frozen in liquid nitrogen. Leaf material was homogenized using a TissueLyser (Qiagen) at 30 Hz for 90 sec. Per 50 mg leaf, 100 μ l lysis buffer (150 mM NaCl, 1% Triton X-100, 50 mM Tris (HCl pH 8.0), 0.1% SDS, dissolved in ddH₂O, stored at 4°C; for fresh buffer: add 10 mM DTT and 1x Complete Protease Inhibitor Cocktail (Roche)) were added, incubated for 30 min on ice, and additionally homogenized with a drill (IKA RW 16 basic) for 1 min. After centrifugation for 15 min at 4°C at 16,100g, the supernatant was mixed with 6x protein sample buffer (0.375 M Tris (HCl pH 6.8), 12% SDS, 60% glycerol, 0.6 M DTT, 0.06% bromphenol blue, dissolved in ddH₂O, stored at -20°C), and denatured for 10 min at 95°C.
- Cell culture: 2 ml of the Arabidopsis cell culture were centrifuged for 5 min at 4°C at 11,000g. The pellet was frozen in liquid nitrogen. After adding 500 μ l 6x protein sample buffer, the cells were homogenized by a drill for 1 min and denatured for 10 min at 95°C.

Immunoblotting assay

10 μ l of each protein sample and 5 μ l PageRulerTM Prestained Protein Ladder (10 to 180 kDa, ThermoFisher Scientific) were loaded on an 8% SDS-PAGE (For one separation gel, load directly: 2.3 ml ddH₂O, 1.3 ml 30% acrylamide mix (Rotiphorese Gel 30; Roth), 1.3 ml 1.5 M Tris/HCl (pH 8.8), 50 μ l 10% SDS, 50 μ l 10% ammonium persulfate (APS), 3 μ l tetramethylethylenediamine (TEMED). After polymerization, mix one stacking gel, loaded directly: 0.68 ml ddH₂O, 0.17 ml 30% acrylamide mix, 0.13 ml 1.5 M Tris/HCl (pH 6.8), 10 μ l 10% SDS, 10 μ l 10% APS, 1 μ l TEMED). Protein separation was achieved with 20 mA per gel in chambers containing running buffer (25 mM Tris, 250 mM glycine, 0.1% SDS, dissolved in ddH₂O, stored at room temperature). Semi-dry protein transfer was performed on a PVDF membrane for 17 h at 4°C, which was placed between two Whatman papers, each saturated with anode or cathode buffer (10% Roti-Blot 2A, 5% methanol, solved in ddH₂O; 10% Roti-Blot 2K,

20% methanol, solved in ddH₂O; stored at room temperature). The membrane was blocked by incubation for 1 h with 5% milk powder solved in 1x PBS-T (For 10x PBS: 137 mM NaCl, 2.7 mM KCl, 10 mM Na₂HPO₄, 2 mM KH₂PO₄, dissolved in ddH₂O, adjusted to pH 7.4, stored at room temperature; for 1x PBS-T, 9.9% 10x PBS, 0.1% Tween 20, 90% ddH₂O). α -GFP (mouse, 1:2000 in 1x PBS-T with 5% milk powder, Sucofin) primary antibody was used for YFP and mTurquoise2 detection, α -RFP (rat, 1:2000 in 1x PBS-T with 5% milk powder) primary antibody for RFP detection. The corresponding secondary antibody (1:5000 mouse; 1:10,000 rat) was diluted in 1x PBS-T. Each antibody incubation persisted for 1 h. Membranes were washed in between with 25 ml 1x PBS-T for 5 min. Blocking, antibody incubation, and washing were performed on rolls at room temperature. Protein bands were detected using the SuperSignal™ West Femto Maximum Sensitivity Substrate (ThermoFisher Scientific) and the ImageQuant LAS-4000 (GE Healthcare) detection system.

2.5. Microscopic techniques

2.5.1. Stereo and fluorescence microscopy

Leica MZ 16F, equipped with the LAS V3 software, was used for stereo and fluorescence microscopic work.

2.5.2. Confocal laser scanning microscopy

Confocal laser scanning microscopy (CLSM) was used to generate sharp images of the entire section of interest. Only wavelength-specific fluorescent signals within the focal plane are detected. CLSM was carried out using the Leica TCS SP8 LAS X Version 3.5.7 or the Leica TSC SPE microscope equipped with the Leica LAS AF version 2.6.0 software. Table 12 shows the adjusted excitation and detection wavelengths.

Table 12: Excitation lines and detection ranges.

Excitation line [nm]				
CFP 405	mTurquoise2 458	YFP 488	RFP 561	mCherry 561
Emission spectra [nm]				
CFP 462-481	mTurquoise2 469-486	YFP 511-550	RFP 570-602	mCherry 603-630

2.6. *In silico* techniques

2.6.1. Compiling *GLI* synteny

A. thaliana was used as a reference to elaborate the synteny of *GLI*, comparing it with *A. alpina* and *C. hirsuta*. The *AtGLI* sequence was used to perform a BLAST search against the *C. hirsuta* CDS database (http://bioinfo.mpipz.mpg.de/blast/cgi-bin/public_blast_cs.cgi). More than a dozen loci spanning the first three highest-ranked genes were blasted against *A. thaliana*. The *AaGLI* ortholog and its adjoining genes were identified using the 1x1 orthologs table from the *Arabidopsis alpina* website (http://www.arabis-alpina.org/data/ArabidopsisAlpina/data/Aa_At_ortho_1x1.txt).

2.6.2. Calculation of protein stability in ratiometric approach

Mean gray values for each channel were measured using ImageJ based on CLSM images. Depending on the experiment, YFP/RFP, YFP/mCherry, or mTurquoise2/YFP ratios were determined. Values were normalized to the respective control data set (CFP without protein tag, mCherry without MYC1 tag, or overall mCherry values). In the case of variance homogeneity and normal distribution, the significance tests were conducted using a one-way ANOVA. Otherwise, a Mann-Whitney U test was performed.

2.6.3. Calculation of fluctuation

Temporal fluctuation

Two CLSM images were acquired for each selected time point (before, 0 h, 3 h and 6 h after conversion). Mean gray values were measured using ImageJ and the mean of both values per time point was used for further calculations. Values were normalized to an overall mean of 3 h and 6 h. Pearson's and Spearman's correlation were calculated using Origin.

Spatial fluctuation

Root tips and hypocotyl were imaged via CLSM. Mean gray values of the fluorescence intensities of each nucleus were measured with ImageJ. YFP and CFP values were normalized to the corresponding mean of all data points per biological replicate. Pearson's and Spearman's correlation were calculated using Origin. Due to variance inhomogeneity, significance tests were conducted with a Kolmogorov-Smirnov test.

2.6.4. Calculation of promoter expression

Well-visible trichomes of CLSM images were selected and assigned to a developmental stage. Leaf-wise, mean intensity values of each developmental stage were normalized to the youngest class, emerging trichomes (category 1). The values of each category were averaged over all leaves, and the standard deviation was calculated based on the sum of the square of variation using the formula

$$\sqrt{\frac{1}{n} \sum_{i=1}^n (x_i - \bar{x})^2}.$$

Due to variance inhomogeneity, significance tests were conducted with a Mann-Whitney U test.

3. Results

This study deals with the cross-regulatory interactions of the conserved *TTG1*-dependent network, focusing on the initiation and development of trichome patterning in *Arabidopsis thaliana*. This complex network regulates five different traits in *Arabidopsis*. Among these, trichome patterning is of particular interest, as its manipulation produces easily recognizable phenotypes which do not severely influence plant development. The network is regulated by different gene classes: R2R3 MYB, bHLH, and WD40 factors represent the activators, promoting trichome initiation; while R3 MYB transcription factors were identified as inhibitors, repressing a trichome cell fate. Only an accurate and precise interplay of all involved factors enables a highly reproducible, regularly distributed trichome pattern on rosette leaves. Although this topic has been explored for decades, many aspects of the underlying mechanism are still elusive.

To unravel the *TTG1* machinery in more detail, several experiments were designed on both the transcriptional and translational levels. The obtained results are divided into several topics and briefly depicted in the following: First, a temporal and spatial analysis of gene fluctuation in different *Arabidopsis* tissues was conducted, elucidating the primary source of noisy gene expression. Next, protein stability was addressed using a newly established ratiometric measuring approach, to analyze the stabilization behavior of two protein families quantitatively. The following chapter deals with the expression pattern of *MYC1* and its influence on the trichome pattern. Additionally, the expression strength of further patterning genes was studied in different developmental trichome stages. The last part captures an extensive systematical transcriptional analysis of 15 trichome patterning genes in a multitude of *Arabidopsis* mutants and compares the gene expressions with two related Brassicaceae species.

3.1. Gene fluctuation in *A. thaliana*

Fluctuation, also known as noise, describes the variability in gene expression within supposedly identical cell populations (Raser & O'Shea, 2005). Already first mathematical modeling approaches of the activator-inhibitor model have shown that *de novo* patterning processes, such as trichome and root hair formation, require gene fluctuation (Koch & Meinhardt, 1994; Meinhardt & Gierer, 1974; 2000) and that it accounts for about half of the regulatory processes during trichome development

(Greese et al., 2012). Therefore, it is worth getting a closer look at the impact of noisy gene expression in the plant system.

Gene fluctuation can be split into extrinsic and intrinsic noise. The first depicts global effects such as differences in cell size, number of metabolites, ribosomes, or polymerases, whereas the latter is characterized by molecular mechanisms such as differences in transcription factor binding (Elowitz et al., 2002). Although the processes of plant development are well-coordinated, stochasticity occurs and is needed to break the homogeneity for cell specification and pattern formation (Hong et al., 2016; Raj & van Oudenaarden, 2008). This means that slight differences in transcriptional and translation regulation are required to circumvent the similarity of genetically identical cells and to precisely reproduce tissues and organs. Before Schultheiß Araújo and colleagues in 2017 analyzed gene fluctuation in whole plant tissues (Schultheiß Araújo et al., 2017), it was only described in non-plant single-cell systems and human tissue culture (Dar et al., 2012; Elowitz et al., 2002; Newman et al., 2006; Taniguchi et al., 2010).

In this chapter, examples of temporal fluctuation and extrinsic and intrinsic noise are shown. Further analyses were published by Schultheiß Araújo and co-workers in 2017 (Schultheiß Araújo et al., 2017).

3.1.1. Protein expression fluctuates over time

Until Schultheiß Araújo and co-workers described fluctuation in plant tissue, noisy gene expression has only been studied in single-cell systems (Dar et al., 2012; Elowitz et al., 2002; Newman et al., 2006; Taniguchi et al., 2010). To enable measurements in a non-equilibrated environment, the photoconvertible Kikume green red (KikGR) protein was chosen. After illumination with 405 nm, KikGR is irreversibly converted from a green (KikG) to a red fluorescent state (KikR; Tsutsui et al., 2005). In order to measure temporal fluctuation in an entire tissue, *A. thaliana* rosette leaves stably expressing *p35S:NLS-KikGR* were dissected, and changes in protein levels were recorded in 3 h intervals by CLSM. Through photoconversion, all existing proteins are converted to their red state and the newly occurring green signals equal newly produced protein. To exclude movement into neighboring cells, the tetrameric Kikume version was used. An NLS sequence was linked to the fluorescent protein to achieve accurate measurements of each cell nucleus of the leaf. The fusion construct was driven by the constitutively active 35S promoter, ensuring high expression rates (Munsky et al., 2012). This

promoter limits conclusions due to its constitutively active nature, but since theoretical analyses showed that constitutive promoters generate low degrees of intrinsic noise, the results rather underestimate the natural situation (Elowitz et al., 2002).

Each examined leaf was scanned twice before (pre) and after (0 h, 3 h, 6 h) conversion (Figure 4A), and the average was used for calculating the temporal gene expression. The analysis of nascent KikG proteins revealed a positive correlation between the two time points, but efficiencies were constantly below a perfect match of 1 (Figure 4B, C; Figure S4). This means that noisy gene expression could indeed be detected, and distinct cells of a coherent tissue fluctuate over time.

These results were confirmed in further experiments using the *UBIQUITIN 10* (*UBQ10*) promoter and plants which were previously kept in darkness for 36 h to minimize already converted red NLS-KikR protein (Schultheiß Araújo et al., 2017).

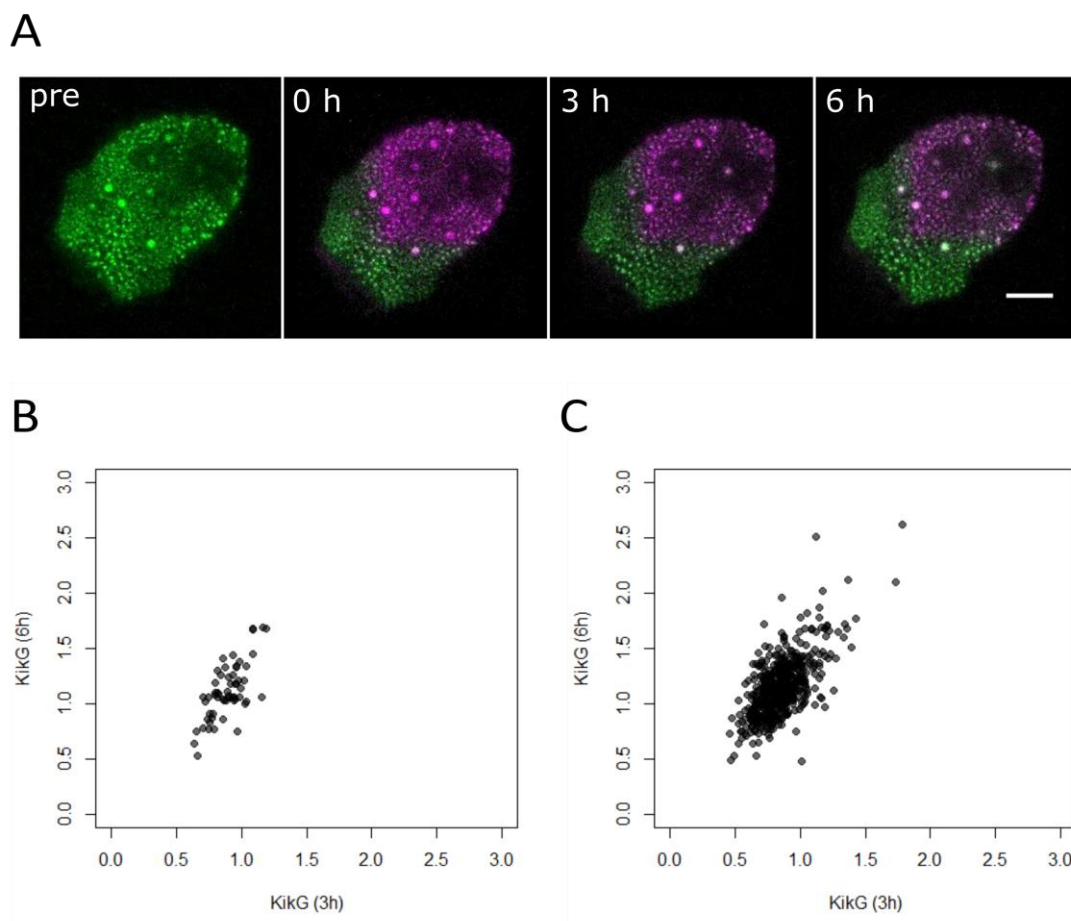


Figure 4: Analysis of temporal fluctuation in stable Arabidopsis *p35S:NLS-KikGR* lines. **A)** CLSM overlay images of one Arabidopsis leaf expressing *p35S:NLS-KikGR* before (pre) and after (0 h, 3 h, 6 h) conversion. KikG is illustrated in green, KikR in magenta. Scale bar indicates 50 μm . **B)** Scatter plot of the nuclei of one representative leaf expressing *p35S:NLS-KikG* ($n = 58$; Pearson's correlation $r = 0.71$, Spearman's correlation $r = 0.60$). **C)** Scatter plot of nuclei cumulating all leaves expressing *p35S:NLS-KikG* ($n = 484$; Pearson's correlation $r = 0.65$, Spearman's correlation $r = 0.57$).

3.1.2. Extrinsic noise is the primary source of fluctuation in root tips and hypocotyls

In order to spatially differentiate between extrinsic and intrinsic noise, a dual reporter system was utilized. *A. thaliana* was transformed with *p35S:2xNLS-YFP* and *p35S:2xNLS-CFP*, generating transgenic plant lines expressing both constructs simultaneously. The double nuclear localization signal (2xNLS) reduces intracellular mobility and enables accurate measurements in a defined compartment. If only extrinsic noise exists, both markers, YFP and CFP, will be expressed in perfect correlation. Single cells of a tissue will differentiate in the absolute amount of the fluorophores, but their ratio would stay constant. In intrinsic noise, the expression of YFP and CFP gets uncorrelated because of different copy numbers within a cell, leading to a field of varying fluorophore proportions. In short: if both markers correlate in the same cell, extrinsic noise is detected. Otherwise, intrinsic noise is observed. Figure 5 presents the dual reporter analysis in root tips and hypocotyls.

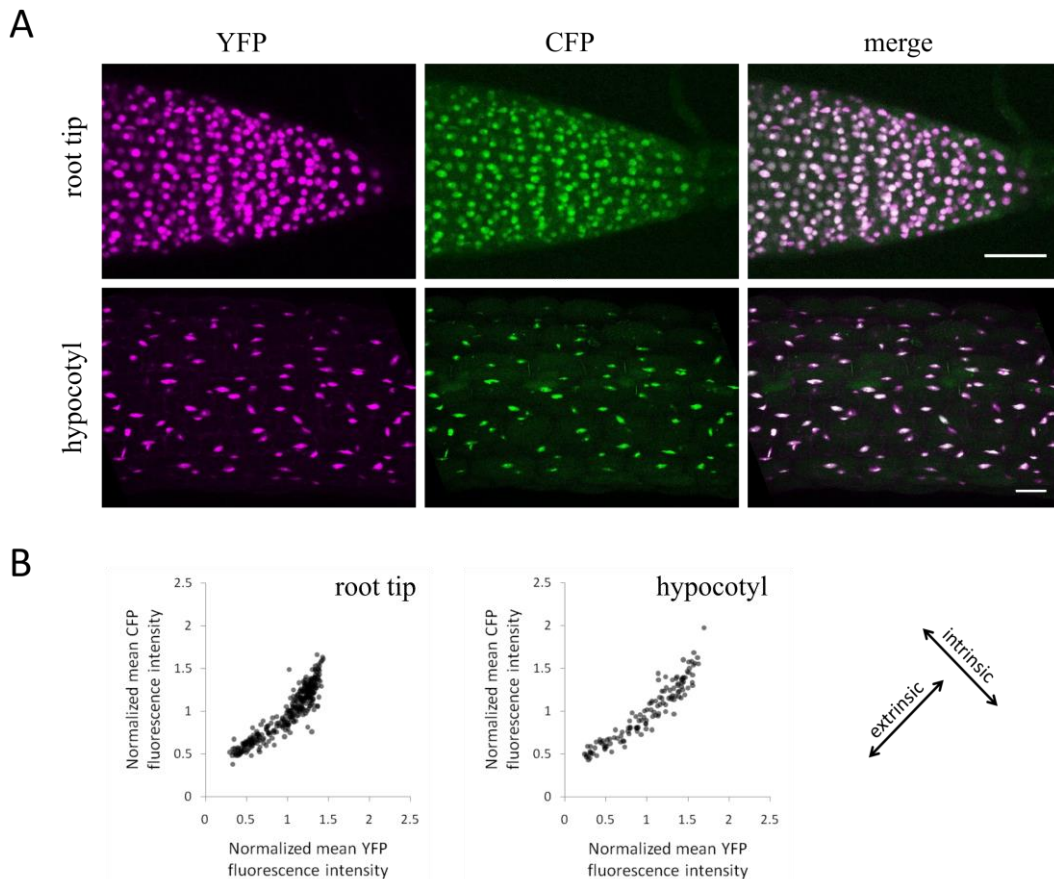


Figure 5: Extrinsic and intrinsic noise in root tip and hypocotyl in *p35S:2xNLS-YFP p35S:2xNLS-CFP* plants. A) CLSM images of a root tip and a hypocotyl stably transformed with *p35S:2xNLS-YFP p35S:2xNLS-CFP*. Scale bar indicates 100 μm . B) Scatter plot of the normalized mean YFP fluorescence intensity against the normalized mean CFP fluorescence intensity of single cells of one representative root tip and hypocotyl. YFP and CFP signal intensities do not differ significantly (Kolmogorov-Smirnov test $p > 0.05$). Root tip: Pearson's correlation $r = 0.922$, Spearman's correlation $r = 0.916$, $n = 328$; hypocotyl: Pearson's correlation $r = 0.942$, Spearman's correlation $r = 0.955$, $n = 129$. Extrinsic noise extends at a 45° angle between the x- and y-axis; intrinsic noise perpendicular to it.

CLSM images illustrate strong YFP (magenta) and CFP (green) signals in both tissues. On the one hand, white-appearing co-expression is recognizable in the overlay channel, suggesting extrinsic noise. On the other hand, single magenta and green-colored nuclei can be identified, indicating intrinsic noise (Figure 5A). Plotting the mean YFP fluorescence intensity against the mean CFP values reveals higher extrinsic (3.5-fold) than intrinsic noise in both tissues (Figure 5B). Hence, extrinsic noise is the primary source for gene fluctuation in root tips and hypocotyls.

3.2. Protein stability of trichome patterning genes

Besides gene fluctuation as part of regular pattern formation, protein concentrations decide the final cell fate. Protein levels are affected by the processes of protein production, stability, and degradation. To shed light on the mutual stabilizing characteristics of the different trichome protein families, the viral 2A reporter system was employed (Ryan et al., 1991). It was utilized to co-express members of different protein classes in an equimolar ratio and to compare their individual influence.

When starting the work on this ratiometric reporter system, little was known about the best 2A peptide for *in vivo* plant experiments. Kim and colleagues concluded that P2A performed best (Kim et al., 2011) and F2A was the only peptide tested in plants at that point (Samalova et al., 2006). In a first step, the cleavage efficiency of P2A and F2A was determined in different plant organisms by Ilka Schultheiß Araújo. She could qualitatively and quantitatively demonstrate that the P2A peptide possessed the higher cleavage efficiency upon transient expressions in leek and tobacco cells, and in Western blot analyses (Figure S5; Schultheiß Araújo, unpublished).

3.2.1. Proof of concept

The multicistronic 2A system enables the measurement of protein stabilities *in vivo* in a temporal or spatial manner. Towards this end, YFP was fused to the protein of interest and linked to the P2A sequence, followed by a fluorescent marker protein (RFP-HA-NLS). This fluorescently labeled marker protein is independent of stability changes of the protein of interest (Matz et al., 1999) and used as reference when calculating the protein stability. The ratio between the protein of interest and the reference marker determines the protein stability quantitatively. Initially, the protein of interest and the reference occur in equimolar rates. If the protein of interest is stabilized, the ratio shifts

in favor of this protein and gets higher. In turn, if the amount of the protein of interest decreases, the ratio gets smaller due to the constant reference protein.

As a proof of concept, the light-perceiving module light oxygen voltage (LOV2) and the murine ornithine decarboxylase (ODC) were utilized. LOV2 describes a light-reactive domain of the Arabidopsis photoreceptor phototropin 1 (Christie et al., 1999) and causes conformational changes upon blue light treatment. These, in turn, activate the ODC cassette, mediating ubiquitin-independent proteasomal degradation of the fusion protein (Renicke et al., 2013). Following an efficient cleavage of the P2A peptide, the marker expression is expected to be unaffected under blue light and control darkness conditions because it is uncoupled from the ODC degradation sensor. A degradation of LOV2-ODC is only assumed upon irradiation with blue light but not in darkness since LOV2 undergoes no conformational change without induction.

To test this theory, the blue light-sensitive *p35S:YFP-LOV2-ODC-P2A-RFP-HA-NLS* and as control *p35S:YFP-LOV2-P2A-RFP-HA-NLS* were transiently expressed in tobacco leaf cells and the YFP/RFP ratio was calculated. Comparable RFP intensities were visible under all tested conditions. YFP-LOV2-ODC levels were clearly reduced upon blue light exposure, whereas YFP-LOV2 remained similar to the darkness sample (Figure 6A). Quantification revealed a significant degradation of LOV2-ODC when treated with blue light ($p < 4 \cdot 10^{-4}$). No significant alteration was determined for the LOV2 control construct under blue light or darkness ($p < 0.35$; Figure 6B). All findings were verified in an additional independent experiment (Figure S6).

Hence, the P2A ratiometric reporter system can be utilized for plant-specific protein stability measurements *in vivo*.

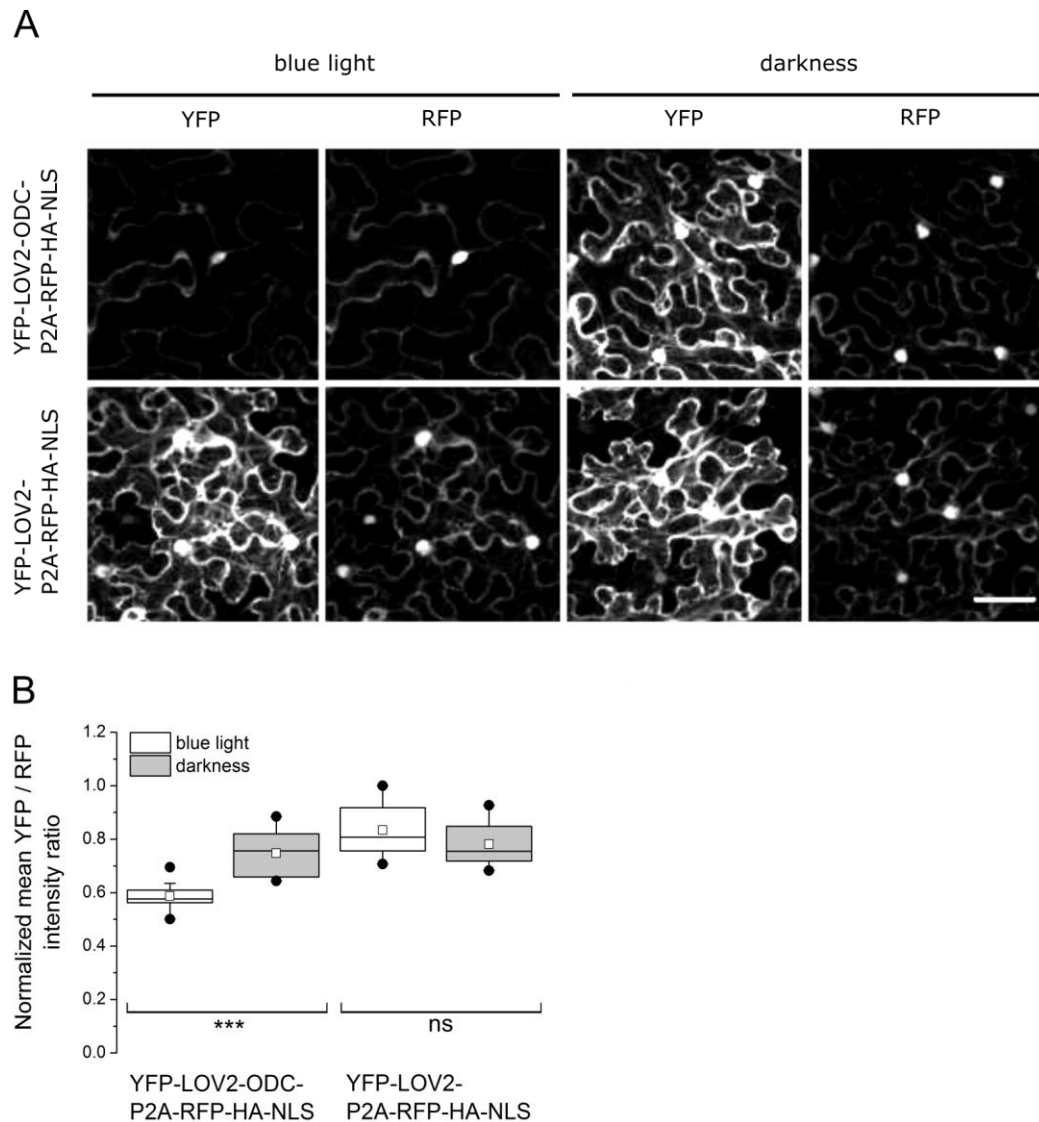


Figure 6: Blue light inducible degradation of LOV2-ODC. **A)** CLSM images of tobacco leaves transiently expressing YFP-LOV2-ODC-P2A-RFP-HA-NLS (upper row) or YFP-LOV2-P2A-RFP-HA-NLS (lower row). The first two columns on the left side illustrate the YFP and RFP channel (gray values) for cells treated with blue light, the two columns on the right the YFP and RFP channel (gray values) for cells kept in the dark, respectively. Images were taken sequentially using Leica TSC SPE with a format of 1024 x 1024 pixels. Scale bar: 50 μ m. **B)** Box plot analysis of the YFP / RFP fluorescence intensity ratio between blue light and dark exposed samples of YFP-LOV2-ODC-P2A-RFP-HA-NLS and YFP-LOV2-P2A-RFP-HA-NLS. LOV2-ODC irradiated with blue light ($n = 8$, median = 0.58) differed significantly from dark kept samples ($n = 10$, median = 0.76; One-way ANOVA $p < 4 \cdot 10^{-4}$). LOV2 did not differ significantly under blue light ($n = 8$, median = 0.81) or darkness conditions ($n = 6$, median = 0.76; One-way ANOVA $p < 0.35$). Mean intensity values were measured using 366 x 366 μ m² CLSM images comprising several cells and normalized to the maximum value. Boxes show median, 0.25 and 0.75 quartiles. Dots indicate 1% and 99% percentiles, rectangles represent mean values.

3.2.2. bHLH proteins are capable to stabilize MYB proteins

MYB and bHLH proteins represent central components in trichome patterning and other traits (Gonzalez et al., 2008; Simon et al., 2007) and are known to physically interact with each other (Payne et al., 2000; Zimmermann et al., 2004). MYB proteins comprise R2R3 and R3 single repeat proteins, which compete for binding to bHLH factors (Esch et al., 2003; Pesch et al., 2015; Schellmann et al., 2002). Protein stability is suggested to

be an essential regulatory factor by experimental work (Bouyer et al., 2008; Tominaga-Wada & Wada, 2017) as well as an essential parameter in pattern formation by theoretical consideration (Bouyer et al., 2008; Digiuni et al., 2008).

Here, the influence of the bHLH proteins MYC1 and GL3 on stabilizing the MYB proteins GL1, TRY, and CPC was investigated with the P2A ratiometric reporter system (Figure 7A). To achieve this, *p35S:YFP-[MYB]-P2A-RFP-HA-NLS* was co-expressed with *p35S:CFP-[bHLH]* in transiently transformed epidermal leek cells.

First, the protein localizations of the different construct combinations were studied based on CLSM images (Figure 7B-D). As expected, the RFP-HA-NLS reference constantly localized in the nucleus and the unfused control of free CFP was cytoplasmic. The localization of the YFP-MYB protein varied depending on the CFP-bHLH construct. YFP-GL1 alone was mainly found in the nucleus. Also the co-expression with CFP-GL3 caused a nuclear localization, whereas YFP-GL1 was trapped to the cytoplasm when co-expressed with CFP-MYC1. Without co-expression, YFP-TRY was localized in the cytoplasm. Together with CFP-MYC1 or CFP-GL3, it was found in the nucleus. YFP-CPC alone and with both CFP-bHLH co-expression was constantly localized in the nucleus. All observations reflected the expected localizations of cleaved P2A constructs and are in line with previous results (Pesch et al., 2013).

Second, the ratio between the YFP-tagged MYB protein to the reference marker RFP-NLS was calculated when co-expressed with or without a bHLH protein. In all examined cases, a constant significant stabilization of the MYB factor was found in the presence of a bHLH protein compared to the control. The influence of the bHLH proteins on the R2R3 MYB activator GL1 revealed a significant stabilization of YFP-GL1 when co-expressed with CFP-MYC1 or CFP-GL3 compared to the unfused CFP w/o control ($p < 1 \cdot 10^{-4}$ and $p < 5 \cdot 10^{-7}$; Figure 7E). Similar results were gained for the R3 MYB inhibitors TRY and CPC. The quantification of YFP-TRY showed a significant stabilization in the presence of CFP-MYC1 and CFP-GL3 in contrast to the control ($p < 2 \cdot 10^{-8}$ and $p < 9 \cdot 10^{-9}$; Figure 7F). YFP-CPC was also significantly stabilized upon the co-expression of CFP-MYC1 and CFP-GL3 compared to CFP alone ($p < 5 \cdot 10^{-8}$ and $p < 1 \cdot 10^{-5}$; Figure 7G). These findings were confirmed independently in tobacco leaves as well as with 2xNLS-mCherry as a different reference marker in leek (Figure S7) and tobacco cells (Schultheiß Araújo, unpublished). Taken together, the presence of bHLH proteins positively influences the stability of activators and inhibitors of the MYB family *in vivo*.

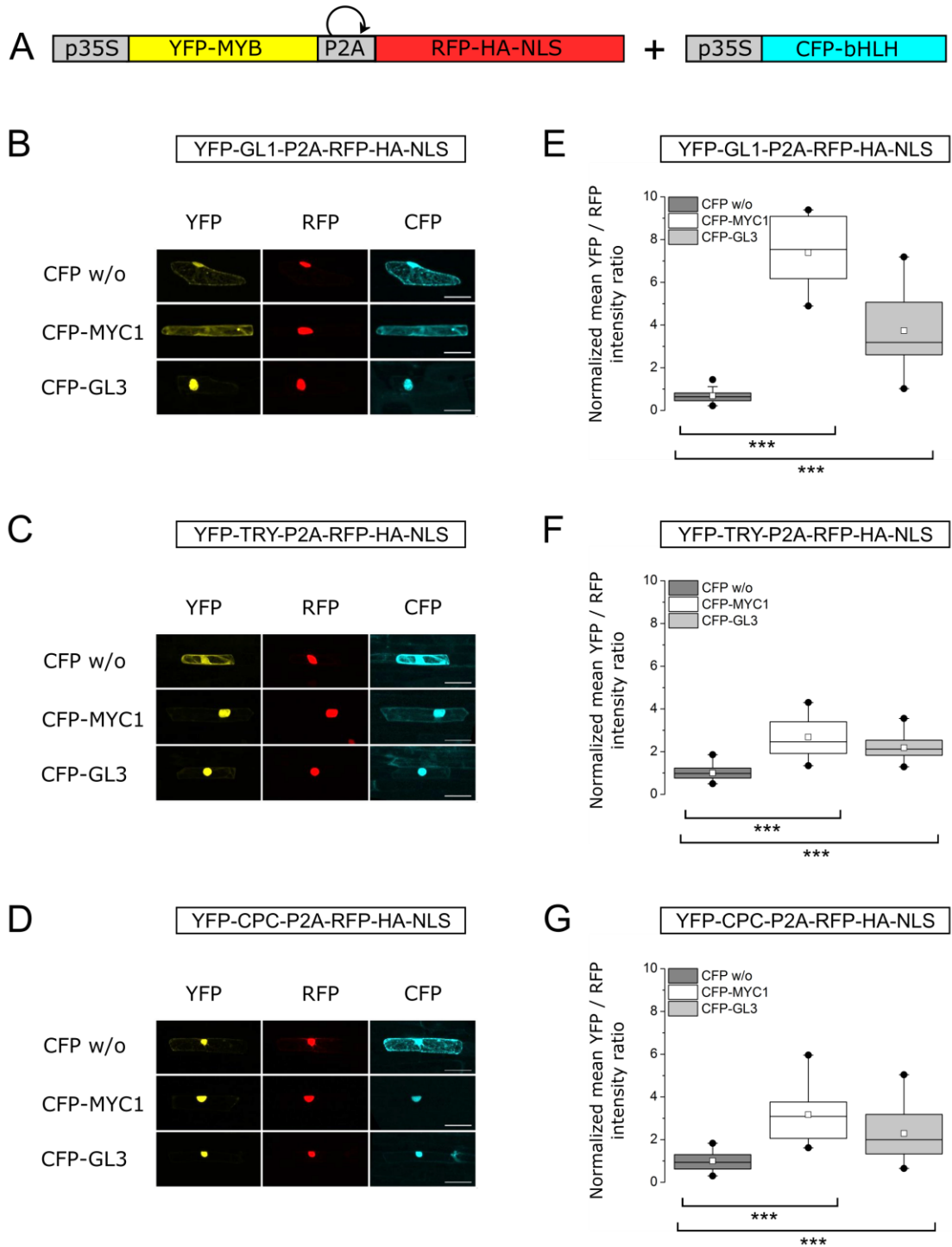


Figure 7: MYB proteins stabilized by bHLH proteins. **A**) Schematic illustration of the used P2A construct. **B - D**) CLSM images of YFP-MYB-P2A-RFP-HA-NLS expression in epidermal leek cells transiently transformed with CFP w/o, CFP-MYC1 or CFP-GL3. Images were taken sequentially using Leica TSC SPE with a format of 1024 x 1024 pixels. Scale bars indicate 50 μ m. **E - G**) Box plot analyses of YFP-MYB-P2A-RFP-HA-NLS co-expressed with CFP w/o, CFP-MYC1 or CFP-GL3. **E**) YFP-GL1 was significantly stabilized when co-transformed with CFP-MYC1 ($n = 9$, median = 7.54, Mann-Whitney U test $p < 1 \cdot 10^{-4}$) or CFP-GL3 ($n = 36$, median = 3.19, Mann-Whitney U test $p < 5 \cdot 10^{-7}$) compared to the CFP w/o control ($n = 12$, median = 0.64). **F**) YFP-TRY was significantly stabilized when co-expressed with CFP-MYC1 ($n = 19$, median = 2.46, Mann-Whitney U test $p < 2 \cdot 10^{-8}$) or CFP-GL3 ($n = 22$, median = 2.12, Mann-Whitney U test $p < 9 \cdot 10^{-9}$) compared to CFP w/o ($n = 29$, median = 0.98). **G**) YFP-CPC was significantly stabilized when co-transformed with CFP-MYC1 ($n = 19$, median = 3.08, Mann-Whitney U test $p < 5 \cdot 10^{-8}$) or CFP-GL3 ($n = 28$, median = 2.00, Mann-Whitney U test $p < 1 \cdot 10^{-5}$) compared to the CFP w/o control ($n = 26$, median = 0.94). Mean intensity values were normalized to the mean of the CFP w/o control. Boxes show median, 0.25 and 0.75 quartiles. Dots indicate 1% and 99% percentiles, rectangles represent mean values.

3.2.3. Dosage-dependent stabilization of TRY by MYC1

In chapter 3.2.2, it was shown that bHLH proteins are capable to stabilize MYB proteins. This finding raised the question of whether this effect is dosage-dependent. To answer this, constructs containing two P2A sequences were generated. A version without MYC1 (*p35S:mTurquoise2-TRY-P2A-YFP-P2A-mCherry*) was used as control. *p35S:mTurquoise2-TRY-P2A-YFP-P2A-mCherry-MYC1* served as singular MYC1 dosage and was enhanced by an additional plasmid carrying mCherry-MYC1 (*p35S:mCherry-MYC1*; Figure 8A).

To verify the correct cleavage of both P2A peptides within one construct in the first place, tobacco leaves and Arabidopsis dark-grown cell culture were transiently transformed with one or the other version. A signal of all three fluorophores was clearly detectable in the same cell (data not shown). Crude protein extracts were analyzed by Western blot to validate the predicted band size. A prominent band at about 30 kDa was observed, corresponding to the inner YFP cleavage product. Partially or uncleaved protein bands were not found (Figure S8), indicating a successful cleavage of both 2A peptides.

Next, the control construct, the singular MYC1-dosed version, and the enhanced variant were transiently expressed in epidermal leek cells (Figure 8B). This time, YFP was used as a reference marker to determine the mTurquoise2-TRY stability in dependence of the mCherry-MYC1 dosages or the control (Figure 8C). The quantification of the mTurquoise2/YFP ratio revealed a significant stabilization of mTurquoise2-TRY in the presence of single mCherry-MYC1 ($p < 5 \cdot 10^{-5}$). Adding the independent plasmid with *p35S:mCherry-MYC1*, thereby increasing the available MYC1 amount in the cell, likewise led to a significant stabilization of mTurquoise2-TRY ($p < 5 \cdot 10^{-9}$). This stabilization was even significantly higher than the singular mCherry-MYC1 expression ($p < 1 \cdot 10^{-7}$), suggesting a stabilizing effect of additional applying MYC1. In order to classify the correlation between TRY stability and MYC1 concentration, the mTurquoise2/YFP ratios were plotted against the mCherry-MYC1 signal intensities. A distinct relationship with a Pearson's correlation coefficient of 0.86 was detected (Figure 8D), indicating the concentration-dependent TRY stabilization by MYC1.

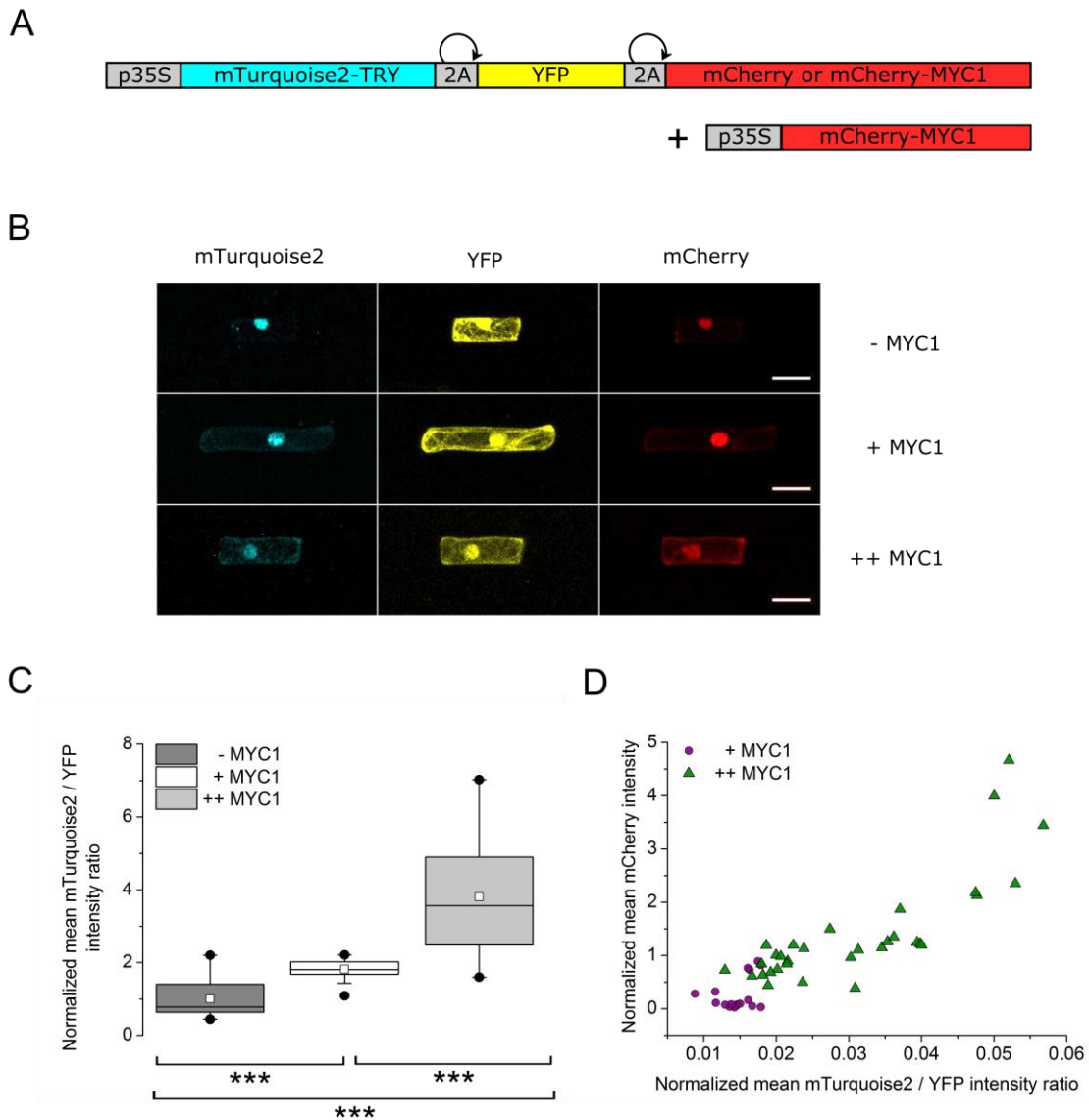


Figure 8: Concentration-dependent stabilization of TRY by MYC1. **A)** Schematic illustration of the construct with two P2A peptides. **B)** CLSM images of mTurquoise2-TRY-P2A-YFP-mCherry, mTurquoise2-TRY-P2A-YFP-mCherry-MYC1 and mTurquoise2-TRY-P2A-YFP-mCherry-MYC1 plus additional mCherry-MYC1 expression in transiently transformed epidermal leek cells. Scale bar indicates 50 μm . **C)** Box plot analysis of the used P2A construct in dependence of the MYC1 concentration. mCherry-MYC1 expression significantly stabilizes mTurquoise2-TRY ($n = 19$, median = 0.78, Mann-Whitney U test $p < 5 \cdot 10^{-5}$) and increases with higher mCherry-MYC1 concentration ($n = 17$, median = 1.80, Mann-Whitney U test $p < 5 \cdot 10^{-9}$) compared to the control as well as compared to one-time mCherry-MYC1 expression ($n = 32$, median = 2.48, Mann-Whitney U test $p < 1 \cdot 10^{-7}$). Mean intensity values were normalized to the mean expression without MYC1. Boxes show median, 0.25 and 0.75 quartiles. Dots indicate 1% and 99% percentiles, rectangles represent mean values. **D)** Dot plot of the correlation between the mTurquoise2 to YFP ratio against the mCherry intensity with one-time (+) or further increased (++) MYC1 concentration. Mean values were normalized to mCherry-MYC1. The additional expression of mCherry-MYC1 correlates strongly with higher mTurquoise2-TRY values (Pearson's correlation $r = 0.86$).

3.3. MYC1 - an outstanding trichome patterning gene

MYC1 is a fascinating, but often neglected gene in the trichome patterning machinery. It belongs to the bHLH family, although it is more distantly related than GL3 and EGL3 (Zhang, 2018). Since *myc1* mutants exhibit fewer trichomes than Col-0 wildtype, it is classified as a trichome-promoting factor (Symonds et al., 2011; Zhao et al., 2012). It is

known to interact with all central components of trichome formation such as the activators GL1/MYB23, GL3/EGL3, TTG1, as well as the inhibitors CPC and TRY (Tominaga et al., 2008; Zhao et al., 2012; Zimmermann et al., 2004). Interestingly, GL3 and EGL3 are able to rescue the *myc1* trichome phenotype, whereas MYC1 cannot substitute their function in *gl3* and *egl3* mutants (Pesch et al., 2013; Zhao et al., 2012). However, MYC1 is indeed able to partially restore the root hair and seed coat mucilage phenotype in *gl3 egl3 tt8* triple mutants (Zhang & Hülskamp, 2019), suggesting redundant yet divergent functions. Controversially discussed is the ability of MYC1 to form homo- and heterodimers. Yeast two-hybrid assays showed no dimerization (Zhao et al., 2012), whereas recent LUMIER assays revealed weak MYC1 homo- and heterodimers together with GL3 and EGL3 (Zhang, 2018). Another striking feature is the nuclear-cytoplasmic shuttling behavior of MYC1. Unbound, it is found predominantly in the cytoplasm, while TRY and CPC are localized in the cytoplasm and the nucleus. Upon co-expression with MYC1, both proteins are trapped in the nucleus. In contrast to that, nuclear localized GL1 is recruited to the cytoplasm when co-expressed with MYC1 (Pesch et al., 2013; Schultheiß, 2015). All these findings indicate not to underrate the impact of MYC1 on trichome patterning.

3.3.1. Comparison of MYC1 splicing variants

While looking for MYC1 sequence information, TAIR (<https://www.arabidopsis.org/>) recently revealed three different splicing variants, leading to the question of which one to choose. Version 1 consists of eight exons (2081 bp), version 2 of nine exons (1894 bp), and version 3 of seven exons (1670 bp). This is of higher relevance for experiments working with the CDS, such as restriction digests or the analysis of protein stabilities. Because the differences occur at the C-terminus, that part of the gene, including the 3'UTR of Col-0 leaf cDNA, was sequenced to compare the variants.

The results pointed out that only version 1 fits the sequence (Figure 9). Version 3 consists only of seven exons, and the sequence broke off exactly at the end of exon seven, where the splicing variant differs from the others. In contrast to version 1, version 2 comprises an additional ninth exon. However, the beginning of exon 9 did not match the sequencing results. Only version 1 reached a perfect consensus on the sequenced cDNA material. It might be possible that other variants predominate in other tissues or organs, but since the primarily investigated system, the trichome patterning

machinery, acts in the analyzed leaf material, version 1 was used as a template for further experiments.

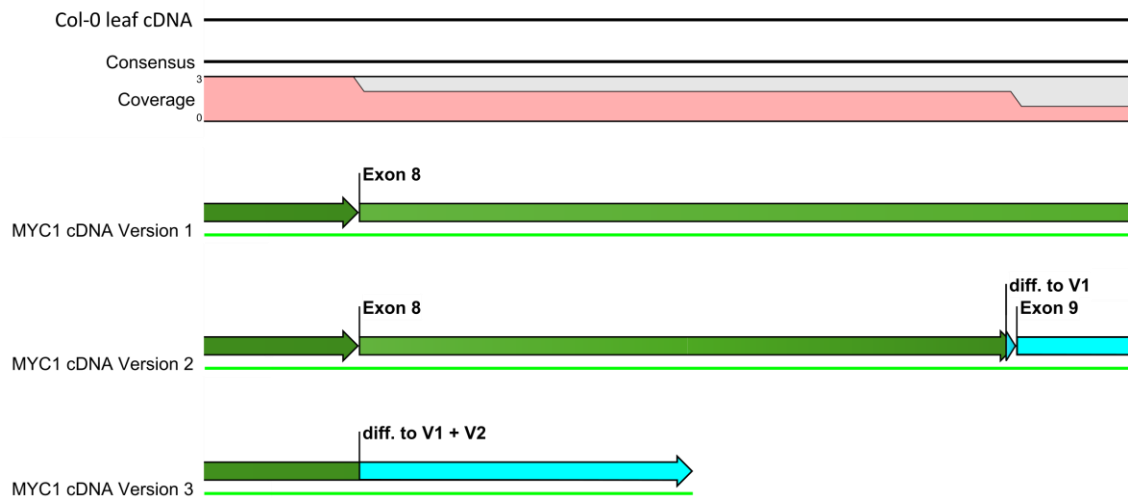


Figure 9: Comparison of MYC1 splicing variants. Sequencing results of version 1 (2081 bp), version 2 (1894 bp), and version 3 (1670 bp) against *A. thaliana* Col-0 leaf cDNA. Sequence similarities are illustrated in green, discrepancies in turquoise.

3.3.2. *pMYC1*_{1970 bp} is equally applicable as *pMYC1*_{2581 bp}

First, to elaborate *MYC1* in more detail, its promoter expression was on closer consideration. In lines stably expressing a 2.0 kb (1970 bp upstream of the transcription start site; TSS) *MYC1* promoter fragment fused to GUS, ubiquitously expression in young *Arabidopsis* leaves was detectable after GUS staining (Figure S9). This observation is contradictory to published *pMYC1:GUS* plants from Zhao and colleagues. They showed a distinct *pMYC1* expression in trichome socket cells, using a 2.6 kb (2581 bp upstream of the TSS) promoter (Zhao et al., 2012). However, this expression pattern could not be reproduced with their plants. Therefore, genetically stable *A. thaliana* plants were generated comparing both promoter regions. Each promoter fragment drives two NLS peptides and mCherry as a fluorescent tag (*pMYC1*_{1970 bp}:2xNLS-mCherry / *pMYC1*_{2581 bp}:2xNLS-mCherry), enabling the selection of single nuclei.

When analyzing these lines, the focus was on answering the following questions: At which developmental trichome stage is *MYC1* expression maximal? Is there expression in trichome surrounding cells? If so, where is the higher expression found: in trichomes or adjacent cells? Leaves stably expressing each construct were imaged by CLSM, and the signal intensity was measured for each nucleus. The nuclei were

classified into four categories according to their developmental stage. Category 0 reflects all epidermal cells which did not face a trichome cell fate, category 1 describes emerging trichomes, category 2 expanding trichomes, and category 3 branched trichomes (Figure 10A).

For both promoter fragments, the quantitative analysis of several stably transformed plants revealed striking differences between younger and older trichomes. The youngest, just emerging trichomes (category 1) showed a significantly higher expression of *pMYC1* compared to both, expanding and branched trichomes (category 2 and 3; Figure 10B, C). The shorter fragment revealed no differences between undifferentiated epidermal cells and the first trichome developmental stage (category 0 vs. 1). However, a differential expression was found for the longer version. Here, the youngest trichomes expressed significantly less *pMYC1* than non-specialized epidermal cells.

Another way to consider this data is to focus on trichomes of the same category and their adjacent epidermal cells (Figure 10D). The quantified fluorescence intensities of trichomes were correlated with the signal intensities of all epidermal cells in the first and second tiers around them. Epidermal cells which belonged to tiers of more than one trichome were excluded. For plants stably transformed with *pMYC1*_{1970 bp}:*2xNLS-mCherry*, the analysis revealed a significantly increased expression in the area around emerging trichomes (category 1) compared to expanding trichomes (category 2). In contrast, the expression in epidermal cells surrounding branched trichomes (category 3) was significantly reduced (Figure 10E). This indicates that the younger the trichome, the higher the expression of *MYC1* in adjacent cells. A slight, but significant difference between tier one and two was seen for expanding trichomes. The same behavior was observed for plants expressing *pMYC1*_{2581 bp}:*2xNLS-mCherry*, although there was almost no significant difference between expanding and branched trichomes (Figure 10F). In respect to Zhao et al., 2012, it was an important finding that the longer *pMYC1*_{2581 bp} is less expressed in the surrounding tiers than in the trichome cell itself (Figure 10E, F), as this is opposite to their published images. Taken together, one can state that both promoter variants exhibited a similar expression of *MYC1* and can be equally used for further studies.

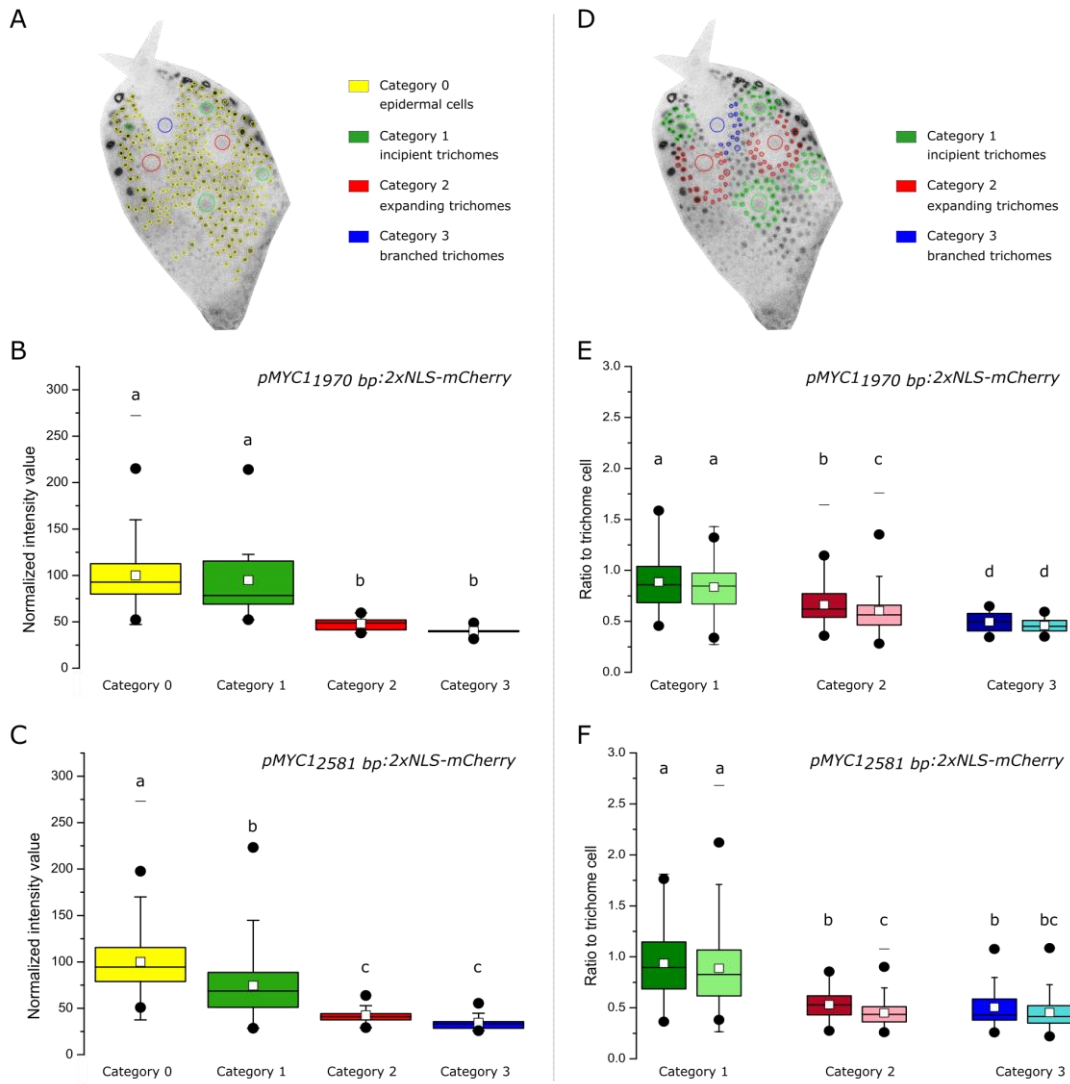


Figure 10: Comparative study of *pMYC11970 bp* and *pMYC12581 bp*. **A)** Epidermal cells and trichomes grouped by developmental stage. **B, C)** Quantitative analysis of Arabidopsis leaves stably transformed with either *pMYC11970 bp:2xNLS-mCherry* (**B**) or *pMYC12581 bp:2xNLS-mCherry* (**C**). Category 0 displays non-specialized epidermal cells, category 1 emerging trichomes, category 2 expanding trichomes and category 3 branched trichomes. Dunn test with Bonferroni adjustment. Same letters above the box plot indicate no significant difference. **B)** Category 0 did not differ significantly from category 1 ($p < 0.7$), but differed significantly from category 2 ($p < 4 * 10^{-11}$) and category 3 ($p < 8 * 10^{-5}$). Category 1 differed significantly from category 2 ($p < 4 * 10^{-4}$) and category 3 ($p < 9 * 10^{-3}$). Category 2 and 3 did not differ significantly ($p = 1$). **C)** Category 0 differed significantly from category 1 ($p < 3 * 10^{-8}$), category 2 ($p < 1 * 10^{-15}$) and category 3 ($p < 8 * 10^{-12}$). Category 1 differed significantly from category 2 ($p < 5 * 10^{-3}$) and category 3 ($p < 6 * 10^{-3}$). Category 2 and 3 did not differ significantly ($p = 1$). **D)** Trichomes and their surrounding epidermal cells marked by developmental stage. **E, F)** Quantitative analysis of expression intensities of trichome cells depending on their adjacent epidermal cells stably transformed with either *pMYC11970 bp:2xNLS-mCherry* (**E**) or *pMYC12581 bp:2xNLS-mCherry* (**F**). The left box plot of each category illustrates the first tier of epidermal cells surrounding a trichome, the right box plot the second tier. Emerging trichomes (category 1) and their first two tiers are colored in green, expanding trichomes (category 2) in red and branched trichomes (category 3) in blue. Dunn test with Bonferroni adjustment. Same letters above the box plot indicate no significant difference. **E)** The first tier of category 1 differed significantly from the ones of category 2 ($p < 3 * 10^{-7}$) and category 3 ($p < 2 * 10^{-9}$) and category 2 differed significantly from category 3 ($p < 2 * 10^{-3}$). The second tier of category 1 differed significantly from the ones of category 2 ($p < 8 * 10^{-14}$) and category 3 ($p < 2 * 10^{-13}$) and category 2 differed significantly from category 3 ($p < 1 * 10^{-3}$). Thereby, in category 2 first and second tier differed significantly from each other ($p < 0.022$). **F)** The first tier of category 1 differed significantly from the ones of category 2 ($p < 1 * 10^{-16}$) and category 3 ($p < 3 * 10^{-11}$) but category 2 did not differ significantly from category 3 ($p < 0.679$). The second tier of category 1 differed significantly from the ones of category 2 ($p < 1 * 10^{-36}$) and category 3 ($p < 1 * 10^{-17}$) but category 2 did not differ significantly from category 3 ($p = 1$). Thereby, in category 2 first and second tier differed significantly from each other ($p < 9 * 10^{-5}$).

3.3.3. Endogenous MYC1 is expressed in nucleus and cytoplasm

The intracellular shuttling behavior characterizes MYC1 as an exceptional trichome gene. Depending on the interaction partner, its localization varies between the nucleus and the cytoplasm (Pesch et al., 2013; Schultheiß, 2015). Initially, this property was observed in transgenic expression studies under the *35S* promoter (Pesch et al., 2013), raising the question whether this phenomenon also occurs under endogenous conditions.

To test this, stable *Arabidopsis* lines expressing *pMYC1_{1970 bp}:YFP-MYC1* were created. As it is known that MYC1 protein interaction varies in different ecotypes (Symonds et al., 2011), the expression was also studied in the Wassilewskija (WS) accession. Similarly to Col-0 (Schultheiß, 2015), YFP-MYC1 was expressed in the nucleus in cells close to trichomes and trichomes themselves. More distantly, it was shifted to the cytoplasm (Figure 11A, B). Next, YFP-MYC1 expression was analyzed in different mutant backgrounds. In the *ttg1* mutant, an overall expression was found in the nucleus in young leaves. In further developed leaves, *pMYC1_{1970 bp}:YFP-MYC1* expression was restricted to the basal half of the leaf (Figure 11C, D). YFP-MYC1 was also expressed in the nucleus in the *gl3 egl3* double mutant with seldom occurring cytoplasmic expression at the leaf basis (Figure 11E, F). Different to the first glabrous mutants, *pMYC1_{1970 bp}:YFP-MYC1* expression in *gll* is localized in the cytoplasm. It is ubiquitously found in young leaves, and restricted to the basal region in older ones (Figure 11G, H). The latter observation is in line with a previous study (Schultheiß, 2015). The inconsistent expression in the three analyzed glabrous mutants was surprising, suggesting either further influences on the MYC1 localization beyond the presence of trichomes or a more distinct cross-regulatory function of MYC1 within the trichome patterning genes.

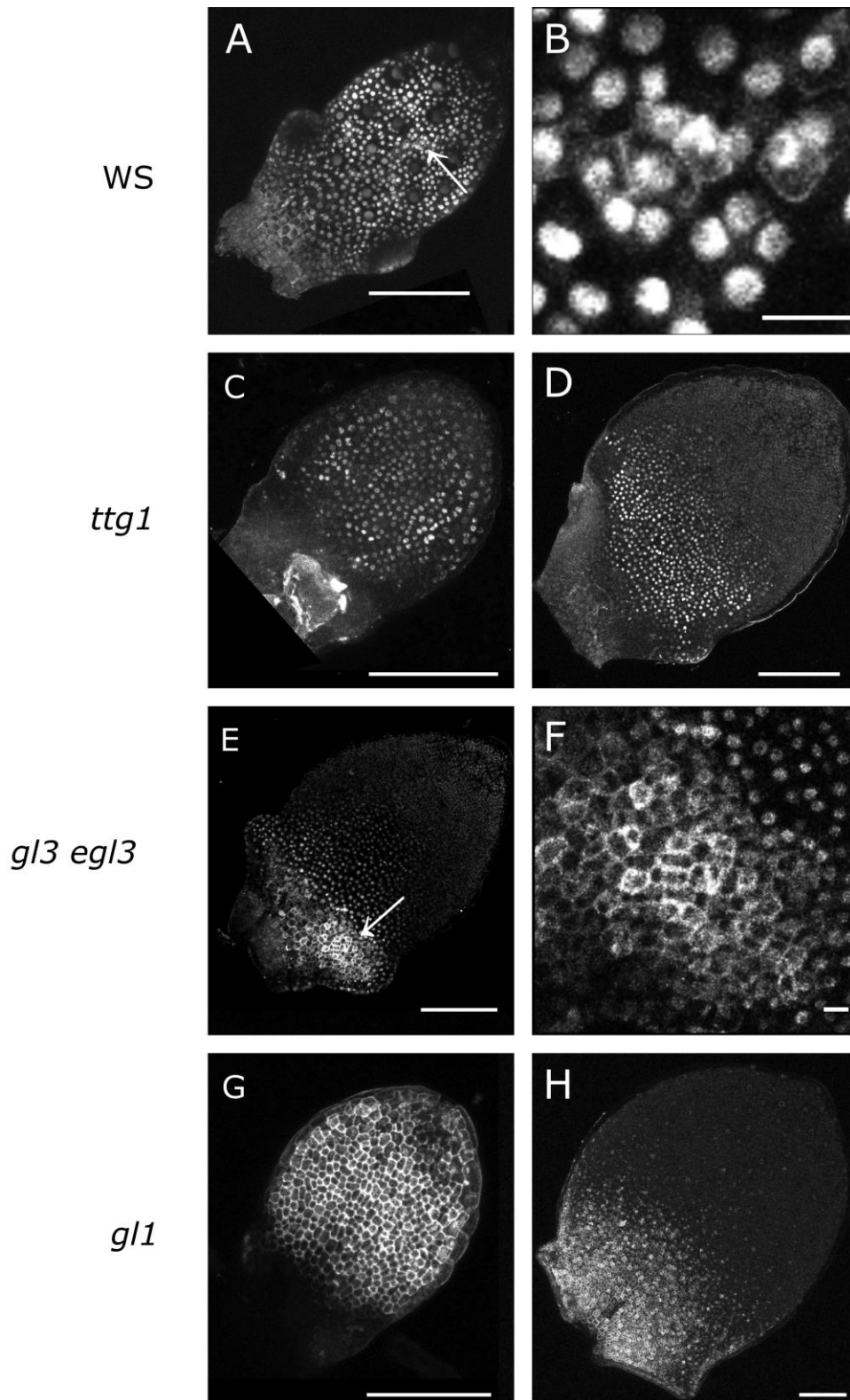


Figure 11: CLSM images of Arabidopsis plants stably transformed with $pMYC1_{1970 bp}:YFP-MYC1$ in different backgrounds. A, B) In the WS ecotype, YFP-MYC1 is expressed in the nucleus in trichomes and their closest surrounding cells. Arrow indicates cytoplasmic expression distant to the trichomes. Region is magnified in B. C, D) Nuclear YFP-MYC1 expression in the *ttg1* mutant in a younger (C) and further developed leaf (D). E, F) In the *gl3 egl3* background, YFP-MYC1 expression is found in the nucleus. Arrow indicates occasional cytoplasmic expression and is magnified in F. G, H) Cytoplasmic YFP-MYC1 localization in the *gl1* background. Expression is restricted to the leaf basis in further developed leaves (H). Scale bars: 100 μ m A, C, D, E, G, H; 10 μ m B, F.

3.3.4. *MYC1* influences trichome patterning

In transient experiments, it has been shown that bHLH proteins are able to stabilize MYB proteins (Chapter 3.2.2) and that *MYC1* significantly stabilizes TRY in a dosage-dependent manner (Chapter 3.2.3). Thus, *MYC1* turned out to be an attractive factor of trichome patterning. To shed light on *MYC1* in Arabidopsis plants under non-transient conditions, its influence on trichome density and intercalation was analyzed in *myc1* mutants and *35S:MYC1* overexpression lines. Light microscopy revealed a decreased trichome density in the *myc1* mutant and a higher density in overexpression leaves compared to Col-0 wildtype (Figure 12A).

For the quantitative analysis, leaves of two developmental time points were chosen to capture the impact of *MYC1* during trichome patterning. Younger leaves comprised up to two mature trichomes - a time point with on-going trichome initiation. Older leaves were characterized by at least three mature trichomes. Individual trichomes might not be fully outgrown at that time point, but trichome initiation should no longer occur and each single trichome should still be identifiable on the leaf blade.

While the *35S:MYC1* overexpression line showed no differences to the control in young leaves ($p < 0.625$), *myc1* mutants exhibited a significantly reduced trichome density ($p < 5 \cdot 10^{-8}$). In further developed leaves, *myc1* mutants were still significantly reduced compared to Col-0 ($p < 0.021$), whereas the overexpression line reached a significantly higher trichome density than Col-0 ($p < 0.021$). Comparing the two developmental time points, the trichome density only changed in Col-0 plants. Thereby, older leaves were significantly less dense than younger ones ($p < 0.006$). The *myc1* mutant as well as the *35S:MYC1* overexpression line revealed similar trichome densities between younger and older leaves (Figure 12B).

Next, the focus was on intercalation, which describes the initiation of trichomes between already developed ones. The same lines were analyzed in both developmental stages for the influence of *MYC1* on intercalating trichomes. First, it was considered how many leaves of each line showed intercalation. Most Col-0 plants exhibited intercalation (82%) in young leaves, followed by *35S:MYC1* (56%), and the *myc1* mutant (46%). Later in development, the amount increased to 100% for the wildtype and the overexpression line. Two thirds of the *myc1* mutant leaves developed intercalating trichomes (67%; Table 13). Second, the relative amount of intercalation compared to the total trichome number was analyzed for individual leaves, elucidating whether they emerge in similar rates. Here, only leaves exhibiting any intercalation

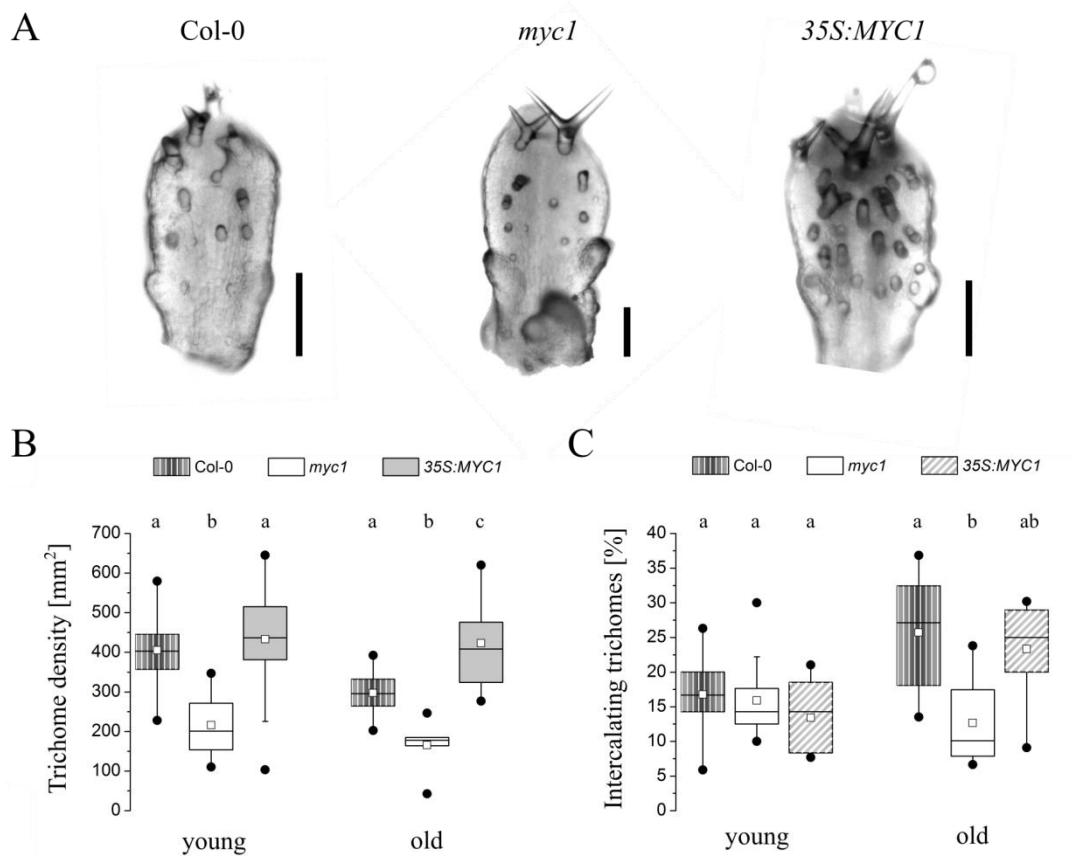


Figure 12: The influence of *MYC1* on trichome patterning. A) Microscopic images of young Col-0, *myc1*, and *35S:MYC1* Arabidopsis leaves. Scale bars indicate 100 μ m. B) Box plot analysis of trichome density. Different letters indicate significant differences between lines for each developmental stage. Box plots with striped pattern indicate significant difference between the developmental stages for each line. A one-way ANOVA was conducted for each comparison. Further developed Col-0 leaves exhibit a significantly reduced trichome density than younger leaves ($p < 0.006$). In young leaves, *myc1* mutants show a significantly reduced trichome density than Col-0 and *35S:MYC1* ($p < 5 \cdot 10^{-8}$ and $p < 3 \cdot 10^{-8}$). In older leaves, *myc1* mutants are significantly less dense than Col-0 and *35S:MYC1* plants ($p < 0.021$ and $p < 7 \cdot 10^{-5}$). *35S:MYC1* overexpression lines show a significantly increased trichome density than Col-0 ($p < 0.021$). C) Box plot analysis of intercalating trichomes. Different letters indicate significant differences between lines for each developmental stage. Box plots with striped pattern indicate significant difference between the developmental stages for each line. A one-way ANOVA was conducted for each comparison. Young Col-0 and *35S:MYC1* plants produce significantly less intercalating trichomes than further developed stages ($p < 0.013$ and $p < 0.001$). In older leaves, *myc1* develops significantly less intercalating trichomes than Col-0 ($p < 0.040$). Boxes show median, 0.25 and 0.75 quartiles. Dots indicate 1% and 99% percentiles, rectangles represent mean values.

were considered. The ratio of intercalating trichomes did not differ significantly between the three lines in young leaves. Over time, Col-0 wildtype as well as plants overexpressing *MYC1* exhibited significantly more intercalation ($p < 0.013$ and $p < 0.001$; Figure 12C; Table 13).

Table 13: The influence of *MYC1* on intercalation in different leaf developmental stages. Depicted are the relative amounts of leaves showing intercalation and the relative number of intercalating trichomes per leaf for younger and further developed leaves.

	Young leaves		Older leaves	
	leaves with intercalation [%]	intercalation per leaf [%]	leaves with intercalation [%]	intercalation per leaf [%]
Col-0	82	16 ± 6	100	26 ± 9
<i>myc1</i>	46	15 ± 9	67	13 ± 8
<i>35S:MYC1</i>	56	13 ± 5	100	23 ± 7

The findings indicated that *MYC1* is at least required for trichome patterning in the long term since older leaves lacking *MYC1* exhibited a reduced trichome density, whereas overexpression lines showed a higher density. Whereby, the reduced density for *myc1* mutants was already measurable in an earlier stage. While the amount of intercalating trichomes did not differ between the time points in *myc1* mutants, Col-0 as well as *35S:MYC1* exhibited more intercalation over time, suggesting a promoting influence of *MYC1* on intercalating trichomes in *A. thaliana*.

3.4. Expression of patterning genes in trichomes and epidermis cells

The main research focus of this work is to deepen the knowledge of the trichome patterning machinery. An indispensable requirement in each experimental assay is to catch the developmental time point where the involved genes are most active. If the leaves are too young, it is possible that not all patterning genes have been activated yet. If they are too old, it may be that some genes have already been switched off again. Therefore, Arabidopsis leaves of only a few hundred micrometers in length were chosen as biological material. Leaves of that size contain trichomes of all developmental stages and reflect the best possible overview of patterning gene activity. A drawback of using whole leaves for expression analyses is that they consist of a lot of undifferentiated epidermal cells next to trichomes. This may dilute the concentration of the expressed patterning genes and does not elucidate the network dependencies within trichome cells. To overcome this issue, a spatial *in vivo* analysis of patterning genes was conducted. The idea was to express key patterning genes bound to a fluorescent marker in stable Arabidopsis lines and determine the expression ratio between trichomes and undifferentiated epidermal cells. In this context, also the generation of stable lines in different mutant backgrounds would allow conclusions about the impact of the

individual missing gene in the patterning gene network machinery. However, first attempts unraveled that gene expression was hardly measurable and, in most cases, not detectable at all in trichome-surrounding epidermal cells. This raised the question of whether the rarely and weakly occurring epidermal expression has biological relevance.

3.4.1. Expression can be neglected in undifferentiated epidermal cells

Since it was often unfeasible to detect patterning gene expressions in non-trichome cells, the GUS reporter system (Jefferson et al., 1987) was utilized as a sensitive staining method to generate increasing staining intensities in dependence on the staining duration. The longer the incubation time, the more substrate is hydrolyzed, leading to a more intense staining, which reflects different signal intensities of fluorescent markers. Based on this characteristic of the GUS system, the expression in trichomes was compared to undifferentiated epidermal cells.

Exemplarily, *A. thaliana* plants stably transformed with *pTRY:GUS* were analyzed regarding the mean gray value intensity in trichomes and epidermal cells depending on the staining duration (Figure 13). Although the differences between trichomes and epidermal cells seemed to be low at a given time point, they were significant for the test period 3-7 h (black bar). After 2.5 h of incubation, neither trichomes nor epidermis cells were stained. An increase of the staining was measurable after 3-4 h in trichomes, followed by a stagnation of the signal intensity for up to 6.5 h.

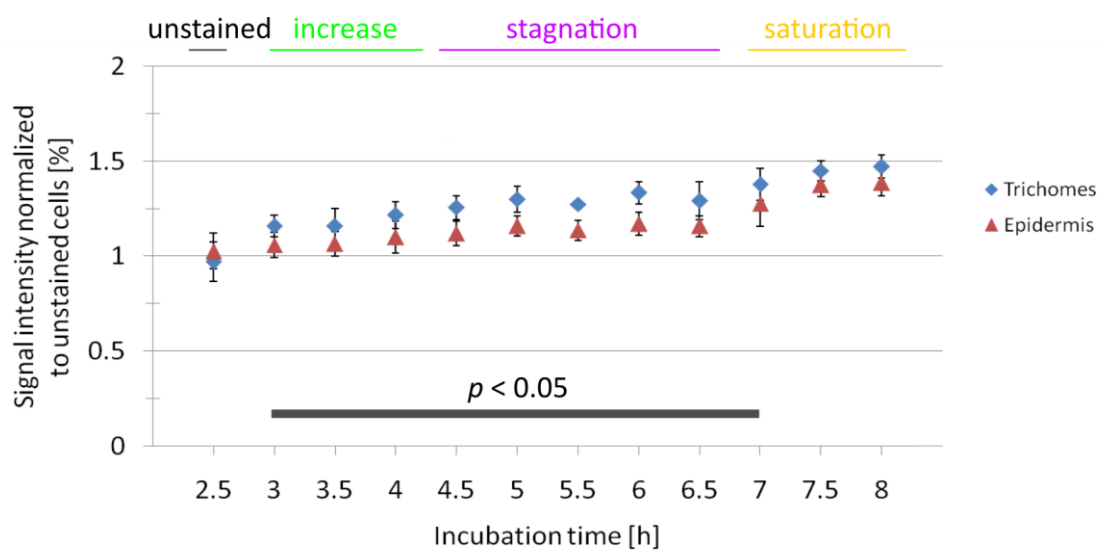


Figure 13: *pTRY:GUS* expression in trichomes and undifferentiated epidermal cells in dependence of staining duration. After 2.5 h of incubation no staining is detectable, the subsequent staining intensities can be grouped into increase, stagnation and saturation. Bottom bar indicates significant difference between trichome and epidermis at each time point (Student's t-Test).

After 7 h, the GUS signal began to saturate. However, the epidermal signal remained unaffected towards the end of the stagnation phase. Only during saturation, the signal intensity of undifferentiated epidermal cells increased. This investigation allowed conclusions about fluorescent marker lines. As long as one works with unsaturated gene expressions, almost no expression of trichome patterning genes would be expected besides trichomes. Therefore, the biological relevance of patterning gene expression in the undifferentiated epidermis may be neglected.

3.4.2. Results of *pGL2* / *pCPC* / *pTRY* / *pETC1* / *pETC2* in Col-0

With the aid of stable fluorescent marker lines, a temporal resolution of the expression of patterning promoters in different developmental stages was achieved. *A. thaliana* plants were transformed with the promoters of *GL2*, *CPC*, *TRY*, *ETC1*, and *ETC2*, driving 2xNLS and 2xCFP, facilitating accurate expression measurements. Trichomes were grouped according to their developmental phase. Newly emerged trichomes were allocated to category 1. Category 2 described expanding trichomes. The first branching event classified category 3. Higher branched and mature trichomes comprised category 4 (Figure 14A, B). To enable a comparison, signal intensities were normalized to the mean value in trichomes of category 1. Figure 14C shows the ratios of all five tested promoter expressions. Generally, it was found that the older the trichome, the higher the expression. In all lines, the strongest increase was detected in expanding and early branched trichomes (2- to 4-fold). A further enhancement to more than 5-fold was often observed in two-branched and higher-ordered trichomes. In contrast to the other promoters, the expression of *pTRY* rises in expanding and two-branched trichomes but decreased during subsequent development. This may indicate a shorter functionally active time period of *TRY*. Interestingly, *pETC1* expression was higher in expanding and two-branched trichome (category 2 and 3) than *pCPC* or *pTRY*, indicating an important role of *ETC1* for trichome patterning.

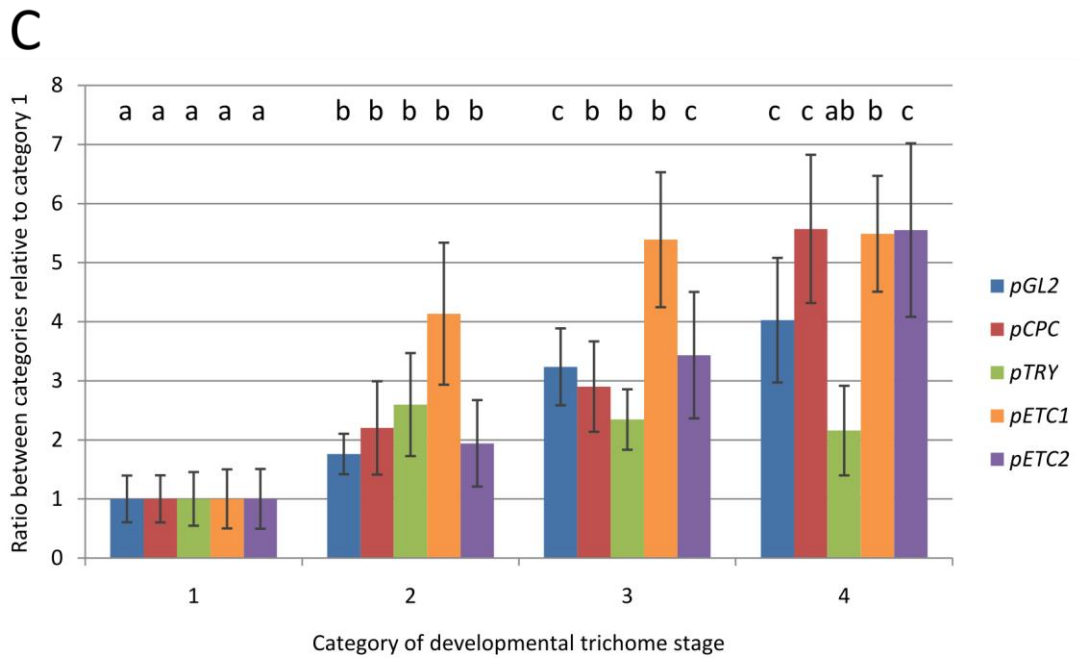
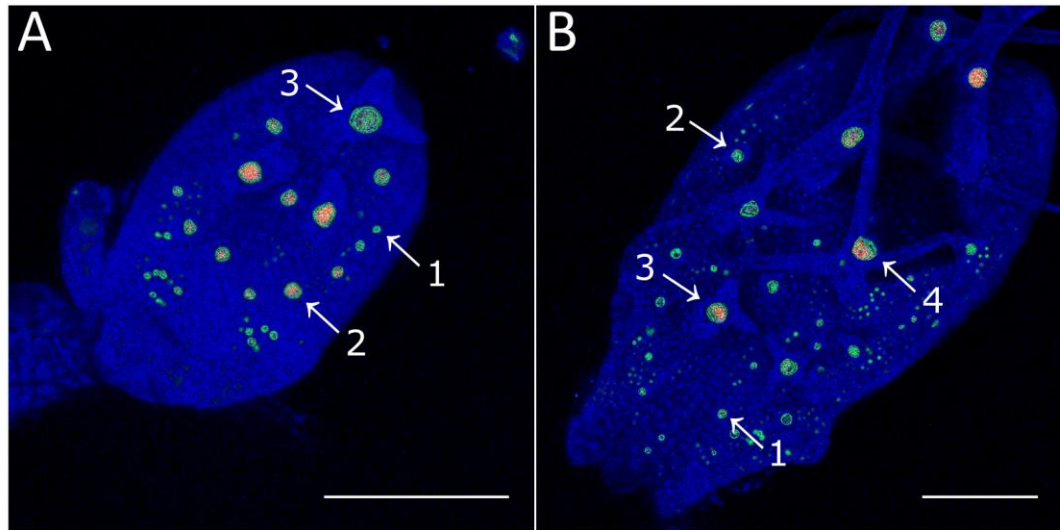


Figure 14: Expression of patterning promoters in different trichome developmental stages. **A, B)** CLSM images expressing *pENSG:pETC1:2xNLS-2xCFP* (A) and *pENSG:pGL2:2xNLS-2xCFP* (B). Numbers refer to trichome class. Scale bar indicates 100 μ m. **C)** Expression of patterning promoters relative to the trichome developmental phase. Category 1 displays emerging trichomes, category 2 expanding trichomes. Two-branched trichomes belong to category 3 and further developed trichomes to category 4. Different letters indicate significant differences for each line (Mann-Whitney U test).

3.5. Cross-regulatory interactions of *Arabidopsis thaliana* and its mutants

Gene fluctuation is essential to initiate cell specification, such as the formation of tissues and organs or the establishment of a trichome pattern (Raj & van Oudenaarden, 2008). In this chapter, *A. thaliana* Col-0 and 21 single and double patterning mutants were studied. On the one hand, all these lines were investigated morphologically to determine and compare the differences in trichome density. On the other hand, the focus was on the transcriptional gene expression of the entire patterning network, to systematically elucidate the underlying mechanisms required for a regularly distributed trichome pattern on *A. thaliana* rosette leaves.

3.5.1. Comparison of trichome density in *A. thaliana* wildtype and various patterning mutants

It is known that trichome patterning on *Arabidopsis* rosette leaves is mainly achieved by the interplay of promoting and repressing factors. Generally, the absence of an activator leads to fewer trichomes and the lack of an inhibitor to more trichomes. In order to quantify that phenotypical impression and elucidate the impact of trichome patterning genes in *A. thaliana*, Col-0 wildtype and 21 mutant lines were compared regarding their trichome number, density, and branching behavior (Figure 15; Figure 16; Table S5). The density was determined from the quotient of the area by the trichome number. Hereby, the more difficult part is to correctly determine the trichome number. This can be challenging, especially for mutants with many trichomes. To avoid this, young leaves were used to identify the trichome density. In order that the density is not biased by leaves of different sizes, the leaf area was limited to 22 mm². The leaves of *gl2* and *ttg1* were slightly larger with a maximum of 31 mm². But since these are almost glabrous mutants, this should be of no consequences.

cpc, *etc1*, *etc1 etc3*, *etc2*, and *etc3* produced more trichomes and reached a higher density than Col-0 wildtype. This was not unexpected as one or two inhibitors were missing in all these lines. Activators had a wider effective range, and more trichomes could develop. The density of the inhibitors *tcl1* and *tcl2* was at wildtype level, indicating less importance or more redundancy for trichome formation.

Compared to wildtype, fewer trichomes and a lower density were identified for *gl2*, *myc1*, *myc1 egl3*, *try*, *ttg1* and *ttg2*. This was especially interesting for *try* as it is one of the key inhibitors in trichome patterning and all others were activator mutants. *try* produced small trichome clusters of up to three trichomes. Not only the decreased

trichome numbers and the cluster formation but also the trichome shape was striking with an increased number of trichome branches in this mutant. A few percent of trichomes showed 4-branched trichomes even in Col-0 wildtype, however, *try* produced approx. 90% trichomes with five or more branches. The absence of *TTG2* led not only to a reduced trichome number but also to trichome developmental defects. Mostly, differentiation stopped before branching, leading to a bulge-like shape.

As the reduced density in *myc1 egl3* was as strong as in the *myc1* single mutant, the lack of *EGL3* seemed to have no further impact. This was underlined as the *egl3* single mutants showed trichome numbers and density equal to Col-0. Redundancy was only seen in the *gl3 egl3* double mutant with its entirely glabrous leaves, while both single mutants displayed comparable values to wildtype. Similar observations were made for *myb23*. Only in combination with *gll*, an effect was countable. *myb23* single mutants depicted wildtype-like values, whereas the *gll myb23* double mutant appeared completely trichome-free. *gll* was the only single mutant without any trichomes; *gl2*, as well as *ttg1*, only rarely formed trichomes, preferably on the leaf margin.

A striking phenotype was found for the *cpc try* double mutant. Massive trichome clusters with up to 50 trichomes were formed without spacing between the trichomes. Considering the estimated absolute trichome number, this mutant exhibited significantly more trichomes than the wildtype.

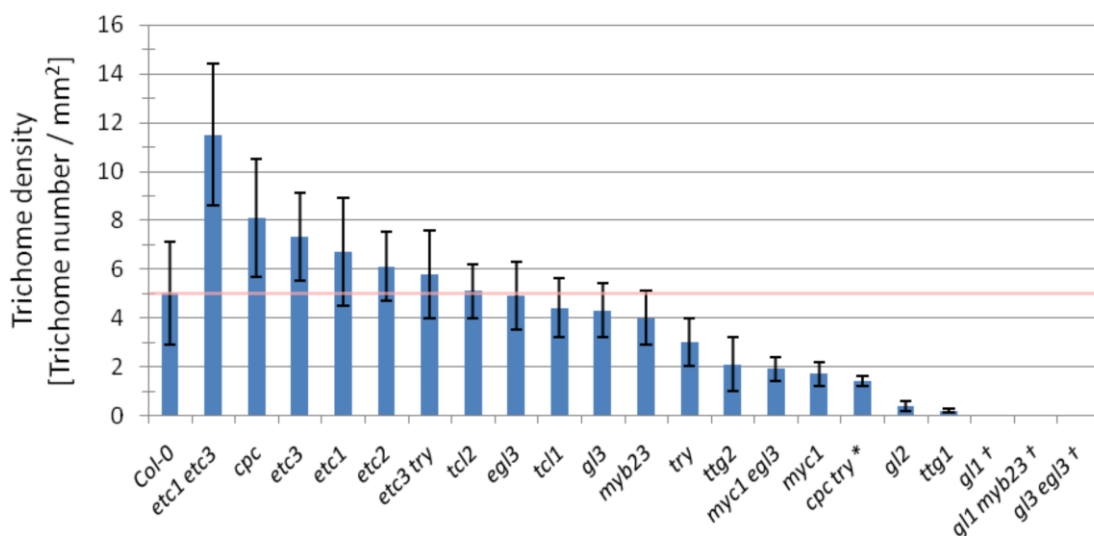


Figure 15: Trichome density in *A. thaliana* wildtype and various patterning mutants. Mean values and standard deviations represent the combination of leaves three and four and are given for 9-19 replicates each. Light red line indicates reference value. * For *cpc try* not single trichomes but trichome clusters (trichome initiation sites) were measured. † These lines are entirely glabrous.

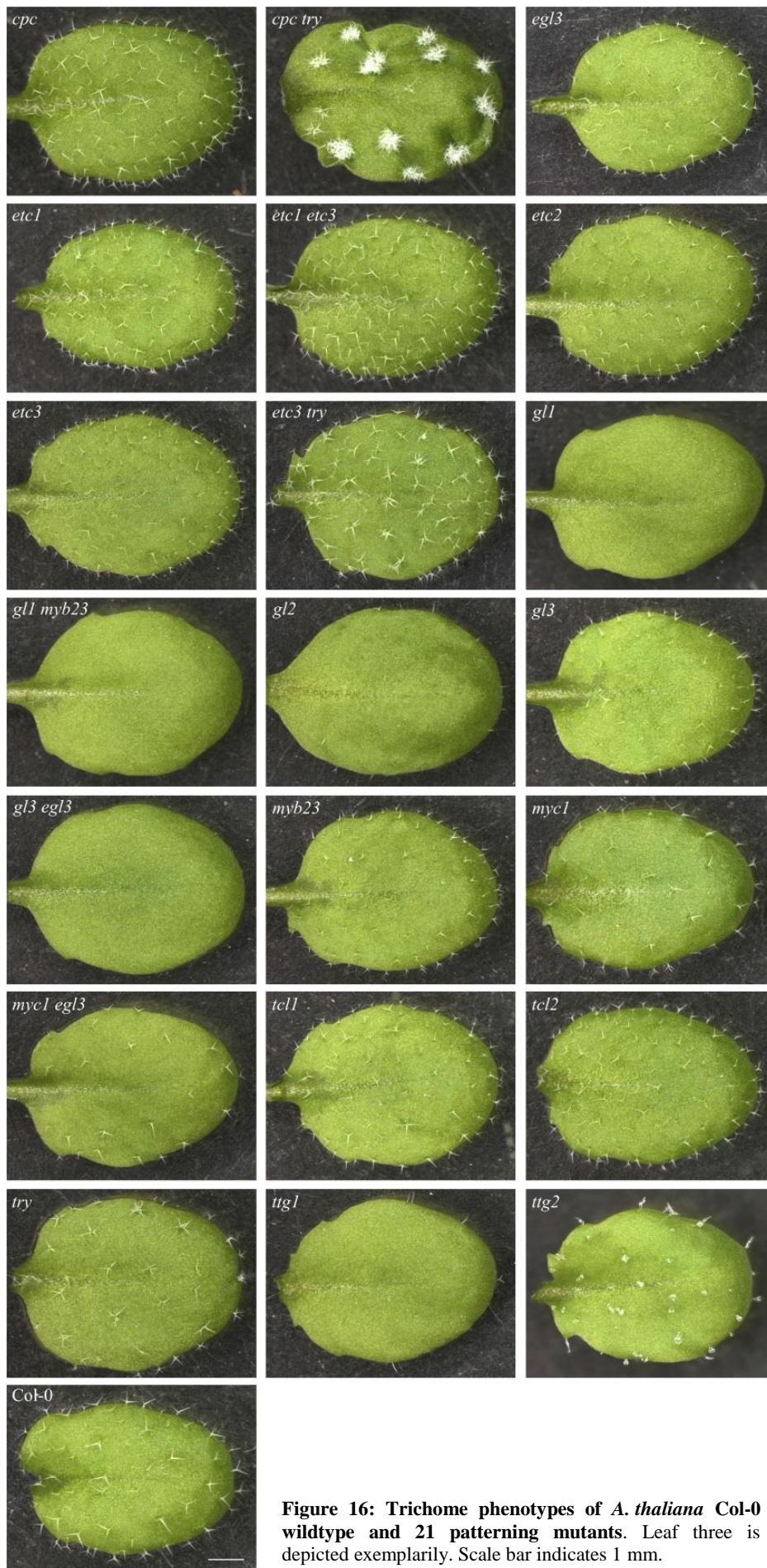


Figure 16: Trichome phenotypes of *A. thaliana* Col-0 wildtype and 21 patterning mutants. Leaf three is depicted exemplarily. Scale bar indicates 1 mm.

3.5.2. Transcriptional expression of trichome patterning genes in *A. thaliana*

More than a dozen genes are involved in the cross-regulatory *TTG1* network, forming the regularly distributed trichome pattern on *A. thaliana* rosette leaves. General dependencies are known, e.g. activators promote inhibitors, which in turn repress the activators. However, the exact levels at which the genes regulate one another are uncertain.

To elucidate the transcriptional expression of the trichome genes in more detail, a vast systematical qPCR approach was employed. The differential regulation of 15 patterning genes was analyzed in *Arabidopsis* Col-0 wildtype and 21 mutant backgrounds. Investigating the cross-regulatory changes in the absence of one gene may indicate its role within the network, i.e. functional dependencies. Moreover, this approach may shed light on the impact of gene redundancies.

The aim of this intraspecies strategy was not only to quantify the cross-regulatory interactions of the complex *TTG1* network but also to contribute to a theoretical trichome patterning model, which was developed by Anna Deneer from the Wageningen University & Research. This model combines the activator-inhibitor and the activator-depletion model and comprises the core components *TTG1*, *GL3*, *GL1*, *CPC*, and *TRY* (Balkunde et al., 2020). *TTG1* and *GL3*, as well as *GL1* and *GL3*, form dimeric activator complexes, activating *TRY* and *CPC*, respectively. In turn, the inhibitors bind to *GL3*, thus forming inactive complexes. Recently, *ETC1* was added to the model (Figure 17). It shares redundant functions with *CPC/TRY* (Wester et al., 2009) and operates as one possible representative for the inhibitors to enable the simulation of the *cpc try* double mutant. The model is based on parameters including the rates of basal production, activation, degradation, diffusion, and the binding strength of the proteins. Experimentally obtained data were used to calibrate and improve these parameters and strengthen the conclusiveness. Together with this modeling approach, the following questions were addressed to contribute to the main objective: How robust is the regulation of trichome density by the *TTG1* network? This includes: a) Can the genes be randomly regulated to generate the familiar trichome pattern, or are there certain genes that are more sensitive than others? If so, b) which one would crash the trichome phenotype if severely up- or downregulated? Or, to put it another way: Which criteria must be fulfilled for a proper operating network? c) Can changes in the expression be mimicked, e.g. by overexpression lines?

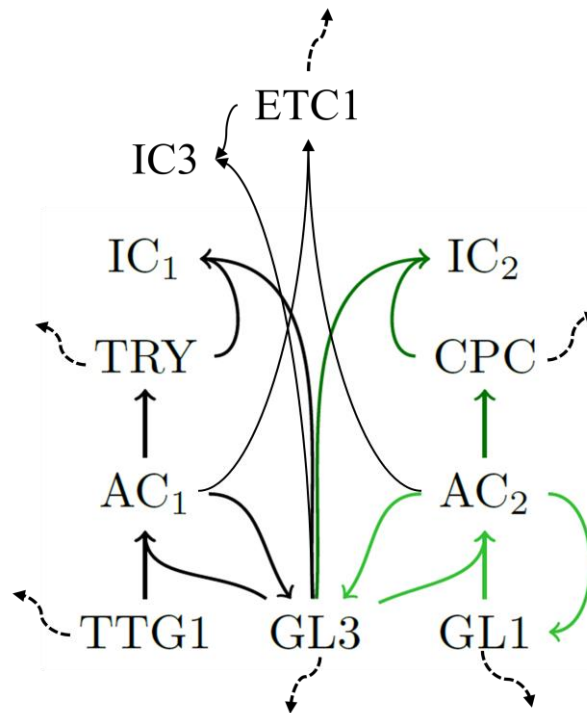


Figure 17: Interaction scheme of the trichome patterning network. GL3 binds either to TTG1 or GL1, resulting in active complexes (AC). They activate TRY, CPC, or ETC1, forming inactive complexes (IC). Dashed lines indicate mobility. (Modification from Anna Deneer based on her figure in Balkunde et al., 2020.)

In order to map the processes during trichome patterning as best as possible, tiny, trichome-developing rosette leaves of 200-400 μm length were harvested. Due to the juvenile leaf shape and altered trichome initiation of the first two true leaves in *A. thaliana* (Park et al., 2017; Telfer et al., 1997), sample collection started from rosette leaf three after phase transition and is illustrated in Figure 18. Root and hypocotyl, as well as the cotyledons and the first two rosette leaves, were removed to gain leaf material with on-going trichome initiation and formation.

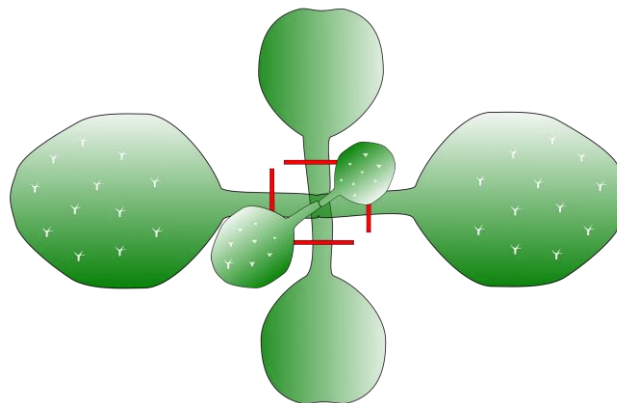


Figure 18: Dissection scheme of Arabidopsis plants. Cotyledons and the first two true leaves were removed (red bars), as well as root and hypocotyl, to harvest tiny leaves with on-going trichome development.

Some premises were set to obtain conclusive examination results of the extensive expression approach. The fold changes were calculated based on the gene expressions of each individual Arabidopsis mutant compared to the Col-0 wildtype. To exclude slight differences in gene expressions due to natural variations, only values passing a 2-fold threshold were considered, meaning that the expression of a certain gene is either halved or doubled in the mutant compared to the wildtype reference. This cut-off approximately reflects the deviation of the two used reference genes upon all experiments. In the attempt to transfer the gene expressions to known trichome phenotypes, it is assumed that RNA level equals protein concentration. Graphs and tables comprising the complete data set with and without the cut-off can be found in the appendix (Figure S10; Figure S11; Table S6; Table S7). The expression of a gene in its corresponding mutant was not considered and was marked by an “x” in all tables. Genes, which were not detectable due to their low expression, were put into brackets.

Gene expression in Col-0 wildtype

First, the transcriptional expression results were analyzed for all 15 investigated trichome patterning genes in the Arabidopsis Col-0 wildtype. The expression data were normalized to two reference genes and adjusted to the highest value to simplify the comparison. The bars in Figure 19 depict the relative expression of each individual gene.

Strikingly, *TTG1* is by far the highest expressed gene. The difference to the second-highest gene might be surprising, but not the finding that it is generally highly expressed as *TTG1* regulates five different traits. Interestingly, it is followed by *TCL2*, an inhibitor that receives little attention. Here, the inhibitors *CPC* or *TRY* would have been expected as they are believed to play important roles in pattern formation due to their mutant trichome phenotype. *GL2*, known to be expressed during trichome outgrowth (Rerie et al., 1994), was the third-highest expressed gene. Among the key components, *GL1*, its homolog *MYB23*, and *CPC* were expressed in a similar range. Interestingly, *GL3/EGL3*, essential for building the trimeric MBW activator complex and the dimers with *GL1* or *TTG1*, were only lowly expressed. *TRY*, the other most prominent inhibitor, was only half as much expressed as *CPC*. *ETC1* and *ETC3* showed a comparable expression to *CPC*, whereas *ETC2* was almost nonexistent, suggesting a minor role.

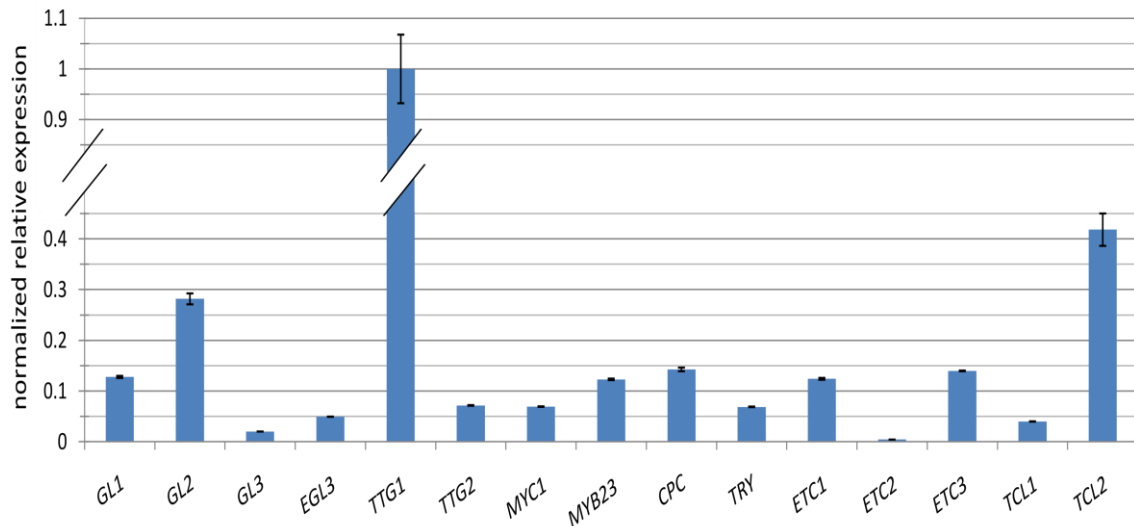


Figure 19: Transcriptional patterning gene expression in *A. thaliana* Col-0 wildtype. Depicted are the relative expressions of 15 patterning genes normalized to the highest value.

Activators

First, transcriptional gene regulation was studied among the activators. The corresponding results are depicted in Figure 20. Comparisons to the trichome phenotype refer to Table S5.

Looking at the key components, the extreme downregulation of *MYB23* in the glabrous *gl1* mutant was striking, suggesting a strong dependency of *MYB23* on *GL1* expression (both MYB factors). As *MYB23* was also moderately to strongly reduced in the *gl2* and *ttg1* mutants - both exhibiting an almost glabrous phenotype with only a few trichomes on the leaf margin -, suggested that the *MYB23* activation is abolished in glabrous mutants. In contrast, the expressions of *GL1*, *GL2*, and *TTG1* were unchanged in the *myb23* mutant. Since the other activators were also not affected, this may explain the wildtype-like trichome phenotype of *myb23*. The same explanation may apply to the *gl3* mutant. The transcriptional expression revealed a slight decrease only for *MYB23*, which might be compensated by its homolog *GL1*, leading to a trichome pattern similar to Col-0.

The WD40 factor *TTG1* turned out to be a stable and robust key player, as none of the activator mutants influenced its expression, not even the entirely trichome-free mutant *gl3 egl3* or *gl1 myb23*. In contrast, the *ttg1* mutant caused the downregulation of many genes, including the activators *GL1*, *GL3*, and *MYB23*. This prevented the formation of the activator complex, which in turn reduced *GL2* and *TTG2*. Consequently, key inhibitors such as *CPC* and *TRY*, but also *ETC1* were downregulated.

However, *ETC2* and *TCL2* were upregulated. For *ETC2* it has to be considered that being very lowly expressed in wildtype, already minor differences caused high fold changes and, therefore, a 1.9-fold reduction of *ETC2* connoted an absence of that gene.

Next, the less prominent activators were analyzed. Exclusively, the loss of *TTG2* (WRKY transcription factor) caused the upregulation of an activator, *MYB23*, and an increased expression of the inhibitor *ETC1*, whereas *CPC* and *TRY* were reduced. Since not many genes respond to the loss of *TTG2*, the reduced trichome density and defects in branching (Figure 16) in these mutants appear to be due to the absence of *TTG2* itself or are regulated on the protein level. In contrast, the loss of individual activators often affected the *TTG2* expression. Moderate reductions were found in *gl2*, *egl3*, *ttg1*, *gll myb23*, and *myc1 egl3* mutants, and *TTG2* expression was absent in the *gl3 egl3* double mutant. The absence of neither inhibitor caused any changes in the *TTG2* expression. That is interesting as *TTG2* is assigned to share redundant functions with *GL2*, but in contrast to *GL2*, *TTG2* did not respond to the loss of any inhibitor.

In the following, particular features of the activators are described. As expected, the homeodomain transcription factor *GL2* was downregulated in the glabrous mutants *gll*, *gll myb23*, *gl3 egl3*, and *ttg1*. Less expected was the finding that the loss of *GL2* influenced both, activators and inhibitors. Whereas all affected activators (*GL1*, *MYB23*, *TTG2*) were negatively regulated, some inhibitors were down- (*CPC*, *TRY*, *ETC1*) or upregulated (*ETC2*, *TCL1/2*). This suggests that *GL2* cannot be considered as an exclusive downstream gene of the network, but its function is relevant for the expression of most patterning genes, and it contributes actively to the cross-regulatory interactions. In *gl2* mutants, first trichomes are initiated but do not develop properly. This could be because some activators (*GL3*, *EGL3*, *TTG1*) are not affected, and some inhibitors are upregulated.

Besides *MYB23*, none of the genes primarily contributing to the activator complex was upregulated in any inhibitor single mutant. This may indicate that the inhibitors work in concert to repress the activators and that the loss of one repressor can be compensated by others or that their regulation takes place on the protein level.

MYC1 seems to represent an exception among the activators. Although, as far as it is known, the absence of *MYC1* does not appear to be compensated by other activators, the *myc1* mutant caused only a slight decrease in the expression of *GL3* and a moderately altered regulation of three inhibitors (*ETC2*, *ETC3*, and *TCL1*).

Results

Furthermore, none of the activator mutants and only strong double mutants such as *gl3 egl3* or *gl1 myb23* influenced the *MYC1* transcriptional expression level.

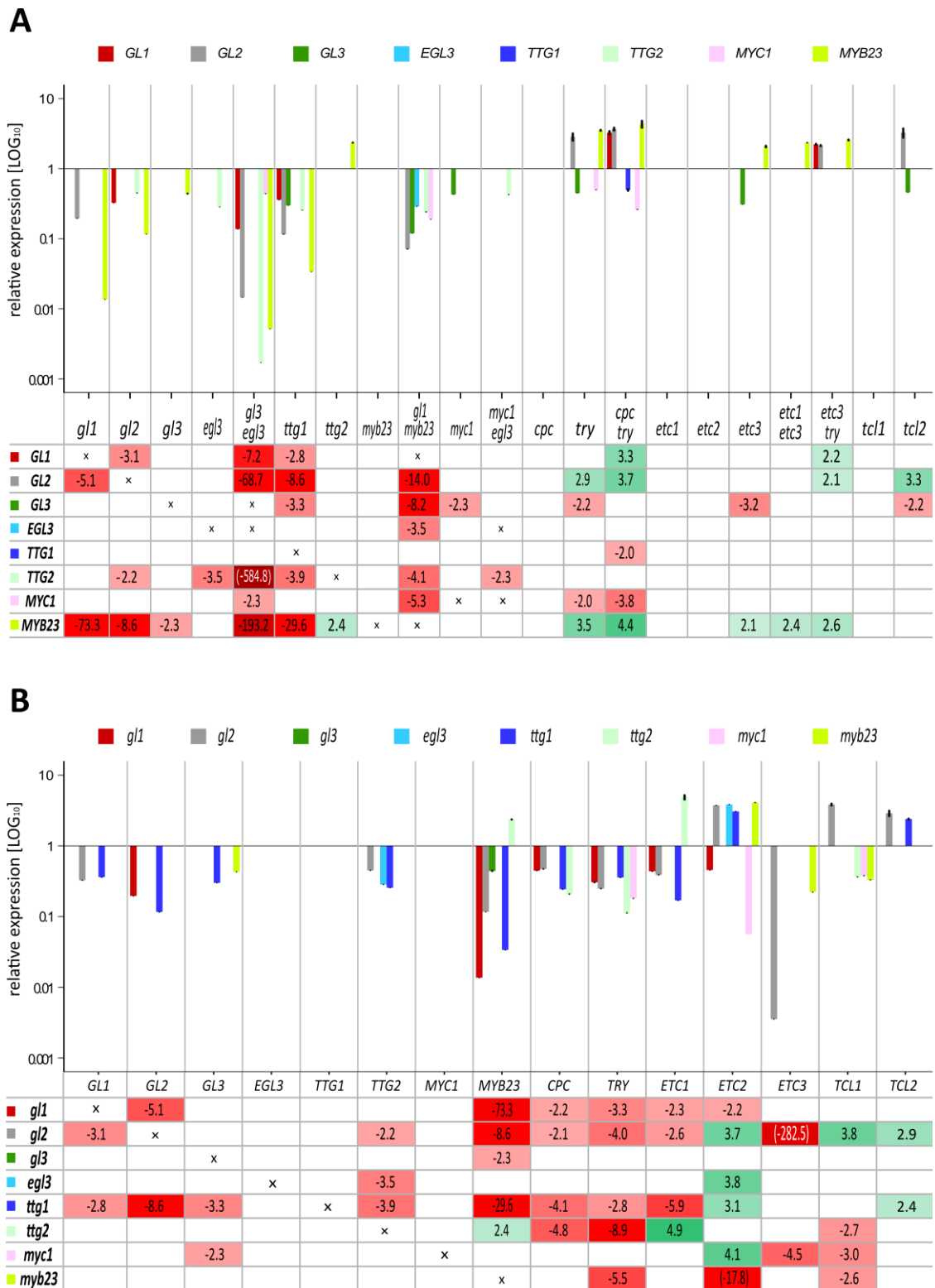


Figure 20: Transcriptional expression analysis of the activators in *A. thaliana* mutants. Depicted are the bar plots with the relative expression changes compared to Col-0 wildtype and the corresponding fold changes upon a 2-fold cut-off ordered by mutants (A) or genes (B). Expression differences less than the 2-fold threshold lead to empty fields. Upregulations are indicated in green, downregulations in red; the darker the color, the stronger the regulation. Individual gene expressions in the corresponding mutant background were not considered and are indicated by an x. Values of unexpressed genes are bracketed.

Inhibitors

In the following section, the transcriptional expression of the inhibitors was analyzed. All graphs and values can be found in Figure 21 and comparisons to the trichome phenotype refer to Table S5.

CPC and *TRY* represent the key players among the R3 MYB inhibitors. As expected, both inhibitors were often downregulated in the absence of their activators. Interestingly, the expression of *CPC* or *TRY* was moderately reduced but not abolished in glabrous mutants such as *gll* or *ttg1*, indicating other sources for their activation besides properly formed activator complexes. While *CPC* expression was not altered in *gl3* and *egl3* single mutants, it was strongly reduced in the *gl3 egl3* double mutant. Less severe, this effect was also found for *TRY*.

In contrast, the absence of either *CPC* or *TRY* caused fewer expression alterations among the patterning genes. A dependency of *CPC* by *TRY*, but not vice versa, was indicated by the upregulation of *CPC* in *try* mutants. Moreover, the *GL2*, *MYB23*, and *ETC2* expressions were increased in *try*. As the *try* mutant exhibits fewer trichomes, the increased activator expressions of *GL2* and *MYB23* seem to be compensated by reducing *GL3* and *MYC1*. Generally, the absence of *CPC* caused no differential regulations of any patterning genes, neither activators nor inhibitors. This was interesting as *cpc* mutants develop a higher trichome density.

Next, the other five inhibitors were investigated in more detail. *ETC2* represents a particular case among the inhibitors. It is differentially expressed in many mutant backgrounds and, strikingly, often upregulated when other inhibitors were downregulated. The *ETC2* reduction in *etc1* and *etc3* was so substantial that the expression was completely abolished. This dependency was not detected the other way around, indicating a divergent functionality of *ETC2* in contrast to *ETC1* and *ETC3*. The loss of *ETC2* had no consequences on any other trichome patterning gene either. In contrast to that and the expression of all other inhibitors, the *ETC2* expression was often increased in the absence of one or two activators. However, it has to be considered that *ETC2* was very lowly expressed in the Col-0 reference background, so that even a 5-fold increase in an individual mutant still results in low copy numbers.

The loss of *TCLI* caused almost no changes in the transcriptional expressions of other patterning genes, despite a slight upregulation of *TRY*. However, this repression of *TCLI* on the key inhibitor *TRY* is interesting as it was the only inhibitor mutant affecting the *TRY* gene expression. Due to the stable expression of the patterning genes

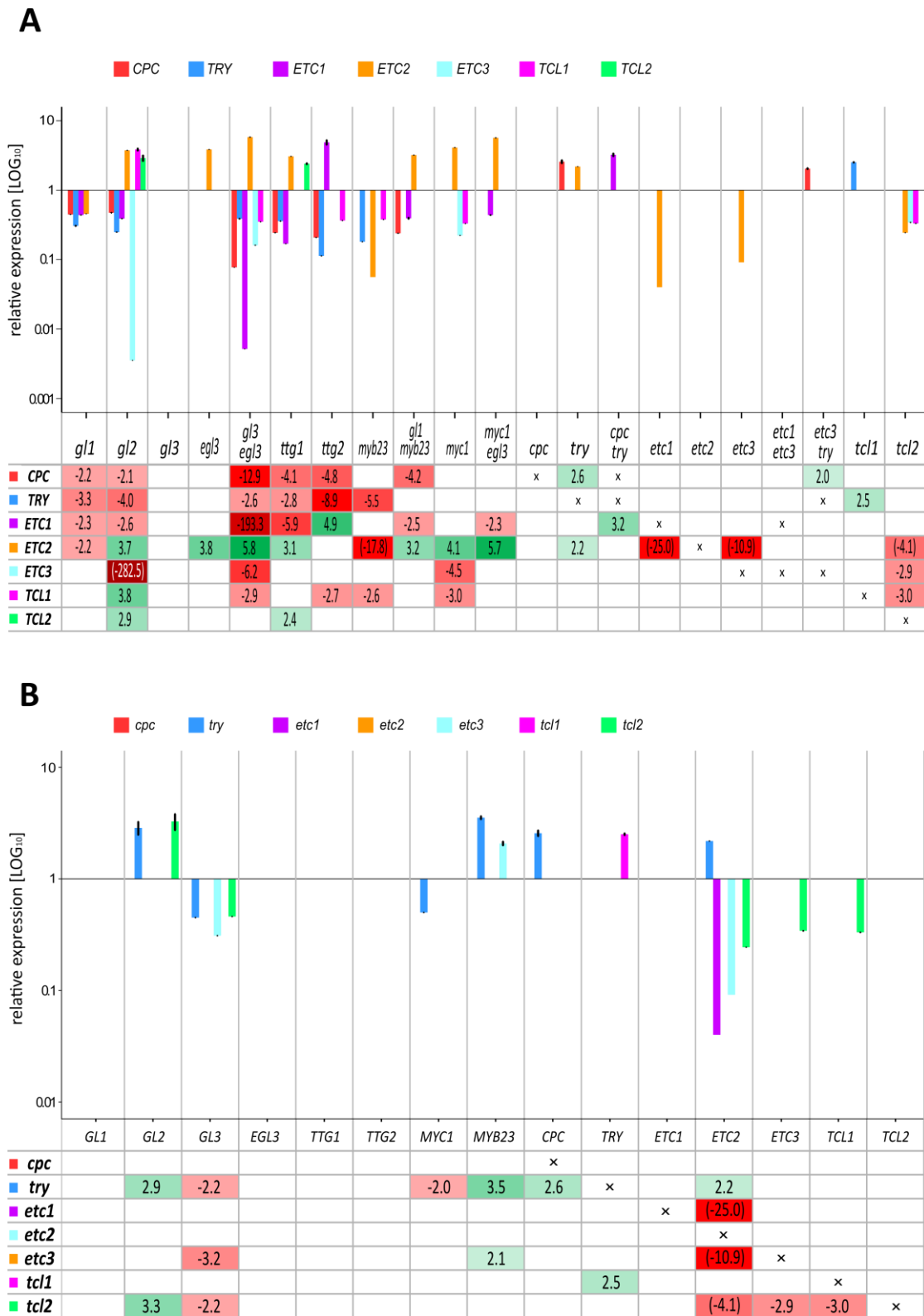


Figure 21: Transcriptional expression analysis of inhibitor mutants in *A. thaliana*. Depicted are the bar plots with the relative expression changes compared to Col-0 wildtype and the corresponding fold changes upon a 2-fold cut-off ordered by mutants (A) or genes (B). Expression differences less than the 2-fold threshold lead to empty fields. Upregulations are highlighted in green, downregulations in red; the darker the color, the stronger the regulation. Individual gene expressions in the corresponding mutant background were not considered and are indicated by an x. Values of unexpressed genes are bracketed.

and the wildtype-like trichome pattern in *tcl1* mutants, its loss suggests no drastic effects on the entire network. In contrast, the *TCL1* expression was influenced by some activators. The *myb23*, *myc1*, and *ttg2* single mutants, as well as the *gl3 egl3* double mutant, showed a slight downregulation, whereas the absence of *GL2* resulted in a comparable increase of *TCL1* expression. Thereby, *TCL1* was similarly affected as other inhibitors. Interestingly, the loss of *TCL2* caused a reduction of *TCL1*, whereas the *TCL2* expression was not altered in the *tcl1* mutant, indicating a unidirectional dependency of *TCL1* on *TCL2*.

Two notable characteristics among the inhibitors were found. Besides the unexpected influence of the homeodomain transcription factor *GL2* on the activators, also the regulation of all inhibitors was changed in the absence of *GL2*. Here, the extreme downregulation of *ETC3* was striking, which led to no detectable expression. This suggests a direct dependency of *GL2* on *ETC3* within the network. Moreover, the transcriptional reduction of *GL3* in the *try*, *etc3*, and *tcl2* mutants suggests a positive feedback loop of these inhibitors on the activator.

Double mutants

This chapter deals with the analysis of several double mutants. Together with their corresponding single mutants, they represent an excellent tool to uncover redundant genes and gain more insights into their overlapping functions. In the following, two groups of double mutants, established and non-established, are described.

Here, the popular and frequently used double mutants of the key components of the patterning network were examined, namely *gl3 egl3*, *gll myb23*, and *cpc try*. The corresponding bar plot and the fold changes are depicted in Figure 22. Comparisons to the trichome phenotype refer to Table S5.

gl3 egl3

Both *gl3* and *egl3* single mutants caused almost no differential regulation, including no mutual control and therefore no direct hierarchical dependency on each other. This explains the wildtype-like regular trichome distribution on Arabidopsis rosette leaves. The absence of *GL3* reduced the *MYB23* expression, the loss of *EGL3* influenced *TTG2* negatively and *ETC2* positively. However, the *gl3 egl3* double mutant revealed a strong additive effect, highlighting the considerable functional redundancy of these genes and indicating the bHLH factor *GL3* and its homolog *EGL3* as essential for the activator

complex formation. Due to their loss, also the activation of the inhibitors is abolished, leading to moderate to extreme downregulation on the activator as well as on the inhibitor side. Only *TTG1* and *TCL2* were unaffected, and *ETC2* was enhanced compared to Col-0. Genes such as *GL2*, *TTG2*, *MYB23*, and *ETC1* were so strongly reduced that their expressions were almost undetectable and probably exhibited no biological relevance for the network in the *gl3 egl3* double mutant. Together, this resulted in a completely glabrous phenotype. Interestingly, the reductions were even more severe than in other glabrous mutants such as in *gll* or *ttg1*, suggesting a fundamental role for *GL3/EGL3* during the transcriptional interactions.

In addition to the single mutants, also the *GL1/MYB23* and *CPC/TRY* homologs were partly tremendously reduced, indicating a direct relationship between the key components. Based on the strong additive effects and the non-compensable consequences for the patterning system, *GL3/EGL3* could be considered as a functional unit and is thus combined in further theoretical approaches.

gll myb23

A different picture emerged from the analysis of the *gll myb23* double mutant. A direct dependency between the two participating MYB factors was found. While the *GL1* expression was unaffected in the *myb23* mutant, *MYB23* was strongly reduced in the *gll* background. Thus, it can be assumed that *GL1* activates *MYB23* expression, but not vice versa.

In contrast to *GL3/EGL3*, *GL1* and *MYB23* are less redundant. A decrease of the *TRY* expression in the *gll* and *myb23* single mutants was compensated and unaffected in the corresponding double mutant. However, the transcriptional expressions of many genes of the trichome patterning system were not altered in the single mutants but moderately to strongly reduced in *gll myb23* double mutants, highlighting the redundant function of the two MYB homologs. Therefore, *GL1/MYB23* was also considered as one functional unit in follow-up experiments. Since the *gll* mutant already produces glabrous leaves, the same phenotype was not unexpected for the *gll myb23* double mutant with even more downregulated activators and inhibitors. The decreases in expressions were less substantial than in the *gl3 egl3* double mutant due to either a lower additive effect or the already glabrous phenotype in the *gll* mutant. Again, *ETC2* represented an exception, being upregulated in the double mutant but reduced in both single mutants.

When looking at the reduced *GL3* and *EGL3* expression, a positive feedback loop was identified. Just as they activated *GL1* and *MYB23*, the latter promoted *GL3* and *EGL3* expression. This self-activating step may harbor an enormous biological relevance as activators require a self-enhancing loop to break the initial homogeneity of the cells and to start the trichome patterning process.

cpc try

Next, the fascinating *cpc try* double mutant with its large trichome clusters was studied on the transcriptional level. Since the *try* single mutant exhibits fewer trichomes but a higher cluster frequency, and *cpc* mutants have more trichomes but no clusters, additive as well as divergent functions were expected. Although the loss of *CPC* did not affect other genes, the differential regulation of the patterning genes in the *cpc try* double mutant could not only be explained by the impact of *TRY* alone. This suggested an additive and redundant effect of both inhibitors. Looking at the two genes revealed a unidirectional relationship between them. Whereas the loss of *CPC* did not influence *TRY*, the transcriptional gene expression of *CPC* was enhanced in *try* mutants, interestingly indicating that *TRY* represses *CPC* in wildtype, but not vice versa. The increased expression of *CPC* and *ETC2* as well as the reduced *GL3* expression may explain the lower trichome density in the *try* mutant.

As expected for a scenario missing two important inhibitors, an increased gene expression among the activators was found. *GL1* and *MYB23* were upregulated upon the loss of *CPC/TRY*. Interestingly, the absence of *TRY* caused downregulation of *GL3*, meaning that the inhibitor *TRY* promoted - and not repressed - the expression of the activator *GL3* in wildtype. However, this effect was not detectable in the *cpc try* double mutant, underlining the diverse functions of both genes. However, the activation of *GL1/MYB23* could also contribute to the unaffected *GL3* expression in the *cpc try* double mutants. The upregulated *GL1/MYB23* expression may also explain the increased expression of the inhibitor *ETC1*, underlining the importance of adding another inhibitor when modeling the *cpc try* double mutant. Interestingly, the otherwise unaffected *TTG1* gene expression reached the 2-fold threshold in the *cpc try* double mutant.

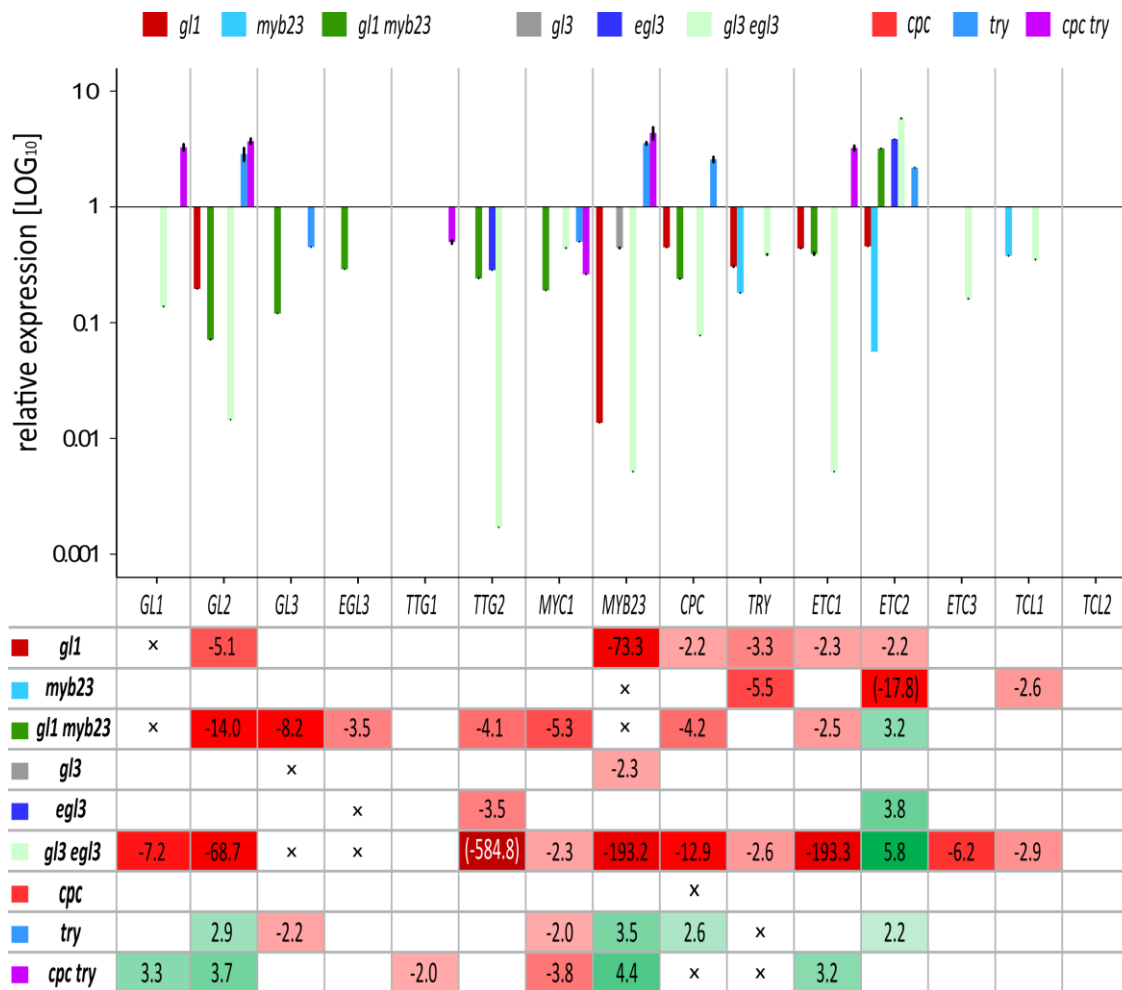


Figure 22: Transcriptional expression analysis of prominent double mutants in *A. thaliana*. Depicted is the bar plot with the relative expression changes compared to Col-0 wildtype and the corresponding fold changes upon a 2-fold cut-off. Expression differences less than the 2-fold threshold lead to empty fields. Upregulations are highlighted in green, downregulations in red; the darker the color, the stronger the regulation. Individual gene expressions in the corresponding mutant background were not considered and are indicated by an x. Values of unexpressed genes are bracketed.

In the following, the less established double mutants - *myc1 egl3*, *etc1 etc3*, and *etc3 try* - were analyzed. Figure 23 represents the corresponding relative expression levels and fold changes.

myc1 egl3

First, the transcriptional cross-regulation in the *myc1 egl3* double mutant and their single mutants was investigated. There was neither an effect on *EGL3* in the *myc1* background, nor on *MYC1* in *egl3* mutants, revealing no direct functional dependency of these two bHLH activators. Generally, the single as well as the double mutants altered the expressions of only a few of the different trichome patterning genes.

Strikingly, only the *ETC2* expression was upregulated; slightly higher in the *myc1 egl3* double mutant than in the individual single mutants. However, due to the very low expression of *ETC2* and its exceptional role, it is difficult to speak of an additive or redundant function. Besides *ETC2*, none of the other inhibitors were increased, but *ETC3* and *TCL1* were downregulated, which could explain the decreased trichome density. On the activator side, only *GL3* was reduced, and other activators were unaffected. *TTG2* was reduced in the *egl3* single and the *myc1 egl3* double mutants, which was surprising as it was otherwise only downregulated in glabrous mutants.

Interestingly, although fewer trichomes emerge on *myc1* mutants, only *GL3* was reduced and other activators were unaffected. The finding that the most genes were not altered in this mutant and the system was not buffered by another bHLH, as the *myc1 egl3* double mutant revealed, supports the idea that *MYC1* is not a classical activator but has a different mechanistic purpose within the patterning network.

etc1 etc3

Next, the two ETC mutants, *etc1* and *etc3*, were analyzed in more detail. *ETC1* expression was not changed in the *etc3* background and vice versa, indicating that both genes do not regulate one another on the transcriptional level. Generally, only three patterning genes were affected by the loss of the genes (*GL3*, *MYB23*, and *ETC2*). Interestingly, both single mutants caused a drastic decrease of the *ETC2* expression, leading to the absence of that gene and indicating a positive regulation of both *ETC1* and *ETC3* on *ETC2*. However, an additive effect was not found in the *etc1 etc3* double mutant but a wildtype-like expression level. Looking at the trichome phenotypes, an additive effect was indeed observed. Both single mutants showed an increase in trichome density, which was even higher in the corresponding double mutant. The enhanced trichome number was only reflected by upregulation of *MYB23* in the double and the *etc3* single mutant. The latter actually revealed a decrease in *GL3* expression, suggesting that *ETC3* activates *GL3* but represses *MYB23* in wildtype. Together, the results indicated no functional redundancy of *ETC1* and *ETC3* beyond the set threshold.

Another interesting point is that although the ETCs are classified as “enhancer of triptychon and caprice”, neither *TRY* nor *CPC* were influenced in the *etc1* or *etc3* single mutant or the corresponding double mutant. Thus, enhancement does not appear to occur at the transcriptional level.

etc3 try

Last, the transcriptional cross-regulation of *ETC3* and *TRY* were studied in each single and the corresponding double mutant. Again, both genes did not regulate each other since the *TRY* expression was unchanged in the *etc3* mutant and vice versa. Generally, the absence of the genes influenced few other patterning genes and revealed no strong redundancy. Interestingly, most gene regulations were slightly weaker in the double mutant than in the *try* single mutant, although *ETC3* is declared to enhance *TRY*. Only the *GL1* expression was increased in the double mutant but unaffected in the corresponding single mutants, indicating an overlapping function.

The increased *MYB23* expression in the single and the double mutant indicates that the R3 MYB inhibitors *ETC3* and *TRY* repress *MYB23* in the wildtype situation, fitting the common opinion that they inhibit one of the activators with which they compete for binding to the bHLH factor. The same result was found for the *GL1* expression, as it was upregulated in the *etc3 try* and *cpc try* double mutants.

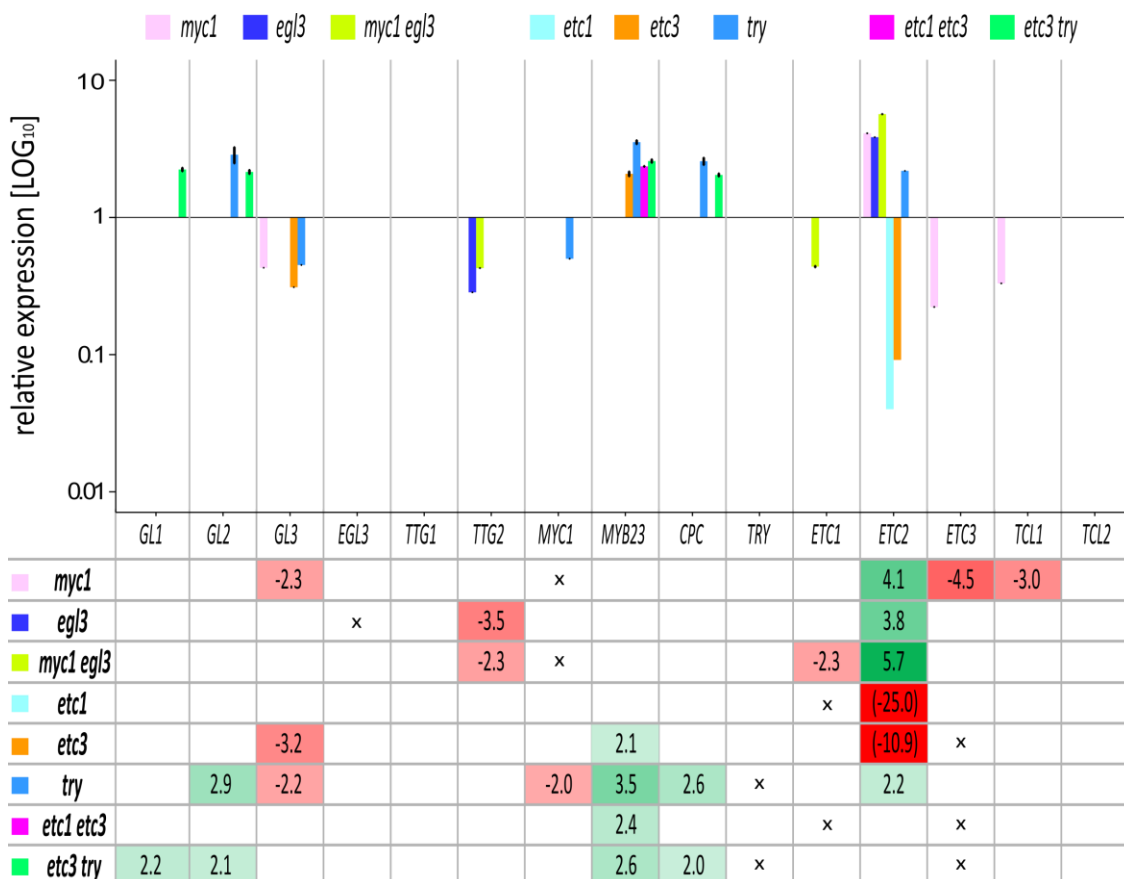


Figure 23: Transcriptional expression analysis of subordinated double mutants in *A. thaliana*. Depicted is the bar plot with the relative expression changes compared to Col-0 wildtype and the corresponding fold changes upon a 2-fold cut-off. Expression differences less than the 2-fold threshold lead to empty fields. Upregulations are highlighted in green, downregulations in red; the darker the color, the stronger the regulation. Individual gene expressions in the corresponding mutant background were not considered and are indicated by an x. Values of unexpressed genes are bracketed.

Summary of transcriptional expression in *A. thaliana* and its mutants

This section shortly summarizes the key results of the intensive intraspecies transcriptional expression study in *Arabidopsis thaliana* and 21 mutants. An interaction scheme was worked out, illustrating the mutual positive or negative regulatory influences of the core components (Figure 24). Although many indications claim a third inhibitor, none can be clearly named on the basis of the conducted transcriptional analysis. Therefore, the scheme is restricted to the inhibitors *CPC* and *TRY*. The entire network interaction scheme can be found in the appendix (Figure S12).

TTG1 was by far the highest expressed gene in Col-0. It was very stable and robust in all mutant backgrounds, but regulated many other genes.

GL2 cannot be considered a pure downstream gene of the network. The effects on other patterning genes - activators and inhibitors - in the *gl2* mutant suggest an active function in the cross-regulatory machinery.

GL3/EGL3 and *GL1/MYB23* can be considered as functional units. A mutual activation loop was detected as *GL3/EGL3* activates *GL1/MYB23* and vice versa. This positive feedback loop is essential to pass the activation threshold and establish the trichome patterning machinery. The most and strongest expression reductions were found in the *gl3 egl3* double mutant, suggesting a fundamental role of *GL3/EGL3*. *GL3* expression was downregulated in the mutants of *try*, *etc3*, and *tcl2*, indicating a positive influence of these inhibitors on *GL3*.

The loss of *MYC1* was not compensated by another bHLH factor, and the analysis revealed no redundant function. Together with the generally low impact on the patterning genes, *MYC1* is likely an activator with a unique purpose in the system.

Interestingly, the inhibitor *TRY* repressed the inhibitor *CPC*, but not vice versa. Both genes showed redundant and divergent functions. All investigated genes were unaffected upon the loss of *CPC*.

ETC2 was by far the lowest expressed gene and revealed no impact on other patterning genes. Its expression was absent in various *Arabidopsis* mutants.

TCL2 promotes the expression of *TCL1*, but not vice versa.

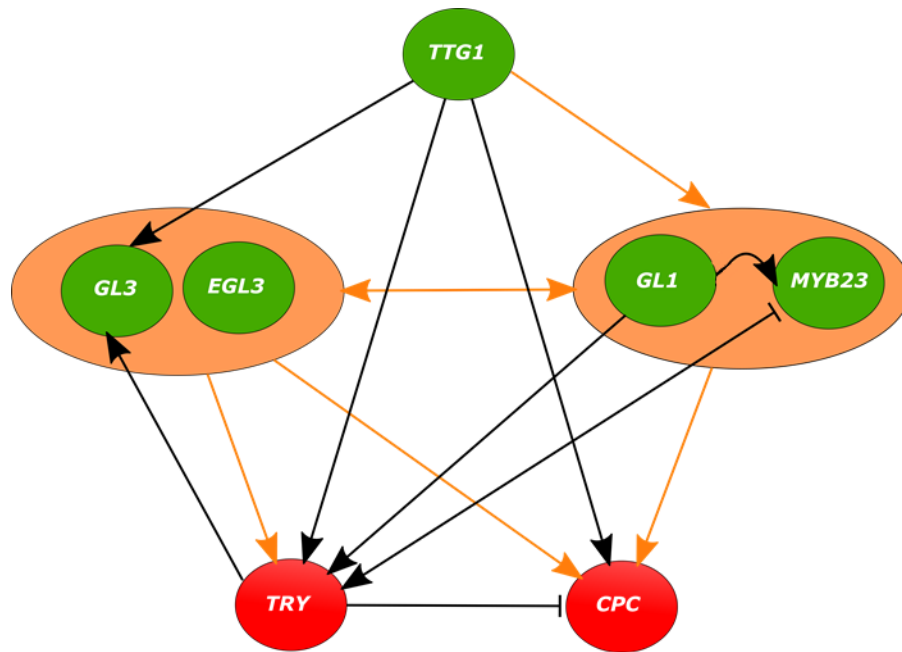


Figure 24: Cross-regulatory interaction scheme of the core components. Illustrated are the interaction dependencies based on the transcriptional expression profile upon a 2-fold cut-off. Activators are indicated in green, inhibitors in red. Orange ellipses contain functional units. Orange lines refer to functional units, black lines to single genes. Promoting regulations are marked by arrowheads, repressing regulations by blunt ends.

3.6. Trichome patterning in different Brassicaceae

Although the trichome patterning network consists of 15 genes, different trichome phenotypes can already be explained by far fewer genes. To identify the relevant core components, a comparative interspecies approach was chosen to analyze the patterning genes in *A. thaliana*, *A. alpina*, and *C. hirsuta*. The known activator and inhibitor complexes of Arabidopsis were in the focus of this study to answer whether the involved genes exhibit similar expression levels in all three species.

Most of the *TTG1* network genes are already annotated in *A. alpina*. No gene ortholog was so far identified for *AaETC2* and *AaTCL1*. Here, a BLAST search was performed with the *A. thaliana* sequence against the *A. alpina* genome. The intron/exon structure was rebuilt based on Arabidopsis, and primer pairs were subsequently designed and tested.

The *A. thaliana* CDS of the patterning genes was utilized to employ a BLAST search within the *C. hirsuta* genome. The most promising hit was verified by synteny, and primer pairs were designed according to the intron/exon annotations. Short annotations were found for *ChTCL1* and *ChTCL2*, but the fragments could not be amplified.

All core components and most of the other patterning genes are present in the three species, and rosette leaves produce a regularly distributed trichome pattern. However, a previous work revealed differences in trichome density and first functional diversifications; i.e., in *Arabidopsis*, simultaneous mutations in *AtGL3* and *AtEGL3* are required to obtain glabrous leaves, whereas *Aagl3* is sufficient to generate the same phenotype (Chopra et al., 2019). Trichome phenotypes in *Cardamine* were so far not in the focus of research, but may be interesting as *C. hirsuta* is more closely related to *A. thaliana* than *A. alpina* (Koch et al., 2001).

To enable an optimal comparison of trichome formation and its underlying cross-regulations in the three Brassicaceae, a comparable leaf development stage has to be selected. As in *A. thaliana*, rosette leaves of *A. alpina* and *C. hirsuta* can be classified as juvenile or adult. In *A. alpina*, juvenile leaves are characterized by small and simple leaves with smooth margins, and roundish blades (Park et al., 2017). Based on this morphology, leaf three was chosen as the first adult leaf in *Arabis*. In *Cardamine*, leaves one to three exhibit a more rounded terminal leaflet and less than four leaflets (Cartolano et al., 2015), announcing them as juvenile. Therefore, *Cardamine* leaves were considered adult from leaf number four and taken for further experimental work.

3.6.1. Comparison of trichome density in Brassicaceae

At first glance, trichome distribution might appear similar in *A. thaliana*, *A. alpina*, and *C. hirsuta* mature leaves. Taking a closer look, differences between the species become apparent. To compare the three Brassicaceae, trichome density was determined on mature leaves. Again, density was determined from the quotient of the area by the trichome number. The juvenile-to-adult phase transition occurs later in *Cardamine*. Therefore, leaf four was analyzed instead of leaf three as in *Arabidopsis* and *Arabis*. As all species exhibit their individual generation time, samples were taken after leaf growth was completed. In contrast to the other two species, *Cardamine* forms compound leaves, and initial experiments revealed that the terminal leaflet is the best to study trichome patterns. Due to its large size, a square, which was comparable to the total leaf size of *A. thaliana* leaves, placed in the same region of each terminal leaflet was investigated. A smaller square was chosen for *A. alpina*, to ensure a feasible counting of the dense growing trichomes (Figure 25).

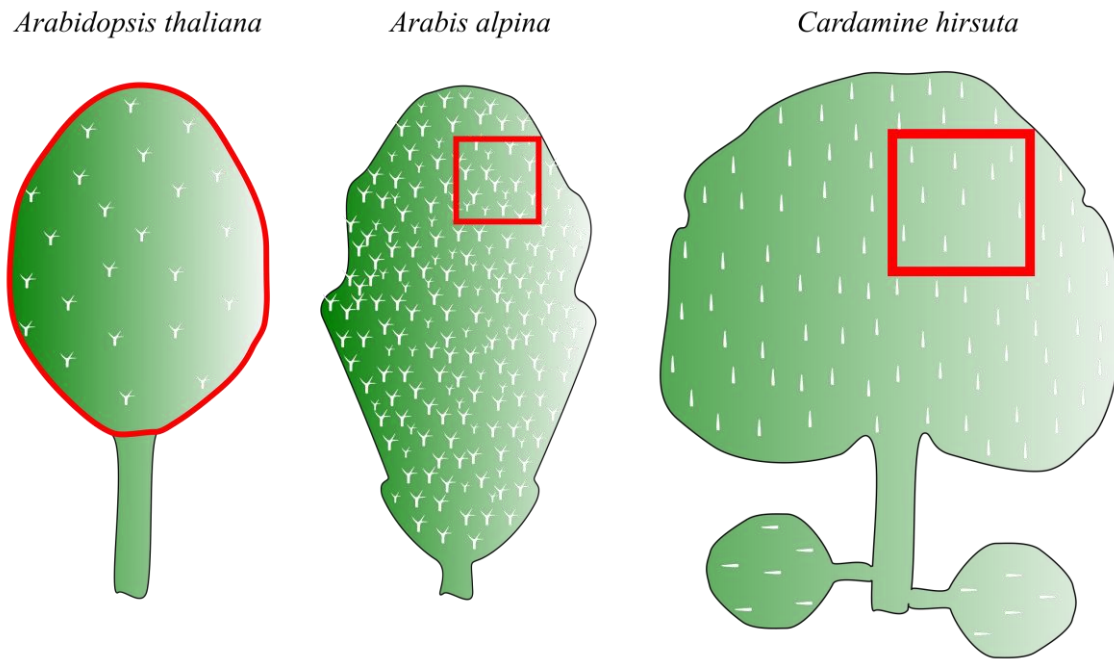


Figure 25: Schematic illustration of trichome counting areas on rosette leaves. Depicted are leaves for *A. thaliana*, *A. alpina*, and *C. hirsuta*. Red borders mark counting regions; entire leaf for *A. thaliana*, 25 mm² for *A. alpina*, and 100 mm² for *C. hirsuta*.

Interestingly, *C. hirsuta* leaves exhibit less than half of the trichomes on the blade than *A. thaliana* (Table 14). However, as expected, trichome density in Arabis is much higher than in the other two species; approx. 3.5-fold higher as in Arabidopsis and even 8-fold as in Cardamine.

Table 14: Leaf area, trichome number, and density of three Brassicaceae. For *A. thaliana* and *A. alpina* leaf three was analyzed, for *C. hirsuta* leaf four. Mean values and standard deviation are given for ten replicates each.

	Area [mm ²]	Trichome number	Density [Trichomes / mm ²]
Arabidopsis	93.2 ± 15.8	88.9 ± 11.4	1.0 ± 0.1
Arabis	25.0 ± 0.0	82.9 ± 13.4	3.4 ± 0.6
Cardamine	100.0 ± 0.0	41.9 ± 6.3	0.4 ± 0.1

3.6.2. Patterning gene expression in different Brassicaceae

This chapter deals with the transcriptional regulation of patterning genes in different Brassicaceae. The expression was analyzed in the wildtype accessions *A. thaliana* Col-0, *A. alpina* Pajares, and *C. hirsuta* Ox.

It is challenging to compare expression levels in different species. Despite the sequence similarity of the patterning genes, different primers were required to perform the experiments, and the results had to be normalized to different reference genes. Therefore, the expression values cannot be directly correlated with each other. To overcome this issue, each species was normalized to the same gene, followed by the comparison of the obtained ratios. Here, *GL3* was chosen as reference gene because of its position as the central and connecting element within the MBW activator complex. Consequently, any ratio changes of the other patterning genes should occur with respect to *GL3*.

The analysis of the transcriptional regulation in *Arabidopsis* and its mutants revealed a strong additive effect and redundant function of *GL3* and its homolog *EGL3* (Chapter 3.5.2). The same result was found for the homologous genes *GL1/MYB23*, albeit less severe. To take this into account, the interspecies approach was finally conducted by studying the gene expression ratios relative to the combination of *GL3/EGL3*, instead of just *GL3*. The theoretical modeling approach supports the idea of combining the redundant homologs (Anna Deneer, personal communication), as the relative expressions obtained from the qPCR experiments fit the model much better and reduce the overall error, suggesting compensatory effects.

In contrast to *A. thaliana*, only some studies exist for *A. alpina* regarding the trichome phenotypes in different mutant backgrounds. In *C. hirsuta*, nothing is known, limiting the conclusions of this comparative analysis. Therefore, the comparison between the species concentrates on the expression shifts after the normalization to the functional unit *GL3/EGL3*, e.g., from an increased to a decreased regulation.

To begin with, the relative expression differences of *GL3* and *EGL3* between the three species were studied (Figure 26A). In *Arabidopsis*, *EGL3* expression was higher than *GL3*. This enhanced expression of *AtEGL3* and the largely overlapping functions of the corresponding proteins were the conceptual basis to consider both genes as functional unit. Remarkably, *EGL3* was lower expressed in *Arabis* and similarly in *Cardamine* compared to *GL3*. On the one hand, the lower *AaEGL3* expression supports less relevance of the corresponding protein for the network, since already *Aagl3* mutants show the same glabrous phenotype as *Atgl3 Ategl3* doubled mutants (Chopra et al., 2019). On the other hand, the combination of *AaGL3/AaEGL3* was required for the developed mathematical trichome patterning model, suggesting a relevant role for the network despite the lower expression of *AaEGL3* and the non-additive phenotype (Anna

Results

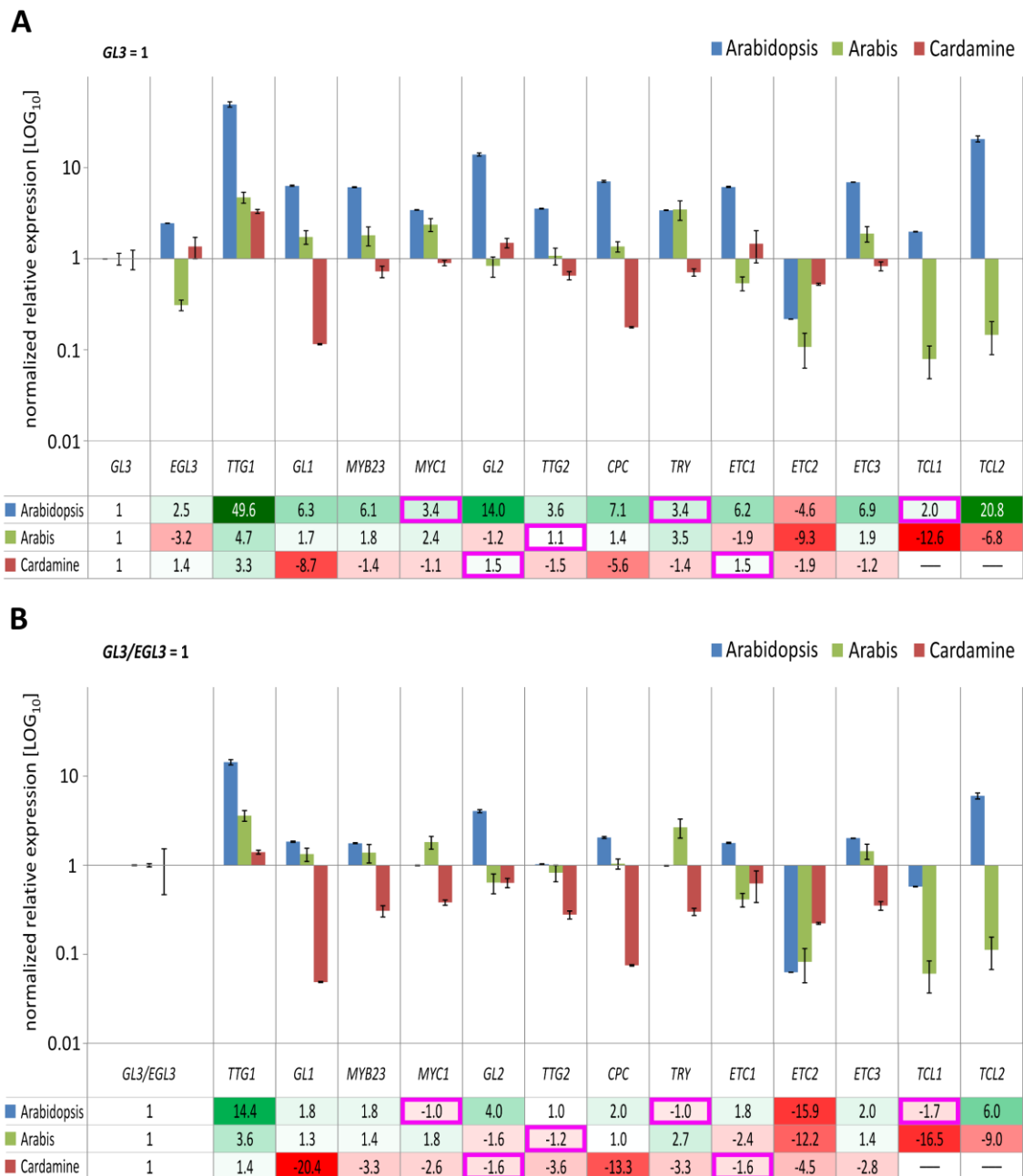


Figure 26: Comparative patterning gene expression in three Brassicaceae. Depicted are the relative expressions and fold changes of 15 patterning genes in *A. thaliana* (blue), *A. alpina* (green), and *C. hirsuta* (red) normalized to *GL3* (A) or *GL3/EGL3* (B). Regulations higher than the reference are highlighted in green, lower regulations in red; the darker the color, the stronger the expression. Pink borders indicate regulatory switches towards a decreased expression upon *GL3/EGL3* combination.

Deneer, personal communication). The similar *ChGL3* and *ChEGL3* transcription levels indicate a balance between both genes and do not exclude a potential consideration of *ChGL3/ChEGL3* as one functional unit.

When considering *GL3/EGL3* a functional unit, particularly the regulatory switches from an increased to a decreased expression are of interest. Among all three species only a few shifts occurred, suggesting a generally stable expression scheme and further supporting the idea of the combined consideration of *GL3/EGL3* (Figure 26B).

In Arabidopsis, switches from increased to decreased expression occurred in *MYC1*, *TRY*, and *TCL1*. This is interesting, as previous experiments suggest that *AtMYC1* is not a classical activator but rather a stabilizing factor. Perhaps, less *AtMYC1* in the system is sufficient to fulfill its stabilization purpose. *TRY* switched from an enhanced to a reduced regulation, while the expression of the other key inhibitor *CPC* remained upregulated, indicating a more dominant role of *CPC* compared to *TRY* within the system. This is particularly interesting, as the intraspecies analysis (Chapter 3.5.2) revealed a negative influence of *TRY* on *CPC*. The downregulation of *TRY* upon the *GL3/EGL3* combination may compensate this regulatory effect. Likewise, the reduced *TCL1* expression may be balanced by the highly expressed *TCL2* gene.

In Arabis, exclusively *TTG2* switched regulatory directionality. However, the difference was slight and may just be a consequence of reduced *GL2* expression, as long as the known overlapping functions of these genes from Arabidopsis (Johnson et al., 2002) also apply for Arabis. Furthermore, it is worth noting that *CPC* was less expressed than *TRY*; the opposite to Arabidopsis, suggesting an exchanged relevance for the Arabis network.

In Cardamine, *GL2*, and *ETC1* were shifted to a reduced expression. This may indicate a lower relevance of these genes within the system. However, besides *TTG1*, *GL3/EGL3* were the highest expressed genes among all Cardamine trichome patterning genes. Consequently, all other genes were reduced when normalized to *GL3/EGL3*, relativizing the significance of downregulation in this species. As in Arabis, *ChCPC* had a minor role than *ChTRY*, again suggesting a shifted importance or regulation of the core component compared to Arabidopsis. Surprisingly, *GL1* was strongly reduced in Cardamine, raising the question of whether it another here not-examined gene compensates it or whether the Cardamine network is fundamentally differently organized and regulated.

Finally, also *GL1/MYB23* were considered as a functional unit, due to their partial redundancy in Arabidopsis. The obtained expression ratios based on the *GL3/EGL3* normalization were supplemented by *GL1/MYB23*. As a result, all other genes were unaffected, and only the individual *GL1* and *MYB23* gene expressions were compared to the *GL1/MYB23* combination (Figure 27). Generally, the same regulatory tendencies were found among all species. In Arabidopsis and Arabis, already the individual genes showed an increased expression compared to *GL3/EGL3*. The *GL1/MYB23* combination enhanced this effect. That is interesting, as a positive

feedback loop was elucidated between both pairs in Arabidopsis. In Cardamine, the individual expressions of *GL1* and *MYB23* were reduced. The combination of both compensated this regulation. Nevertheless, *GL1/MYB23* were less expressed than *GL3/EGL3*. However, it has to be mentioned that the drastically reduced *ChGL1* level was buffered by the combination of *ChGL3/ChEGL3*, demonstrating a potential compensator of *ChGL1*. Taken together, due to the synchronous regulation of *GL1* and *MYB23* in all species, redundancy or the formation of a functional unit cannot be ruled out either in Arabis or in Cardamine. Particularly, the strong compensatory effect of *ChGL1* by *ChMYB23* supports the idea of their consolidation for a proper acting network.

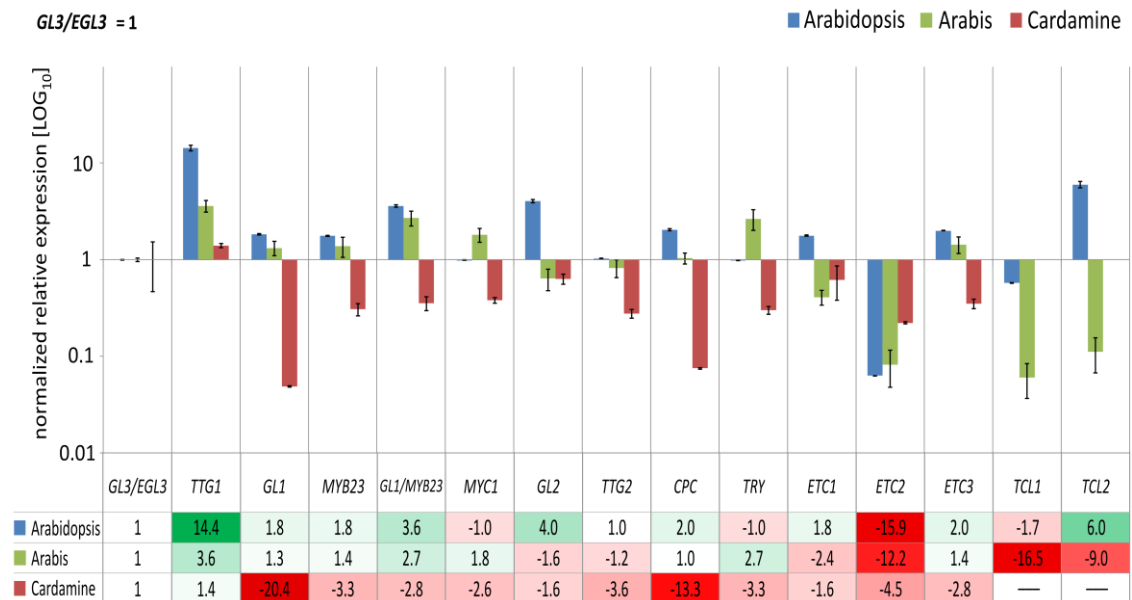


Figure 27: Comparative patterning gene expression combining functional units. Depicted are the relative expressions and fold changes of 15 patterning genes in *A. thaliana* (blue), *A. alpina* (green), and *C. hirsuta* (red) normalized to *GL3/EGL3*. *GL1* and *MYB23* are shown separately or combined. Regulations higher than the reference are highlighted in green, lower regulations in red, the darker the color, the stronger the expression.

3.6.3. Comparison of gene expression in *Atgl2* and *Aagl2* mutants

The previously described comparison of the patterning gene expressions in related species (Chapter 3.6.2), represented a first attempt to elucidate the evolution of the conserved *TTG1* network. However, conclusions are limited since trichome mutant phenotypes are rarely characterized in any Brassicaceae besides Arabidopsis, preventing the correlation of gene expression and phenotype. To partially close this gap and provide some further insights, the gene expression of Arabis *Aagl2* was compared to the *Atgl2* mutant.

The wildtype trichome phenotype in *A. alpina* is characterized by small and large trichomes. In *Aagl2*, the large trichomes are unaffected, but the small ones are underdeveloped (Chopra et al., 2019). In contrast, the *AtGL2* mutation in *A. thaliana* causes glabrous leaves, besides occasional trichomes at leaf margins, which are partially underdeveloped (Figure 16).

Here, the transcriptional expressions were compared between *Atgl2* and *Aagl2* mutants, normalized to their corresponding wildtype (Figure 28). Strikingly, the comparison revealed strong differences in most genes. The gene expressions were mainly reduced in Arabidopsis, but increased in Arabis. *Atgl2* revealed mainly slight to moderate reductions, besides a strong downregulation of *AtMYB23* and absent *AtETC3* expression. Arabis showed moderate to strong enhancements. Particularly, *AaEGL3*, *AaETC1*, *AaETC2*, *AaTCL1*, and *AaTCL2* were drastically increased, suggesting repression of these genes by *AaGL2* in the wildtype situation. Interestingly, an increase was also found for the activators *AaGL3/AaEGL3* and *AaGL1/AaMYB23*, indicating a negative regulation by *AaGL2* in wildtype.

Both species revealed an increased gene expression in *EGL3*, *ETC2*, *TCL1*, and *TCL2*. However, the upregulation was always much higher in Arabis. Only *TTG1* and *TRY* had a negative tendency in both Brassicaceae, and were regulated at a similar level. Interestingly, *AaTRY* was the only inhibitor that was decreased upon *AaGL2* mutation and, behaved differently than *AaCPC*, suggesting a diverse regulation of these putative key inhibitors.

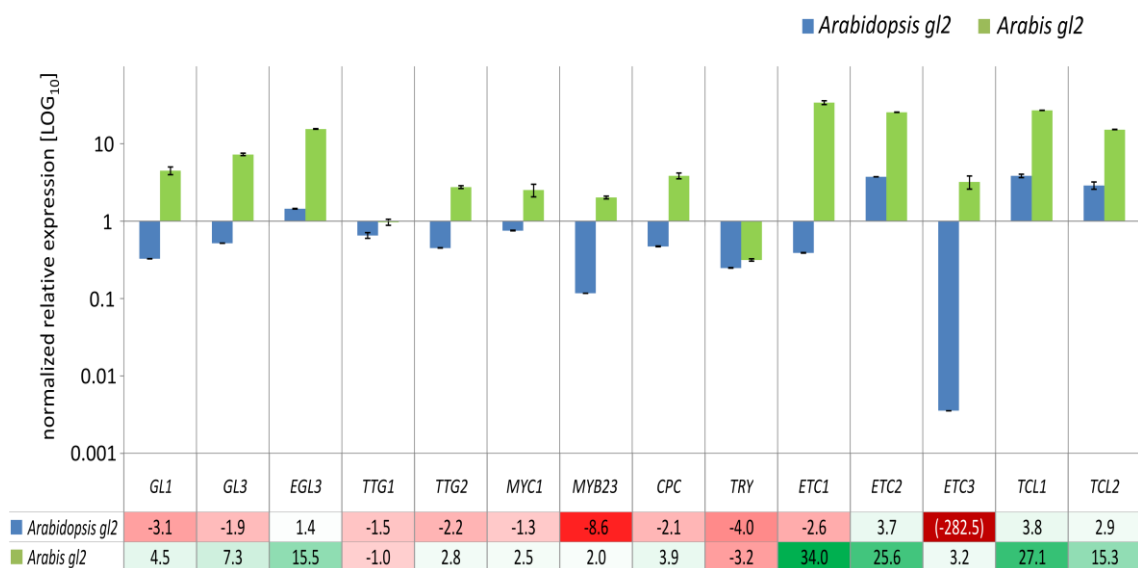


Figure 28: Comparison of gene expressions in *Atgl2* and *Aagl2*. Depicted are the relative expressions and fold changes of 14 patterning genes in *A. thaliana* (blue), and *A. alpina* (green) normalized to its corresponding wildtype. Upregulations are highlighted in green, downregulations in red; the darker the color, the stronger the regulation. The value of an unexpressed gene is bracketed.

It applies for both species that the absence of *GL2* caused many changes in the gene expressions, albeit in different directions. *Atgl2* showed downregulations of most genes, *Aagl2* upregulations. This indicates that *GL2* has an essential function in both species but acts differently. These results indicate that similar to *AtGL2*, *AaGL2* cannot be considered a pure downstream gene of the network, as it cross-interacts with many other patterning genes.

3.6.4. Synteny of *GLI* in related Brassicaceae

As *GLI* is one central component of the trichome network, its relatively low expression in the very young leaf material of Cardamine prompted to confirm the correct selection of this gene. The *GLI* synteny of *A. thaliana*, *A. alpina*, and *C. hirsuta* was compiled, using the first one as a reference. The *AtGLI* sequence was applied to BLAST against the *C. hirsuta* CDS database. Around a dozen genes up- and downstream of the first three highest-ranked hits were investigated by performing a BLAST search against Arabidopsis. To underpin the outcome, the procedure was repeated for the *AaGLI* ortholog. Based on the developed synteny and gene annotations, the first three hits could be identified as the MYB homologs *ChGLI* (CARHR149430), *ChMYB23* (CARHR261770), and *ChWER* (CARHR198560; Figure 29). Thus, the correct sequence was used to study *GLI* expression in *C. hirsuta*.

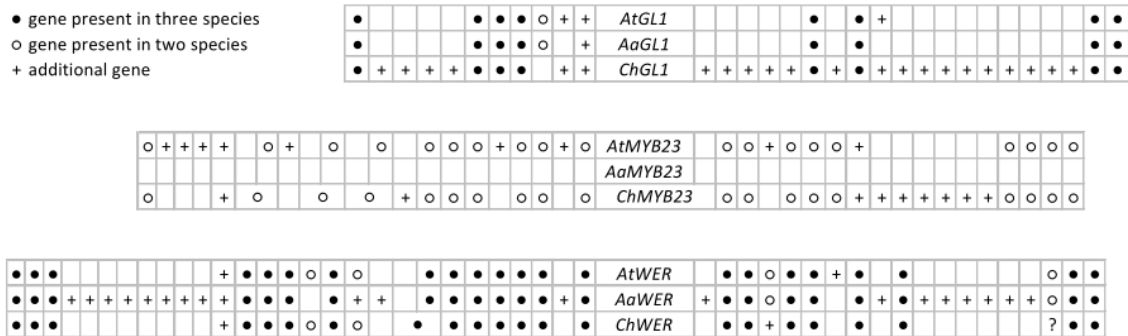


Figure 29: Synteny of *GLI*, *MYB23*, and *WER* in *A. thaliana*, *A. alpina*, and *C. hirsuta*. Each column represents one gene locus. Filled circles display gene orthologs in all three species, empty circles in two species. Pluses indicate additional genes. Merged cells mean that two loci correspond to one gene.

3.6.5. Expression of MYB homologs in multiple tissues

Since *ChGLI* expression was low in developing leaves with on-going trichome patterning, two main questions arose: a) Is *GLI* higher expressed in other tissues, and b) Do homologs compensate for it? A quantitative assay compared the gene expression of *C. hirsuta GLI* with its homologs *MYB23* and *WER* in whole seedling samples, shoot and root, as well as mature leaves, and those with on-going trichome patterning (tiny leaves). The set was completed by investigating *A. thaliana* and *A. alpina* under the same conditions (Figure 30). All results were first normalized species-wise and then related to the expression of *GLI* in tiny leaves to enable a comparison between the different species. Sample integrity was confirmed by actin amplification (data not shown).

Fitting previous studies (Kirik et al., 2001; Larkin et al., 1994), *AtGLI* was not expressed in roots but replaced by *AtWER*. *AtGLI* was moderately expressed in seedlings and shoots, whereas *AtMYB23* was strongly expressed in whole seedling samples, shoots, and mature leaves. *AtMYB23* in mature leaves was similarly high as *AtWER* in roots, in seedlings and shoot samples even higher. This was particularly interesting as *AtGLI* was absent in mature leaves, suggesting a developmental/temporal activity of *AtGLI* in tiny leaves and *AtMYB23* in mature leaves. Surprisingly, *AtWER* was also found in tiny leaves; indeed half as much as *AtGLI*, but clearly detectable, opening new mechanistic windows.

A leaf age-dependent effect was partially found in Arabis and Cardamine. As in Arabidopsis, *AaGLI* and *ChGLI* were very weakly expressed or absent in mature leaves, but *AaMYB23* and *ChMYB23* were found. However, in Arabis, the expression of *AaMYB23* in mature leaves was only half as high as of *AaGLI* in tiny leaves, and *ChMYB23* was similarly to slightly higher expressed in mature leaves than *ChGLI* in tiny leaves. Generally and in contrast to the other MYB homologs, *MYB23* was present in all tissues and species.

Surprisingly, *GLI* was found in roots of Arabis and Cardamine. This was totally unexpected and indicates a divergent gene function between Arabidopsis and the other two Brassicaceae. *ChGLI* expression was absent in the shoot sample, although it was found in tiny leaves. This might be explainable by the small fraction of tiny leaves within the entire shoot tissue.

ChWER was strongly expressed in tiny leaves, even higher than *ChMYB23* and *ChGLI*. This explains the low *ChGLI* expression in the comparative wildtype approach

with all patterning genes (Chapter 3.6.2) and indicates a functional replacement during evolution. Whereas the *AtWER* expression was only high in roots, *ChWER* was highly expressed in roots and tiny leaves, indicating the lack of the tissue-specific diversity of these homologs as in Arabidopsis. In line, *ChWER* was highly expressed in many tissues, while *AtWER* was predominantly found in roots, and the *AaWER* expression was uniquely detectable in roots.

Comparing the three homologs, the *ChGLI* expression was generally low in all examined plant tissues. This raises the question about its general impact on the trichome network in Cardamine. Moreover, it seems that the MYB factors *ChMYB23* and particularly *ChWER* play a major role in the entire plant; the latter especially in young leaves, where trichome initiation and formation is still in progress. The opposite was found for Arabis. There, *AaWER* has a minor role and was almost absent in the whole system, besides its strong function in roots. Surprisingly, *AaGLI* expression was detected in roots, while *AtGLI* was completely absent in Arabidopsis. Generally, the transcriptional expression scheme of Arabidopsis and Arabis are more comparable to each other than to Cardamine.

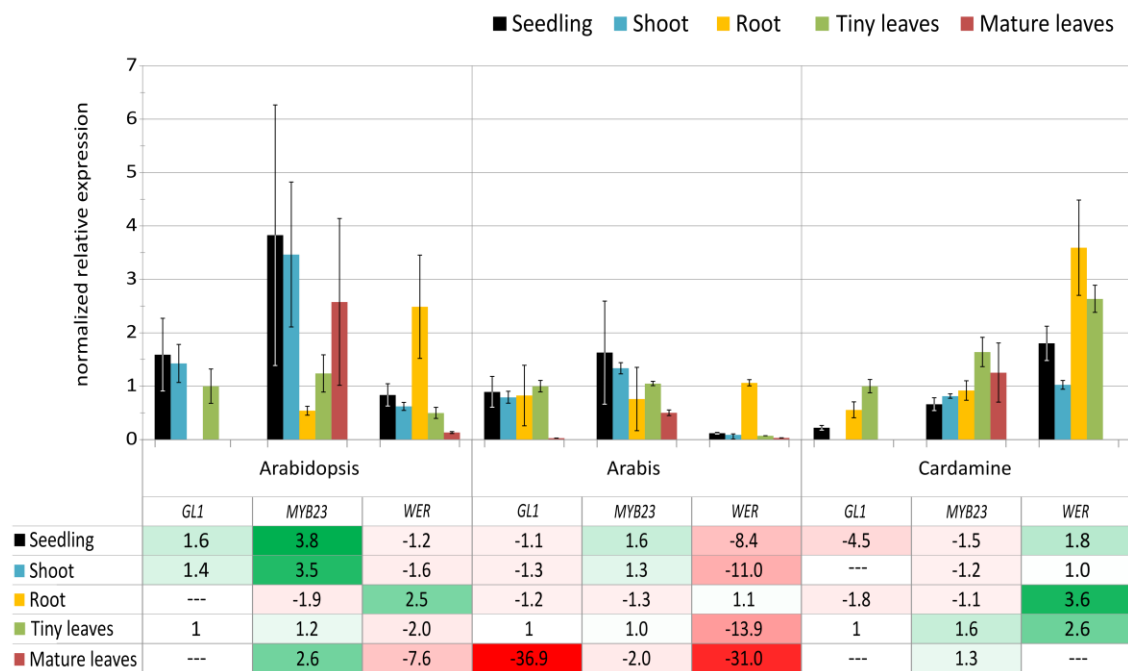


Figure 30: Quantitative expression analysis of three MYB homologs in different species and tissues. Depicted are the relative expressions and fold changes of *GLI*, *MYB23*, and *WER* in *A. thaliana*, *A. alpina*, and *C. hirsuta* in seedlings (black), shoots (blue), roots (yellow), tiny leaves (green), and mature leaves (red) normalized to *GLI* expression in tiny leaves. Upregulations are highlighted in green, downregulations in red; the darker the color, the stronger the regulation.

4. Discussion

The focus of this study was the comprehensive analysis of trichome patterning genes in *Arabidopsis thaliana* and two related Brassicaceae. The investigated patterning genes participate in the conserved antagonistic *TTG1*-dependent network and are in the focus of research for several decades. However, a detailed analysis of the cross-regulatory interactions of all genes remained elusive. To close this gap, an extensive and systematic examination of 15 patterning genes in 21 mutants was conducted, extended by a comparative approach in two related species.

It turned out that only a few of the patterning genes are essential to generate a regularly distributed trichome pattern on rosette leaves. These include the eponymous gene *TTG1*, whose absence causes glabrous leaves; either *GL3* or *EGL3*, due to their high redundancy; and the activator *GL1*, whose absence also causes glabrous leaves. Despite its overlapping function with *GL1*, *MYB23* is not essential. Although the loss of the inhibitor *CPC* does not affect the expression of any other gene, the *cpc try* double mutant underlines the position of both genes as essential core components within the network. However, the *cpc try* double mutant is insufficient to initiate a trichome fate from each epidermal cell. Therefore, an additional third inhibitor is needed to provide the spacing information. *ETC1* is a plausible candidate for this function due to the presumably higher similarity to *CPC* and *TRY*.

The following sections discuss the obtained results of this study gene-wise and provide outlooks for subsequent experimental research.

GL3/EGL3

Many previous studies claim *GL3* and *EGL3* to be functionally redundant proteins within the trichome patterning machinery (Bernhardt et al., 2003; Morohashi et al., 2007; Zhang et al., 2003). However, the amount of affected genes and their strong reductions in the *gl3 egl3* double mutant were unexpected as even other glabrous mutants showed less severe downregulations. Therefore, *GL3/EGL3* should be considered one functional unit and assigned a fundamental role within the network. This essential property may be because *GL3/EGL3* occupy a central position in the MBW complex and are involved in both possible dimers (Balkunde et al., 2010; Pesch et al., 2015). Interestingly, this does not apply to other genes whose mutants lead to glabrous

phenotypes. The remaining activators in other glabrous mutants may still enable the activation of inhibitors, but less strongly than in wildtype.

The theoretical model from Anna Deneer supports the approach to consider *GL3/EGL3* a functional unit, as, e.g., the obtained expression levels fit the model much better when *AaGL3* and *AaEGL3* are combined, leading to an improved parameter search and a decreased overall error. Moreover, although *Aagl3* alone causes a glabrous phenotype, *AaEGL3* seems to be required for the model, suggesting compensatory effects of *AaEGL3* on *AaGL3*.

Exactly those genes identified as direct targets of *GL3* (*GL2*, *CPC*, and *ETC1*: Morohashi et al., 2007; *TTG2*: Ishida et al., 2007), were strongly reduced or even undetectable in the *gl3 egl3* double mutant. Due to the compensatory function of *GL3* and *EGL3*, the *gl3* single mutant may not be sufficient to introduce such severe gene expression reductions.

Interestingly, *EGL3* was higher expressed than *GL3* in Col-0 wildtype, although the latter represents the more prominent gene. However, this result is in line with previous works (Bernhardt et al., 2003; Zhang et al., 2003). Surprisingly, both genes were relatively lowly expressed compared to various other patterning genes, despite their essential role in the MBW complex. A matter of timing may explain this apparently contradictory phenomenon: It seems that not a general stable expression of *GL3/EGL3* is required for the MBW complex, but a defined expression in a distinct period of time. This hypothesis is supported by previous DEX-induced *GL3* and *EGL3* expressions, which reveal 4 h as sufficient to activate trichome initiation (Morohashi et al., 2007).

GL1/MYB23

Identifying a mutual positive feedback loop between *GL1/MYB23* and *GL3/EGL3* was a striking result of the transcriptional expression analysis, which displays another required element to enhance the activator concentration in a given cell to pass the threshold for trichome initiation.

While *GL3/EGL3* showed no mutual dependency, a strong unidirectional influence of *GL1* on *MYB23* was found. In glabrous *gl1* mutants, only *GL2* and *MYB23* were moderately to strongly reduced, some inhibitors slightly, indicating that this regulatory scheme is sufficient to generate a glabrous phenotype. This finding may elucidate the mechanism behind the glabrous *gl1* mutant phenotype. Either the absence

of *GL1* alone causes the glabrous leaves, or a subsequent step-wise regulation leads to this phenotype. The latter is supported by the finding that each glabrous mutant (*gll*, *ttg1*, *gl3 egl3*) exhibits a particular *GL1* reduction, followed by a stronger *GL2* and *MYB23* reduction. This two-step regulation is in line with previous studies demonstrating that *GL2* is directly activated by *GL1* (Kang et al., 2009) and *GL2* directly binds to *MYB23* (Khosla et al., 2014). Furthermore, this unidirectional cascade clarifies the cause for the generally strong reduction of *MYB23* in all glabrous mutants and the unaffected *GL1* and *GL2* expression in the *myb23* single mutant. Moreover, the *MYB23* expression depends on *TTG1*, while *GL1* does not (Kirik et al., 2005), contributing to the frequently occurring differential regulation of *GL1* and *MYB23*. In addition, it was shown that *MYB23* promotes its own expression in the root (Kang et al., 2009). If this also applies to rosette leaves, it should further contribute to the substantial regulation differences.

However, this regulation scheme may only apply for the here investigated tissue material of very young leaves. As observed from the interspecies expression analysis in different tissues and literature, the *MYB23* expression is much lower in tiny leaves than mature ones and correlates with the trichome developmental stage (Kirik et al., 2005). This suggests age-dependent differential regulation of the participating genes and may also involve genes and signaling pathways beyond trichome patterning.

TTG1

TTG1 was by far the highest expressed gene in *A. thaliana* Col-0 wildtype and, except for the *cpc try* double mutant, not affected by the loss of any other patterning gene. What can be the reason for such a high expression level, and how does the network cope with it?

It seems that the strong *TTG1* expression leads to its saturation within the system so that individual mutants do not affect it, designating *TTG1* a stable and robust key factor. A further hypothesis is that the exact *TTG1* expression is not relevant but its general availability. According to the developed mathematical model, the *TTG1* depletion effect, originating from the activator-depletion model (Bouyer et al., 2008; Pesch & Hülskamp, 2009), is required to establish a trichome pattern (Anna Deneer, personal communication). Thus, *TTG1* is not regulated by a positive feedback loop of other core components and fulfills its purpose as long as it depletes. Furthermore, it is assumable that other factors beyond the trichome genes additionally control the *TTG1*

expression, as *TTG1* regulates four other traits besides trichome formation. Among them, anthocyanin production is also localized in Arabidopsis leaves (Lee, 2002; Matsui et al., 2004), perhaps leading to an increased local expression. In line, *TTG1* is also the highest expressed patterning gene in Arabis and Cardamine.

The *ttg1* mutant showed many expression changes in the other patterning genes, mainly reductions. The incapability of forming the trimeric MBW activator complex due to the absence of *TTG1*, and the subsequent non-activation of the inhibitors, may explain the glabrous mutant phenotype and the strong expression differences of the system. Moreover, weak *ttg1* alleles support the hypothesis of *TRY* activation by *TTG1*. Such alleles display a reduced trichome number (Koornneef, 1981; Larkin et al., 1994, 1999), not completely glabrous leaves, and they form trichome clusters reminiscent of the *try* mutant (Balkunde et al., 2020). The authors provide evidence that this phenotype is based on the *TRY* regulation by *TTG1*, which is in line with the results obtained in this study. Further studies substantiate this finding, showing a direct regulation of *TRY* by *TTG1* (Pesch et al., 2015; Schnittger et al., 1999).

GL2

The number of genes affected in the *gl2* mutant suggested, despite its involvement in later trichome developmental stages, a more cross-interactive function of *GL2* within the network than previously thought. This hypothesis is supported by the direct *GL2* binding on the *MYB23* promoter (Khosla et al., 2014). As, in turn, also *MYB23* directly targets *GL2* (Kang et al., 2009), another positive feedback loop was uncovered. The *MYB23* activation by *GL2* is in line with the here obtained results that *MYB23* is strongly expressed in mature leaves but low in younger ones. Additionally, this correlates with an increased *pGL2* expression in further developed trichomes.

As it was shown that *GL1* binds directly to *GL2* (Kang et al., 2009; Morohashi et al., 2007; Zhao et al., 2008) and the *GL1* expression was reduced in *gl2* mutants, it is assumable that the proteins encoded by other differentially regulated genes in *gl2* also directly target *GL2*. This hypothesis needs to be tested in independent experiments such as chromatin immunoprecipitation or *in silico* methods.

Besides the positive feedback loop between *GL2* and *MYB23*, a mutual negative loop was uncovered between *GL2* and *TCL2* as both genes were upregulated in the opposite mutant background, implying a direct regulation. Again, a specific experimental setup is required for verification.

Finally, although *GL2* and *TTG2* act together in trichome cell outgrowth (Ishida et al., 2007; Pesch et al., 2014), it is interesting that *GL2* activates *ETC1*, whereas *TTG2* represses it, indicating contradictory subsequent regulatory purposes.

MYC1

Several indications classify *MYC1* as an outstanding activator among the patterning genes. The *MYC1* expression was often unaffected upon the loss of individual genes, although no apparent compensation existed between the other bHLH factors *GL3* or *EGL3*. Also, neither the glabrous *gl3 egl3* double nor the *myc1 egl3* double mutant showed a drastic effect or revealed clear overlapping functions. A partial redundancy was shown in Arabidopsis rescue experiments, as *GL3/EGL3* could restore the wildtype trichome pattern in *myc1*, but not vice versa (Zhao et al., 2012). However, *MYC1* may be difficult to detect, as its expression is likely to drop after *GL1* and *GL3* induction (Morohashi & Grotewold, 2009). Accordingly, *GL1* and *GL3* are likely to directly target *MYC1* (Symonds et al., 2011), matching the obtained expressions results in this study as *MYC1* regulation was reduced in the *gll myb23* and *gl3 egl3* double mutants. The reduction in these double mutants, but the unchanged *MYC1* expression in the corresponding single mutants, could be further elucidated by the transcriptional analysis in a *gll gl3* double mutant.

The here investigated *MYC1* promoter lines demonstrated the highest *pMYC1* expression in epidermal cells (and youngest trichomes), but a significant reduction in further developed trichomes, reminiscent of a ubiquitous, trichome-unspecific expression. This finding suggests a divergent, rather trichome-independent function of *MYC1*, in contrast to most patterning genes, which are highly active in trichome cells. This may further explain the rarely occurring gene expression changes in the different mutant backgrounds. It prompts *MYC1* as an exceptional activator and promotes the hypothesis of it being a stabilizing factor within trichome patterning.

The outstanding *MYC1* properties continue on the protein level. It was shown that *MYC1* traps *TRY* and *CPC* in the nucleus, preventing their movement into neighboring cells. Thereby, *MYC1* restricts the lateral inhibition of *TRY* and *CPC* and stabilizes the trichome patterning throughout the leaf blade (Pesch et al., 2013; Schultheiß, 2015). This striking trapping mechanism may explain why almost no activator reductions or inhibitor enhancements occurred in *myc1* mutants, although they showed fewer trichomes. This apparent contradictory situation may be explained by the

hypothesis that the inhibitors are not trapped in the nucleus without MYC1, and can also more distantly repress trichome initiations.

Ratiometric measurements utilizing the viral P2A system independently determined the stabilization property of MYC1 on MYB inhibitors and activators. Remarkably, the MYC1 stabilizing function is likely to be accession-dependent, as the Landsberg *erecta* (*Ler*) ecotype harbors a non-functional *MYC1* allele (Symonds et al., 2011). Consequently, this abolishes the interaction with *TTG1* and *GL3* and implements a different stabilization regulation. It may also apply that the prevented fine-tuning of the patterning proteins upon a non-functional *MYC1* allele leads to a slightly more irregularly distributed trichome pattern. A first hint may be provided since *Ler* shows a different variability in trichome regularity upon a slight temperature increase than Col-0 (Okamoto et al., 2020). Since the authors only described the next-neighbor distance but not the general regularity of the trichome pattern, no direct conclusions can be made whether *Ler* has a more irregular pattern than Col-0. If this turns out to be true, it would further support the idea of MYC1 as stabilizing factor.

Trichome intercalation represents another aspect contributing to the regularly distributed trichome pattern in Col-0. It is defined as the trichome initiation between already further developed ones (Jaegle, 2014). There it was demonstrated that *myc1* produces fewer intercalating trichomes than Col-0, and, interestingly, clusters with *Ler*, which shows no intercalation. Accordingly, the here obtained data revealed a lower intercalation rate for *myc1*. The analysis of the trichome distribution in these lines could support the connection between a particular gene and the degree of pattern regularity due to trichome intercalation.

CPC/TRY

The basic models of trichome patterning require an MBW activator complex for trichome initiation and inhibitor activation (Pesch & Hülskamp, 2009). Without the formation of this trimeric complex, trichome cell fates are avoided, and consequently, no inhibitors are activated. Although glabrous mutants indicate the absence of functional MBW complexes, the inhibitors *CPC* and *TRY* were not always strongly affected in glabrous mutants, indicating another activation source than the trimeric MBW complex. This may be explained by the postulated dimer formation promoting inhibitor activation. Here, the TTG1-GL3 dimer (gene homologs are omitted for simplicity) activates *TRY*, and GL3-GL1 promotes *CPC* (Pesch et al., 2015). However,

these assumptions do not match the here obtained expression results, as *TRY* was slightly more reduced than *CPC* in the *gli* mutant and in all other mutants with unchanged *GL3/EGL3* and *TTG1* expression, suggesting a more complex regulation of *TRY* and *CPC* than exclusively by the TTG1-GL3 or GL3-GL1 dimers. Double or higher-ordered mutants of the corresponding dimers could elucidate this discrepancy.

CPC and *TRY* display the same GUS staining with a ubiquitous expression in young leaves, restricted to the trichome initiation zone in later stages. An elevated expression is found in incipient to mature trichomes (Schellmann et al., 2002). The trichome-dependent *CPC* and *TRY* expression is in line with the here investigated promoter marker lines, although different expression strengths were detected. While *pCPC* increased concomitantly with trichome development, *pTRY* first increased and then gently decreased. However, the more sensitive quantification of the fluorescent lines rather than the qualitative impression of the GUS plants may have caused the expression differences. Nevertheless, the promoter expressions in different developmental trichome stages correlates with the postulated short/long-range effect of both inhibitors (Balkunde et al., 2020; Schellmann et al., 2002), highlighting the short-range effect of *TRY* as a result of a lower expression or a shorter period of expression time. In concert with the different effective ranges, small trichome clusters emerge in the *try* mutant, illustrating the *TRY* function in cells closely to trichomes. Additionally, this mutant shows a reduced number of trichomes, suggesting a higher expression of further inhibitors. Interestingly, it turned out that the inhibitor *TRY* repressed the other inhibitor *CPC*, explaining the decreased trichome density in *try* mutants. This regulatory dependence was not found vice versa.

Remarkably, the absence of *TRY* negatively effects the *GL3* expression, indicating that *TRY* promotes *GL3*. This regulation mode was also found for *ETC3* and *TCL2*, but not for *CPC*, suggesting that inhibitors differentially influence activators. At the same time, the *cpc try* double mutant revealed that both genes repress *GL1/MYB23*, which is in line with the current patterning model (Pesch & Hülkamp, 2009). According to the model, the R3 MYB inhibitors (e.g. *CPC*, *TRY*) compete with R2R3 MYB activators (e.g. *GL1*, *MYB23*) for the binding to bHLH proteins (e.g. *GL3*, *EGL3*), rendering the complex inactive. As *CPC/TRY* repress *GL1/MYB23*, they inhibit a factor with which they compete on protein level, thus negatively regulating their own opponent. Indeed, this dual function was also found for *TCL1* and *TCL2* (Wang & Chen, 2014).

ETCs + TCLs

All inhibitors of trichome patterning in *A. thaliana* belong to the family of R3 MYB transcription factors (Gan et al., 2011; Pesch & Hülskamp, 2004), sharing 37-68% amino acid identity (Wang & Chen, 2014). This consensus substantiates the largely redundant but also divergent properties among them. It was demonstrated that the functions of *ETC1* largely overlap with the most prominent inhibitors *CPC* and *TRY* (Kirik et al., 2004a), leading to an additive trichome phenotype in the *cpc try etc1* triple mutant. In contrast, this effect was not observed in the *cpc try etc2* triple mutant (Kirik et al., 2004b). In accordance with this, the gene expressions of *CPC*, *TRY*, and *ETC1* behaved most similarly in several patterning mutants. They showed reduced expressions, whereas *ETC2* and other inhibitors were unaffected or even increased. Additionally, the fluorescent marker lines revealed a relatively higher *pETC1* expression in expanding and two-branched trichomes than in *pCPC* or *pTRY* plant lines, highlighting the involvement of *ETC1* on trichome patterning.

Furthermore, it was shown that *ETC1* is the second-best competitor against *GL1* for the binding to *GL3* after *CPC*, followed by *TRY*, *ETC3*, and *ETC2* (Wester et al., 2009), underlining the higher redundant role of *ETC1*. It remains elusive where *TCL1* and *TCL2* group, but it was shown that both directly suppress the gene expression of *GL1* (Gan et al., 2011; Wang et al., 2007).

Moreover, redundancy was identified among the *ETCs*. Additive effects were quantified in the *etc1 etc3* double mutant with a significantly higher trichome density than their single mutants. While the densities of *etc1* and *etc3* were similar to *cpc*, *etc2* was significantly reduced. These phenotypes may be due to their evolutionary relationship, as *CPC* clusters with *ETC1* and *ETC3*, while *TRY* groups with *ETC2* and the *TCLs* (Wang & Chen, 2014).

TCL1 and *TCL2* influence trichome patterning, however, not in rosette leaves but other plant structures, such as inflorescence stems and pedicels (Gan et al., 2011). This result is in concert with the *tcl1* and *tcl2* mutants' wildtype-like trichome phenotype on mature rosette leaves and their low impact on other patterning genes.

Interspecies comparison

Due to the lack of data on mutant trichome phenotypes in *A. alpina* and *C. hirsuta*, the possible conclusions of the comparative analysis are limited. Nevertheless, some statements can be made about the conserved *TTG1*-dependent network.

Most of the core components identified in *Arabidopsis* likely act comparably in both other Brassicaceae, though fundamental differences were found as well. *TTG1* was the highest expressed gene in all species, although not as pronounced as in *A. thaliana*. As known from previous work, *Aagl3* is sufficient to create glabrous leaves (Chopra et al., 2019). However, the theoretical modeling approach requires the expression of *AaEGL3* to create the expected trichome pattern (Anna Deneer, personal communication). *ChGL3/ChEGL3* were the highest expressed genes after *ChTTG1* in Cardamine, suggesting a major role in trichome initiation or complex formation. Surprisingly, the essential *Arabidopsis* activator *GL1* was almost undetectable in Cardamine, indicating that either *ChTTG1* and *ChGL3/ChEGL3* are sufficient activators or another gene functionally replaced *ChGL1*. A tissue-specific comparison of the three MYB homologs suggested *ChWER* as functional substitute of *ChGL1*.

On the side of the inhibitors, it was shown that *Aatry* exhibits trichome clusters reminiscent of *Attry* (Chopra et al., 2019). This phenotype and the high expression of *AaTRY* compared to all other inhibitors indicate its conserved function. A different situation was found in Cardamine, as *ChETC1* and *ChETC3* represented the highest expressed genes, followed by *ChTRY*. In contrast, *ChCPC* was the lowest expressed and strongly reduced inhibitor, suggesting differential regulation of *ChTRY* and *ChCPC* in this species. Possibly, the *ETCs* are more active in repressing a trichome cell fate, especially when considering the absence of *TCLs* in Cardamine.

Evolution of the R2R3 MYB homologs *GL1*, *MYB23*, and *WER*

Plant MYB genes are supposed to have evolved from the animal c-MYB family (Braun & Grotewold, 1999) and increased the number of their members by multiple gene duplications 200-500 million years ago (Rabinowicz et al., 1999) before plants have split to mono- and dicotyledons. The R2R3 MYBs represent the largest group among this family (Feller et al., 2011). According to Stracke and co-workers, the representatives *GL1*, *MYB23*, and *WER* cluster together in one subgroup with their unique amino acid motif in the eponymous MYB domain (Stracke et al., 2001). Complementation analyses revealed functional redundancies of the homologous MYB genes in *A. thaliana* (Kirik et al., 2005; Lee & Schiefelbein, 2001; Tominaga-Wada et al., 2012), raising the question of whether this exchange is conserved in related Brassicaceae. The low expression of *GL1* in young Cardamine leaves indicates a first hint for functional divergence.

Interestingly, *AtGLI* was expressed in tiny leaves, but not in mature leaves, whereas *AtMYB23* was found in both stages, but at higher levels in mature leaves. This age-dependent behavior also applies partially to *A. alpina* and *C. hirsuta*. In both species, *GLI* was either fundamentally reduced or completely absent in mature leaves. These results perfectly match previous GUS experiments in Arabidopsis. They reveal a ubiquitous *AtGLI* expression in young leaf primordia, increasing in developing trichomes but dropping during trichome branching. In contrast, *AtMYB23* expression is absent in primordia but highly expressed from early to later trichome stages (Kirik et al., 2005).

AtWER was not exclusively found in roots, but lowly, although detectably, expressed in shoots and tiny leaves, contradictory to the knowledge of its distinct spatial regulation (Lee & Schiefelbein, 1999), but in line with a more recent study, which showed *AtWER* expression in roots, young leaves, shoot apices, rosette leaves, stems, and inflorescences (Seo et al., 2011). Strikingly, *ChWER* was strongly expressed in tiny leaves; at higher levels than *ChMYB23* and *ChGLI*. The latter was generally lowly expressed in all tissues, suggesting a minor role in the network. Contradictory, *ChWER* was moderately to strongly expressed in all examined tissues (besides mature leaves), indicating a broader regulation and no tissue specificity. However, spatial control of *WER* was found for the other two species. Compared to other tissues, *AtWER* was predominantly and *AaWER* exclusively expressed in roots. As Arabis is placed to a different lineage than Arabidopsis and Cardamine (Beilstein et al., 2006; Koch et al., 2001; Nikolov et al., 2019), it remains difficult to predict a hypothetical evolutionary course of tissue specification. Whereas Arabis reveals an exclusive root-specific *WER* expression, the Cardamine/Arabidopsis lineage shows a more intermediate to no tissue specificity. However, a different scenario applies for the *GLI* regulation. *AaGLI* and *ChGLI* are found in roots, while *AtGLI* expression is absent in the Arabidopsis root, indicating that the *GLI* specification evolved after the Cardamine/Arabidopsis divergence. Consequently, detailed investigations of several related species within the corresponding lineages would be essential to provide reliable statements on the spatial regulation and the evolution of these homologous MYB genes.

New insights into the evolutionary MYB development could be provided by interspecies promoter swap or rescue experiments of overexpression lines in various tissues as previous studies demonstrated functional substitutions as well as a divergent behavior in Arabidopsis (Kang et al., 2009; Lee & Schiefelbein, 2001; Zhang &

Hülkamp, 2019). Moreover, an extension of the transcriptional gene quantification is required with all patterning mutants. As mutants without an obvious phenotype may cause effects on the gene regulation network (Simon et al., 2013), they should not be neglected in such an approach.

Perspectives

The here obtained results improve our knowledge of the complex cross-regulatory *TTG1*-dependent network, and the applied methods can be easily extended.

As *Arabidopsis* plants may be exposed to altered environmental conditions during their life cycle, various stress conditions offer a suitable option, to gain more insights into the system's robustness. The expressions of patterning genes could be quantified upon abiotic stresses and compared to trichome features such as number and density, morphology and distribution. Moreover, further double or higher-ordered mutants could be included to reveal more transcriptional dependencies.

Overall, interdependencies and influences found in the expression analyses can be of direct or indirect nature. Therefore, it will be essential to uncover direct binding interactions to sharpen the entire interaction scheme.

Furthermore, certain genes should be studied in more detail. *MYC1* represents a conceivable candidate due to its divergent behavior within the group of activators and presumable stabilization function. Unraveling the degree of trichome pattern regularity in several *Arabidopsis* accessions, including the *Ler* ecotype which was described as *MYC1* mutant, may support this hypothesis. Additionally, *GL3/EGL3* could be considered for further research, as they represent an essential element for a proper acting network, despite their relatively low gene expression. This may be due to the fact that *GL3/EGL3* are strongly expressed during a short period of time, followed by a rapid reduction, which was not reflected by the investigated sample material. A detailed time series of marker lines may provide new insights.

A multitude of patterning mutants in both *A. alpina* and *C. hirsuta* is required to correlate their wildtype gene expressions with the mutant regulation scheme and the trichome phenotypes. This experimental setup could be extended by a tissue-specific approach to further elucidate the evolution of the conserved *TTG1* network. Finally, systematical intra- and interspecies promoter swap analyses may highlight functional redundancies of homologous genes among different Brassicaceae.

5. Appendix

Table S1: Oligonucleotide sequences used for construct generation.

Primer ID	Primer name	Primer sequence 5' → 3'
JP_37	BamHI NLS forward	GGGGGGATCCATGCCAAAGAAGAAAAG
JP_41	SgsI pCPC long forward	GGGGGCGCGCCCGCGCCAGAAAAGCTTTGTATACAACAAATG TGCTTCTTTGC
JP_42	pCPC BamHI ClaI long reverse	GGGATCGATGGATCCCGAACTAATCTGAAGACACGAAACACA CAGAGAAAAGAG
JP_43	SgsI pETC1 long forward	GGGGGCGCGCCGAGAAAAGACTTTGAACTTGCACGCCGGCTT GGAGGAAAAG
JP_44	pETC1 BamHI ClaI long reverse	GGGATCGATGGATCCCTCAAAAAGACACCTTAGTACACAAAGA TTTACGATC
JP_46	SgsI pETC2 long forward	GGGGGCGCGCCGGCCATTAAGCCCTGTTTCCTTTTTTAGTCCA ATCAGATCC
JP_47	pETC2 XhoI long reverse	GGGTCGAGTACAGAGAAACTGAAAATGTAGAGTTTGGAGAA TGCAAGATATAG
JP_52	CFP PstI reverse	GGGGCTGCAGCTTGTACAGCTCGTCCATG
JP_54	attB1 NLS forward	GGGGACAAGTTTGTACAAAAAAGCAGGCTTAATGCCAAAGAA GAAAAGAAA
JP_55	mCherry attB2 reverse	GGGGACCACTTTGTACAAGAAAGCTGGGTTGTTAATTAAGTTG TACAGCT
JP_62	SDM_AAC to TAG forward	ACAAGTTAATTAAGTCCAGCTTTCTTG
JP_63	SDM_AAC to TAG reverse	CAAGAAAGCTGGCTAGTTAATTAAGTTG
JP_67	SgsI pMYC1 2581bp forward	GGGGGCGCGCCCGTTGAGTACAAAAGGGTTTTGTCTTTTAC CAC
JP_68	pMYC1 2581 bp XhoI reverse	GGGGCTCGAGATCTAGATATCGTGAAGAACTGAATTTAAAAG TATGG
JP_69	pMYC1 2581 bp forward	GGGGCCGTTGAGTACAAAAG
JP_70	pMYC1 2581 bp reverse	GGGGATCTAGATATCGTGAA

Appendix

Table S2: Oligonucleotide sequences for *A. thaliana* used for qPCR experiments.

Species	Gene	Primer ID	Primer sequence 5' → 3'	Efficiency	Correlation	Fragment length cDNA	
<i>Arabidopsis thaliana</i>	Genes of interest	<i>GL1</i>	AST_467	GTGAACAAAGGCAATTTCACTG	0.96	-0.995	107 bp
		AT3G27920	AST_468	GTTCTTCCCGTACTCTTTTAGC			
		<i>GL2</i>	AST_451	AAGCTCGTCGGCATGAGT	0.90	-0.991	122 bp
		AT1G79840	AST_452	TTCTCTCGATTTCACTGTCTGG			
		<i>GL3</i>	JP_168	GATCCGCAACAGATTCTAGGCG	0.99	-0.994	184 bp
		AT5G41315	JP_169	GCCAGCTTTCACCTGAGAAGC			
		<i>EGL3</i>	JS_07	GGTCTGTCTCTGCTTCTCAAC	0.96	-0.997	132 bp
		AT1G63650	JS_08	GCTCACTTCTCTCAAGACCTAAC			
		<i>TTG1</i>	JS_01	CGCCTCAGAGCTGTAAACATA	1.04	-0.992	125 bp
		AT5G24520	JS_02	CTCCGAACCAGCCGAATAAA			
		<i>TTG2</i>	JP_163	CCAGTAGCAGCTTCGGTCTC	0.99	-0.990	179 bp
		AT2G37260	JP_164	GTTTGTGACGATTCCCTCG			
		<i>MYC1</i>	AST_463	TGGTCGTCTTCACTTACTCAACC	0.93	-0.992	77 bp
		AT4G00480	AST_464	TTCCTTCTTCATATCTCCATTGTA			
		<i>MYB23</i>	JP_170	CCGAACCTATGGCCAGGGCCAC	0.94	-0.995	172 bp
		AT5G40330	JP_171	GCCGAGGAGCTGTGGAGTCTG			
		<i>CPC</i>	AST_455	AAGGCTTCTTGTCCGAAGAG	1.01	-0.988	108 bp
		AT2G46410	AST_456	CCTGTGCCAACGAGTTTAT			
		<i>TRY</i>	AST_457	ACAGACTTGTCCGGTATAGGTG	1.01	-0.994	69 bp
		AT5G53200	AST_458	CTATCTCCTCTGGTTGTCTTCCA			
<i>ETC1</i>	PK_26	CAGCGTAAGTCGAAGCATCTTA	1.08	-0.989	104 bp		
AT1G01380	PK_28	TCTTCTGAGCCATTGCTATTT					
<i>ETC2</i>	JP_208	GATCCCGATATGACTCTGAAGAAGTGA	0.97	-0.993	322 bp		
AT2G30420	JP_209	GTAGCATCGAATGGGAG CAAGATTTGTCTACTTTTATGATTGAA AGCTTTTATTTG					
<i>ETC3</i>	PK_30	GACCAACTCCATCGTTACTTCT	0.96	-0.988	108 bp		
AT4G01060	PK_32	TGCATTGAGAGACCAAATCT					
<i>TCL1</i>	AST_487	GAAATGGGAGTTTATCAATATGACC	1.11	-0.995	109 bp		
AT2G30432	AST_488	ACGTCCCACCACTCTTCTTG					
<i>TCL2</i>	AST_489	GACGGAACAAGAAGAAGATCTCA	0.98	-0.991	97 bp		
AT2G30424	AST_490	CTTTGCCTCTCGTCTACCA					
<i>WER</i>	AS_03	TGCTTGGAATAGGTGGTCTTT	0.92	-0.996	84 bp		
AT5G14750	AS_04	GATGCGTGTCCAATAGTTCTTC					
Reference genes	<i>18S rRNA</i>	EP_75	AAACGGCTACCACATCCAAG	1.00	-0.998	102 bp	
		EP_76	GACTCGAAAGAGCCCGGTAT				
		<i>EF1a</i>	JP_210	CACCACTGGAGTTTTGAGG	0.96	-0.988	137 bp
AT5G60390	JP_211	TGGAGTATTGGGGTGGT					

Appendix

Table S3: Oligonucleotide sequences for *A. alpina* used for qPCR experiments.

Species	Gene	Primer ID	Primer sequence 5' → 3'	Efficiency	Correlation	Fragment length cDNA
<i>Arabis alpina</i>	<i>GL1</i> Aa_G34210	JS_29	CCTCATTATCCGTCCTCCACAAG	0.93	-0.995	112 bp
		JS_30	GCTGAGATGAGTGTCCAGTAG			
	<i>GL2</i> Aa_G239140	PK_17	GGAGGGTGAGGATCTAATG	0.96	-0.995	103 bp
		PK_19	GGTGTGGCGATGATACT			
	<i>GL3</i> Aa_G547900	PK_21	CGACACCGAGTGGTATTA	1.04	-0.990	110 bp
		PK_23	GAGCGTTACACAACCATATC			
	<i>EGL3</i> Aa_G234510	JP_204	CCTTTCCGACACCTTCCACGA	0.95	-0.990	86 bp
		JP_205	GACCTGAGACGCACCACCAC			
	<i>TTG1</i> Aa_G45330	DC_153	GACATTGCTTGGGGAGAAGCTA	0.94	-0.999	135 bp
		DC_154	TCTTAAGAGAGGCGTATCAGGC			
	<i>TTG2</i> Aa_G30000	AS_25	CGGATTCCGGTTGTAGAAGTAG	0.97	-0.996	94 bp
		AS_26	CTTCTCGCTCTCTCTCTCTTG			
	<i>MYC1</i> Aa_G511730	DC_173	GGTTCCTACTGTCAACGAGGTTG	0.88	-0.998	89 bp
		DC_174	GCTCCTCTACTCTTGCCTCAAGT			
	<i>MYB23</i> Aa_G247540	DC_157	GCAACAGATGGTCACTGATAGC	0.96	-0.997	109 bp
		DC_158	GGAATGATCTCCGAGACCAAGT			
	<i>CPC</i> Aa_G196850	JP_182	TGATCGCCGGGAGGATACCG	0.90	-0.997	72 bp
		JP_183	CGACGCCGTGTTTCATGAGC			
	<i>TRY</i> Aa_G156710	AS_15	GTCGGTGATAGGTGGGATTT	0.96	-0.995	121 bp
		AS_16	GATGAAGTTGGCGTCGTTTC			
<i>ETC1</i> Aa_G105910	JP_198	AGTACAAGATGGATAAGCAGCGTAAGT	0.86	-0.993	395 bp	
	JS_26	CTGGAATCCTCCCAGCTATTAATA				
<i>ETC2</i> Chr. 4	JP_188	TGCACAGACTTGTCGGTGATAG	0.87	-0.998	296 bp	
	JP_189	TCGTGTGTTGGAGAAATAGTCTGAGT				
<i>ETC3</i> Aa_G67910	AS_19	GTGAGTAGTCTTGAGTGGGAAG	1.01	-0.996	102 bp	
	AS_20	AGCTATCAATTCCCACCTGTC				
<i>TCL1</i> Chr. 4	JP_196	ATGGATAACACCAACCGTCTTC	0.94	-0.991	280 bp	
	JP_197	CTTGTTCCGGTCATGTTGATAAAC				
<i>TCL2</i> Aa_G645450	JP_186	GGTGGGATTTAATAGCAGGAAGAGTGG	0.88	-0.998	108 bp	
	JP_187	TGGAGTTGGAGTCGTGTGTTGG				
<i>WER</i> Aa_G7920	DC_159	GCTGCTTGGTAATAGTGGTCT	1.00	-0.988	140 bp	
	DC_160	CACCATTATTGCTTGGTTTGGT				
Reference genes	<i>RAN3</i> Aa_G442020	DC_149	CACAGGAAAAACACATTCGT	0.94	-0.997	174 bp
		DC_150	CCATCCCTAAGACCACCAAAAT			
Reference genes	<i>PP2A</i> Aa_G510870	DC_151	AGTATCGCTTCTCGCTCCAG	0.92	-0.992	241 bp
		DC_152	AACCGGTTGGTCGACTATTG			

Table S4: Oligonucleotide sequences for *C. hirsuta* used for qPCR experiments.

Species	Gene	Primer number	Primer sequence 5' → 3'	Efficiency	Correlation	Fragment length cDNA
<i>Cardamine hirsuta</i>	<i>GL1</i>	JP_298	GTGAAGAAAGGCAATTTCACTG	1.11	-0.988	107 bp
		CARHR149430	AST_468			
	<i>GL2</i>	JP_216	TCCACGATCCTGGTGAGCCA	1.03	-0.992	114 bp
		CARHR074650	JP_217			
	<i>GL3</i>	AS_41	TGAAGCCGAGCCAATAGATAC	1.15	-0.996	99 bp
		CARHR213010	AS_42			
	<i>EGL3</i>	AS_29	GACGATTCAAGCAGCGGAAGT	1.17	-0.989	170 bp
		CARHR047690	AS_30			
	<i>TTG1</i>	AS_27	CGGCGATTTCTCCGTCCTCT	0.99	-0.990	146 bp
		CARHR188910	AS_28			
	<i>TTG2</i>	AS_39	TGGAAGGTCAGGTTTCAGAGATTGT	0.98	-0.990	116 bp
		CARHR132330	AS_40			
	<i>MYC1</i>	JP_222	AGACGACGAAGAACCCTTAACGACT	0.86	-0.992	97 bp
		CARHR248590	JP_223			
	<i>MYB23</i>	JP_224	CGGCCAAACCCTCGGAATCT	0.93	-0.987	79 bp
		CARHR261770	AS_34			
<i>CPC</i>	JP_229	TGCGCGTAGGTGGGAATTG	1.04	-0.992	61 bp	
	CARHR141690	JP_230				TCAATCTCTCCGCGTCCT
<i>TRY</i>	AS_49	CTGGAAGACAACCAGAAGAGATAG	1.09	-0.992	125 bp	
	CARHR266270	AS_50				ACGAGGACGATGAAGTTTGG
<i>ETC1</i>	AS_51	TGGATAAGCAGCGTAAGTCAAA	1.00	-0.989	191 bp	
	CARHR001060	AS_52				GCTATTTCTCTCCACTCAAGAC
<i>ETC2</i>	JP_233	CAGGTGGGATTTAATAGCAGGAAGAGT	0.89	-0.991	108 bp	
	CARHR123870	JP_234				AGGTTGCGTCGTTTGTGGGA
<i>ETC3</i>	JP_262	CTTCTTTGTAATACGGTGCCG	0.86	-0.990	254 bp	
	CARHR249240	AS_56				CAGACCAAATCTTCTTCTTCAC
<i>WER</i>	AS_47	GTGGACAGTAGAAGAAGACAAGAT	0.92	-0.995	115 bp	
	CARHR198560	AS_48				TCTACAACCTTTCCGCATCTC
Reference genes	<i>TIP41</i>	JP_174	GATGGTGTGCTTATGAGATTGAGAG	1.02	-0.991	353 bp
		CARHR242510	JP_175			
Reference genes	<i>GAPDH</i>	JP_180	TGACCACCGTCCACTCCATCAC	1.07	-0.991	181 bp
		CARHR013790	JP_181			

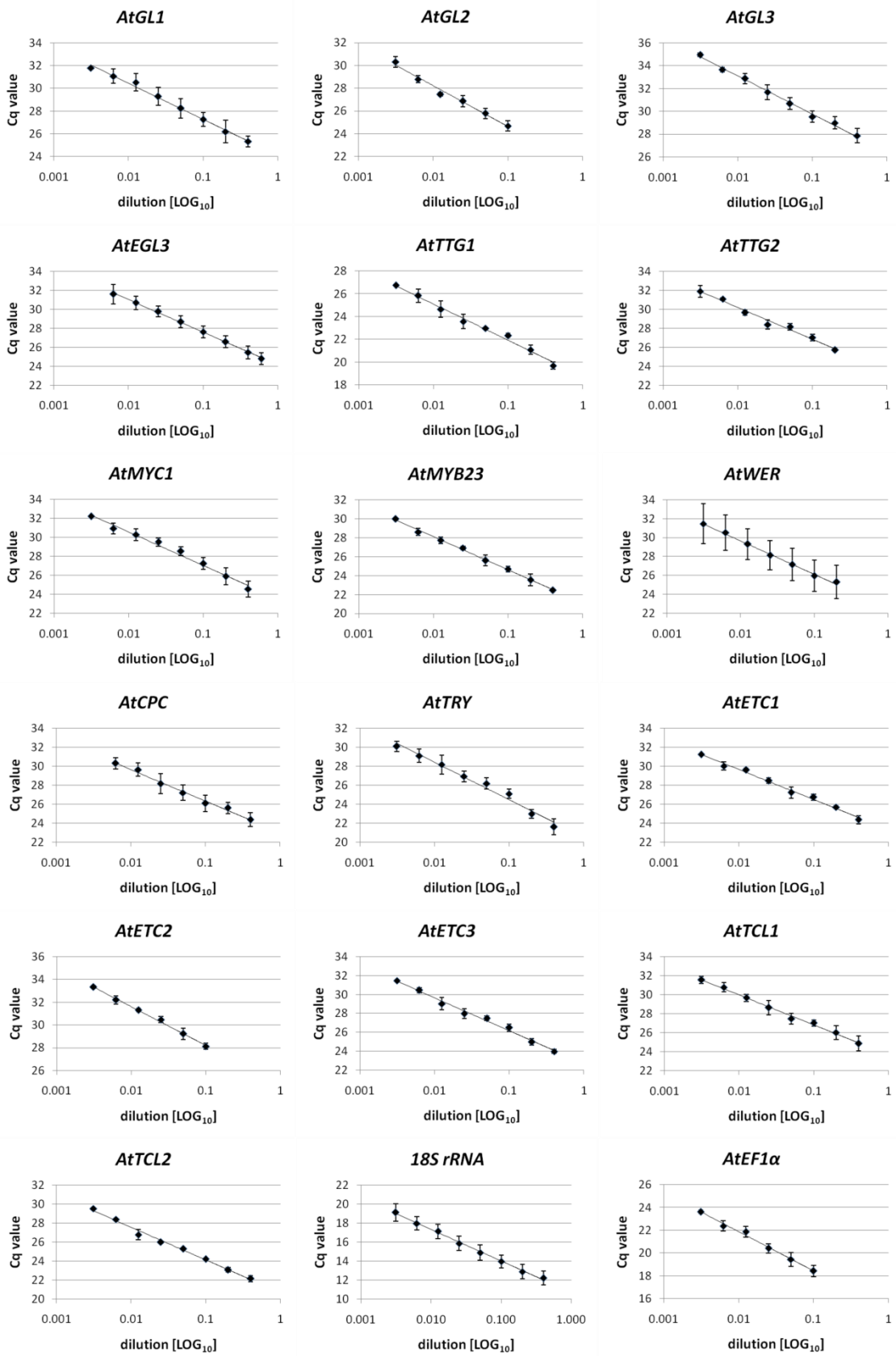


Figure S1: Graphs of *Arabidopsis thaliana* qPCR primer efficiency tests.

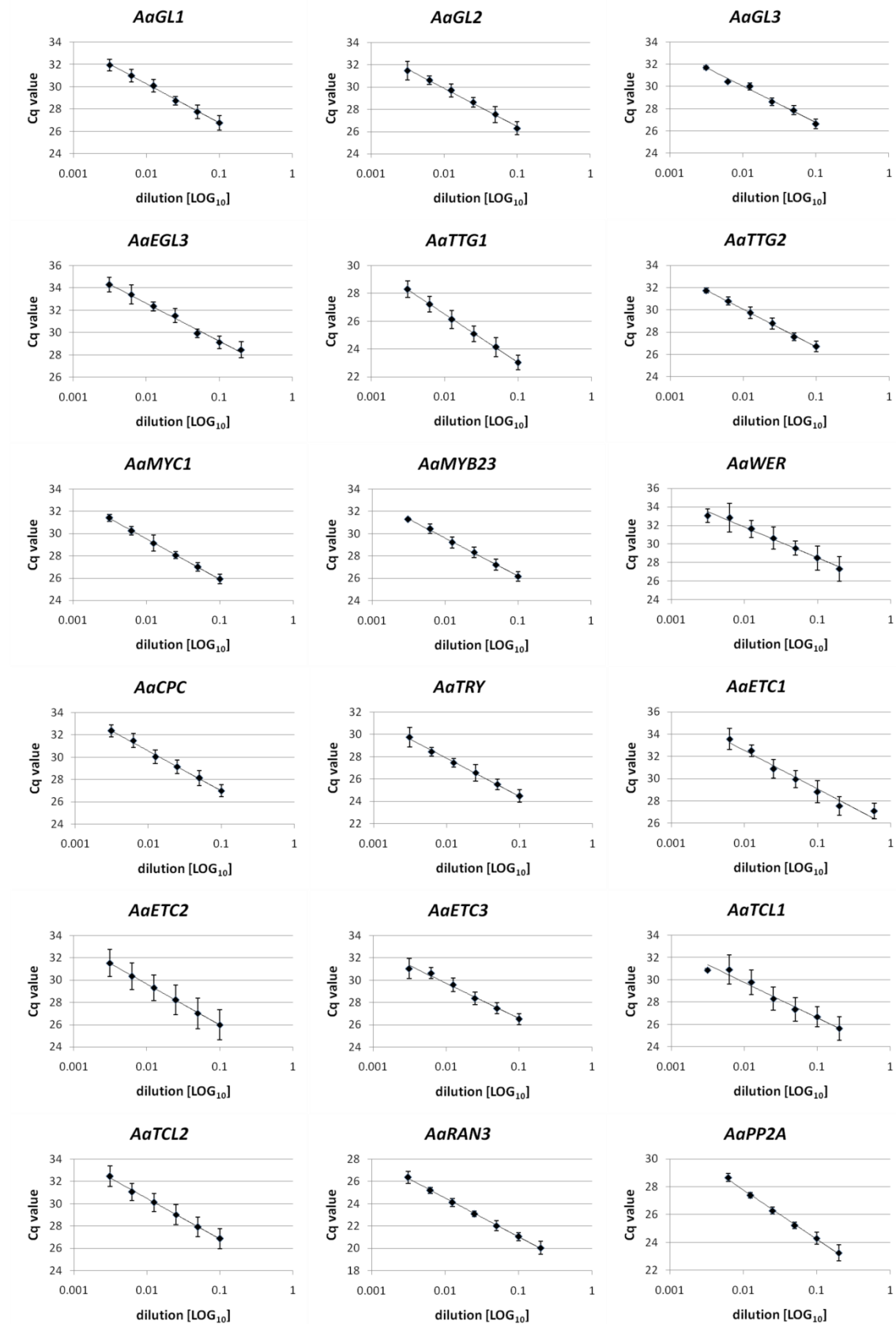


Figure S2: Graphs of *Arabis alpina* qPCR primer efficiency tests.

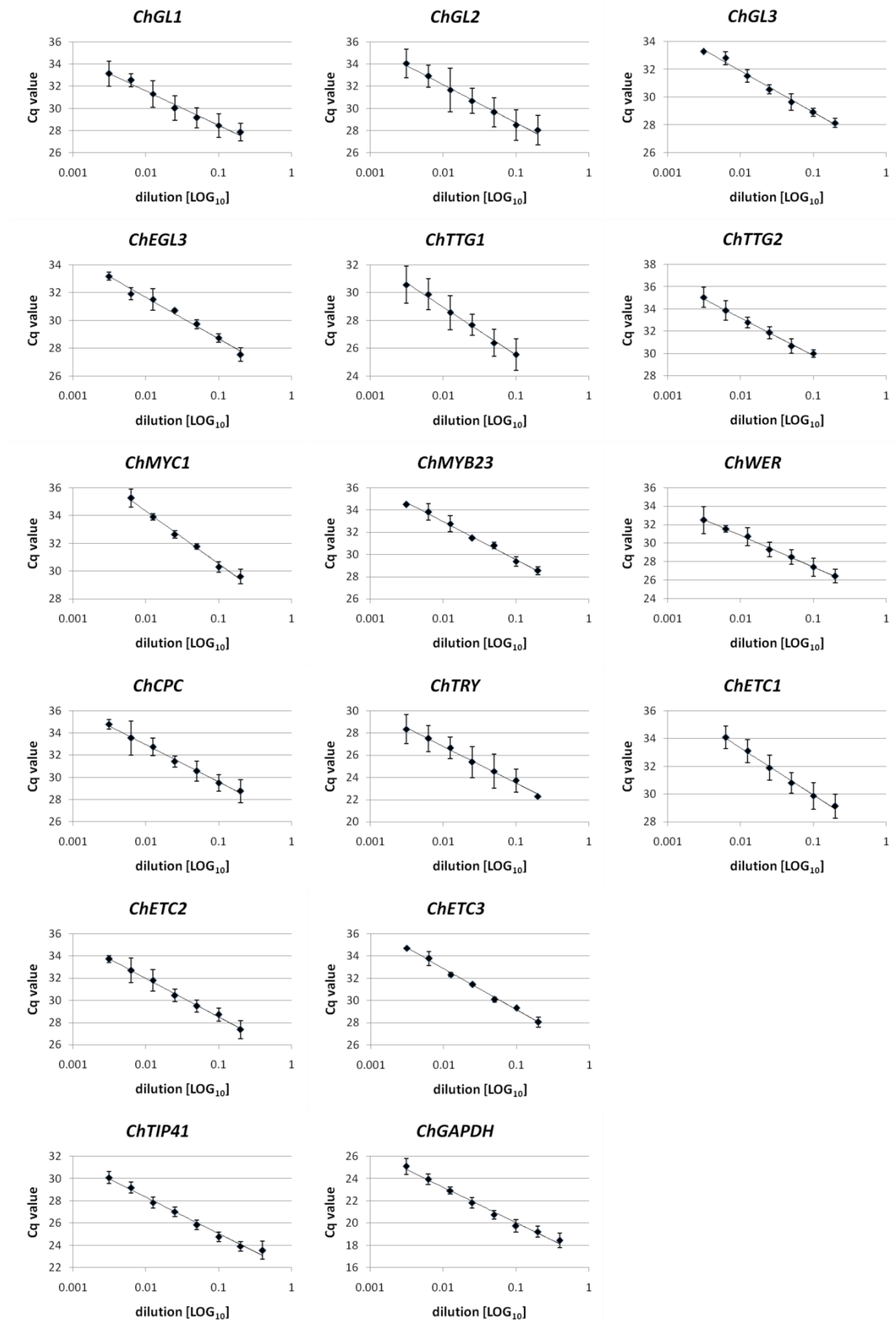


Figure S3: Graphs of *Cardamine hirsuta* qPCR primer efficiency tests.

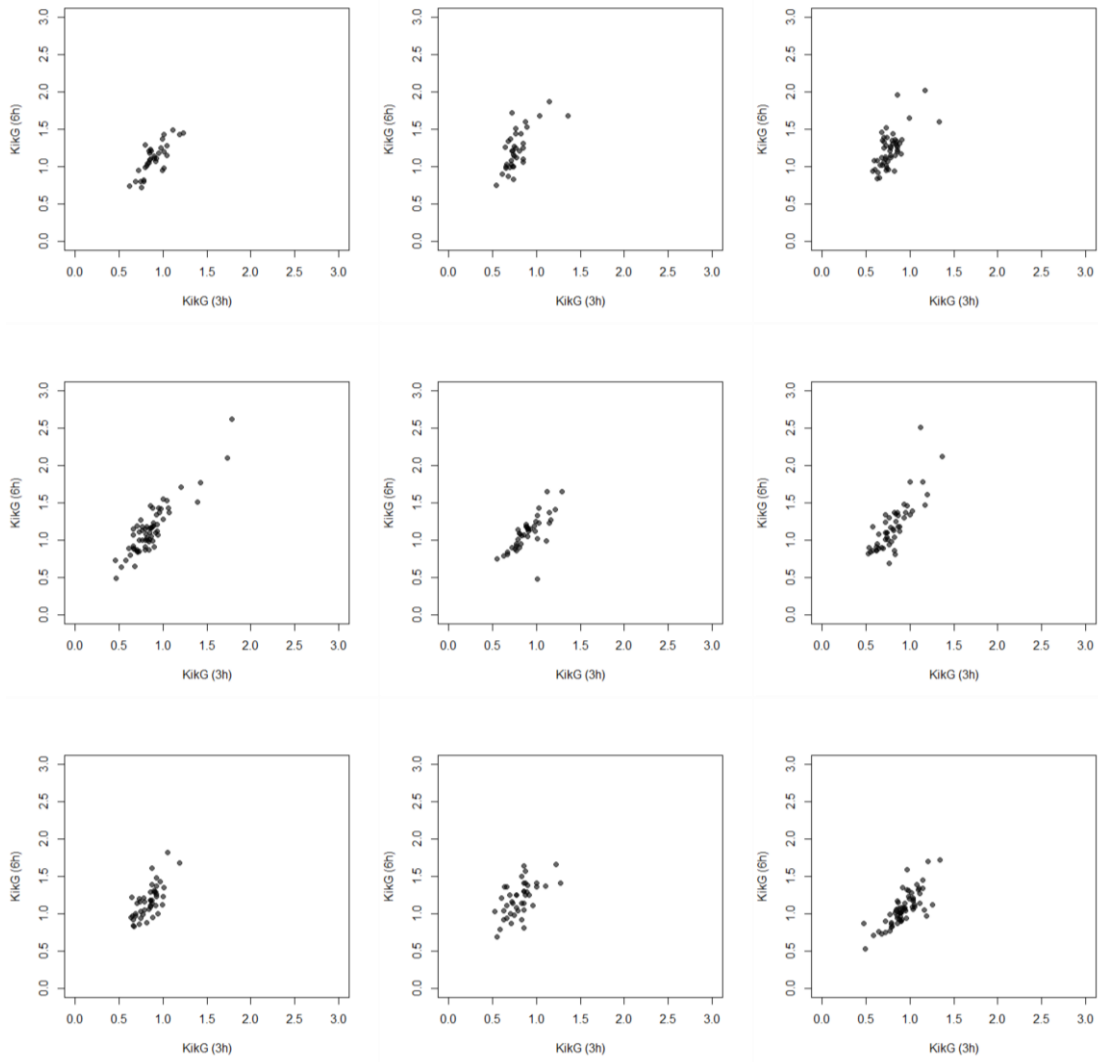


Figure S4: Analysis of temporal fluctuation in stable *Arabidopsis p35S:NLS-KikGR* lines. Scatter plots of nine individual leaves expressing *p35S:NLS-KikG*.

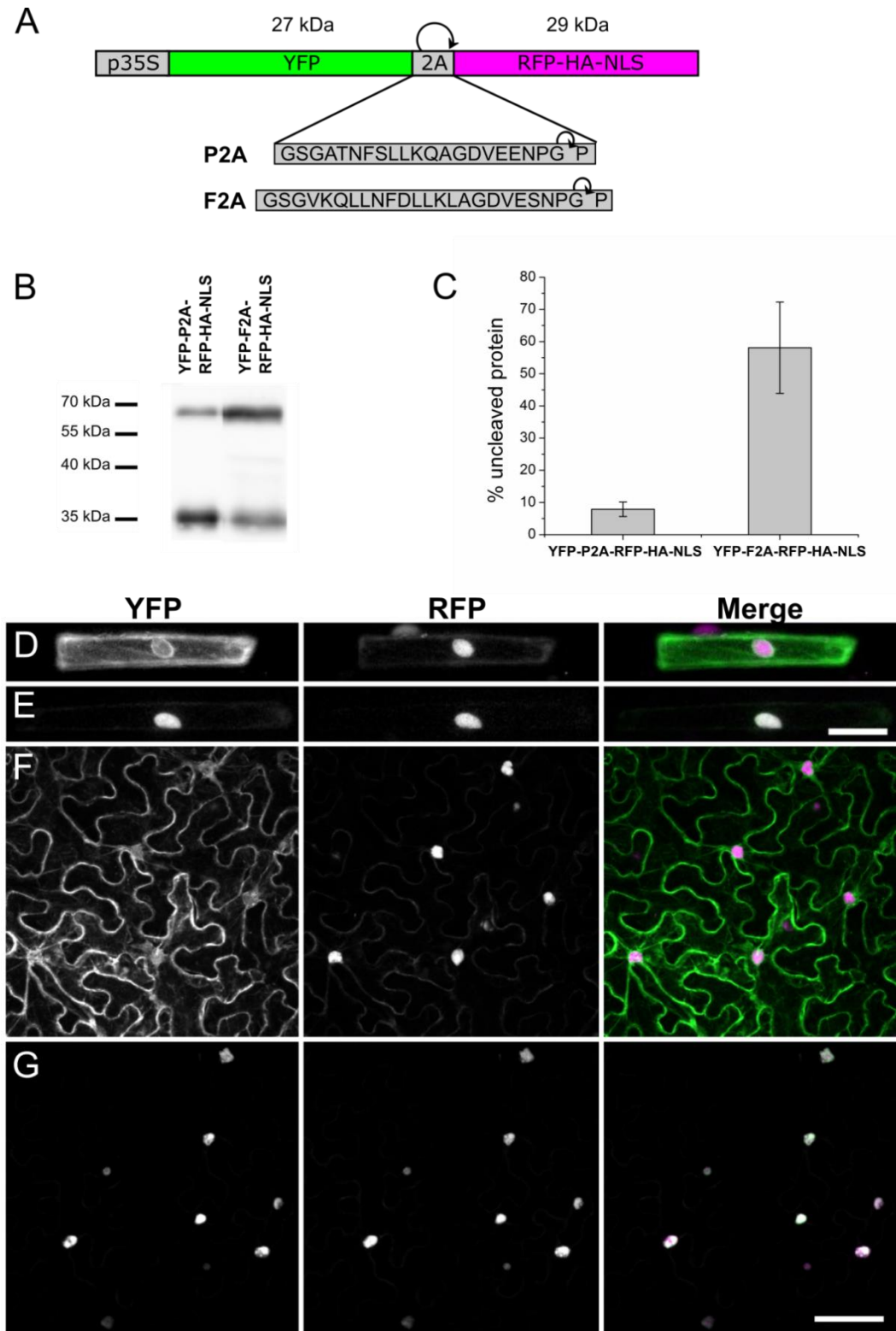


Figure S5: Comparison of P2A and F2A cleavage efficiency. **A)** Schematic illustration of P2A and F2A constructs. **B)** Comparison of cleavage efficiency of YFP-P2A-RFP-HA-NLS and YFP-F2A-RFP-HA-NLS by Western blot analysis of tobacco leaves transiently expressing the two constructs. Uncleaved proteins are expected to run at 56 kDa, RFP-HA-NLS at 29 kDa. **C)** Quantitative analysis of signal intensities of YFP-P2A-RFP-HA-NLS and YFP-F2A-RFP-HA-NLS from three independent tobacco infiltrations. **D-G)** CLSM images of YFP-MYC1-P2A-RFP-HA-NLS (D, F) and YFP-MYC1-F2A-RFP-HA-NLS (E, G) expression in epidermal leek cells transformed by particle bombardment (D, E) and infiltrated tobacco leaves (F, G). Cleaved YFP-MYC1 is expected to localize in the cytoplasm, the uncleaved construct in the nucleus. Left column represents the YFP channel (grey values), middle column the RFP channel (grey values) and right column the YFP (green) / RFP (magenta) overlay (co-localization of YFP and RFP appears white). Images were taken sequentially using Leica TSC SPE with a format of 512 x 512 pixels. Scale bars: 50 μ m. (Adopted from Schultheiß Araújo, unpublished.)

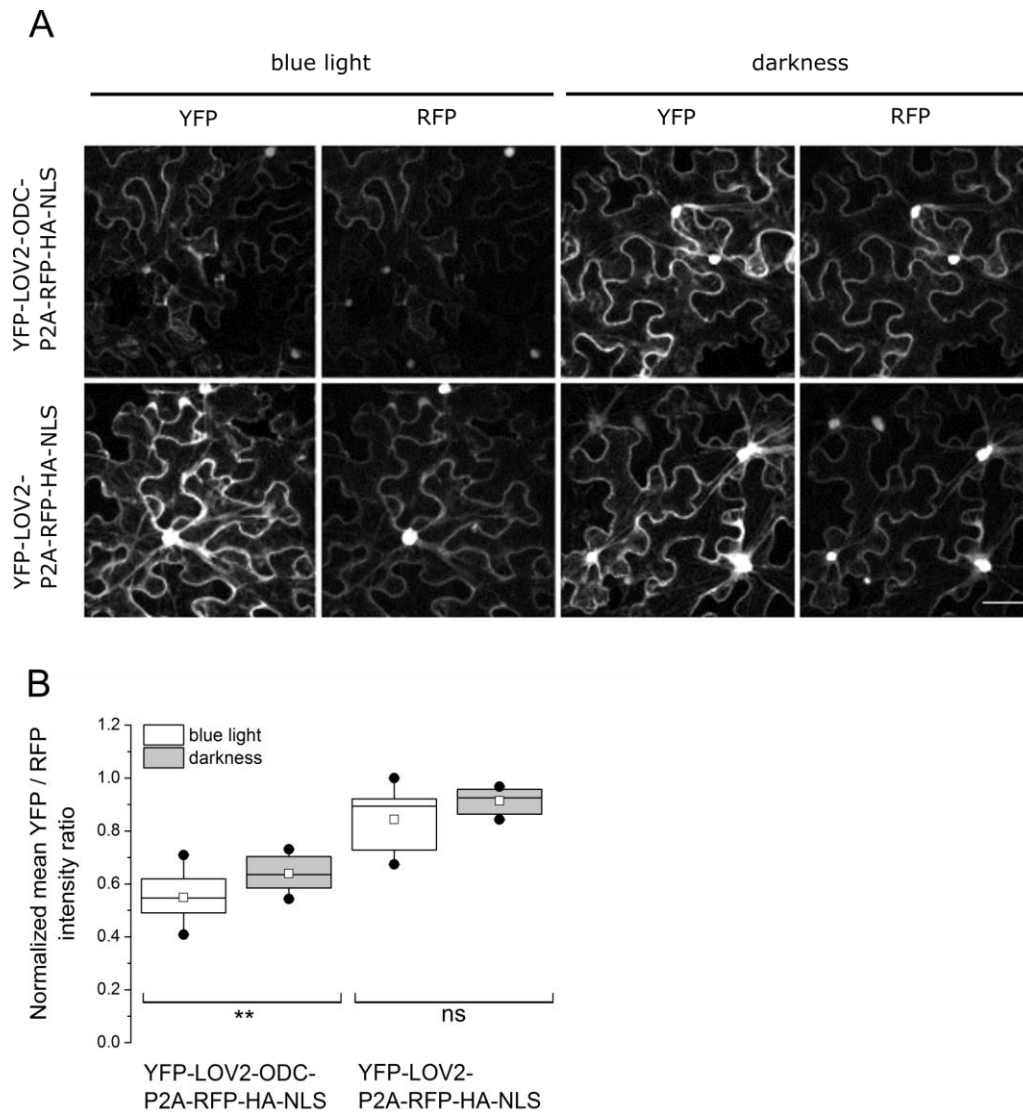


Figure S6: Blue light inducible degradation of LOV2-ODC. **A)** CLSM images of tobacco leaves transiently expressing YFP-LOV2-ODC-P2A-RFP-HA-NLS (upper row) or YFP-LOV2-P2A-RFP-HA-NLS (lower row). The first two columns on the left side illustrate the YFP and RFP channel (gray values) for cells treated with blue light, the two columns on the right the YFP and RFP channel (gray values) for cells kept in the dark, respectively. Images were taken sequentially using Leica TSC SPE with a format of 1024 x 1024 pixels. Scale bar: 50 μm . **B)** Box plot analysis of the YFP / RFP fluorescence intensity ratio between blue light and dark exposed samples of YFP-LOV2-ODC-P2A-RFP-HA-NLS and YFP-LOV2-P2A-RFP-HA-NLS. LOV2-ODC irradiated with blue light ($n = 14$, median = 0.55) differed significantly from dark kept samples ($n = 12$, median = 0.64; One-way ANOVA $p < 6 \times 10^{-3}$). LOV2 did not differ significantly under blue light ($n = 12$, median = 0.89) or darkness conditions ($n = 10$, median = 0.93; One-way ANOVA $p < 0.07$). Mean intensity values were measured using $366 \times 366 \mu\text{m}^2$ CLSM images comprising several cells and normalized to the maximum value. Boxes show median, 0.25 and 0.75 quartiles. Dots indicate 1% and 99% percentiles, rectangles represent mean values.

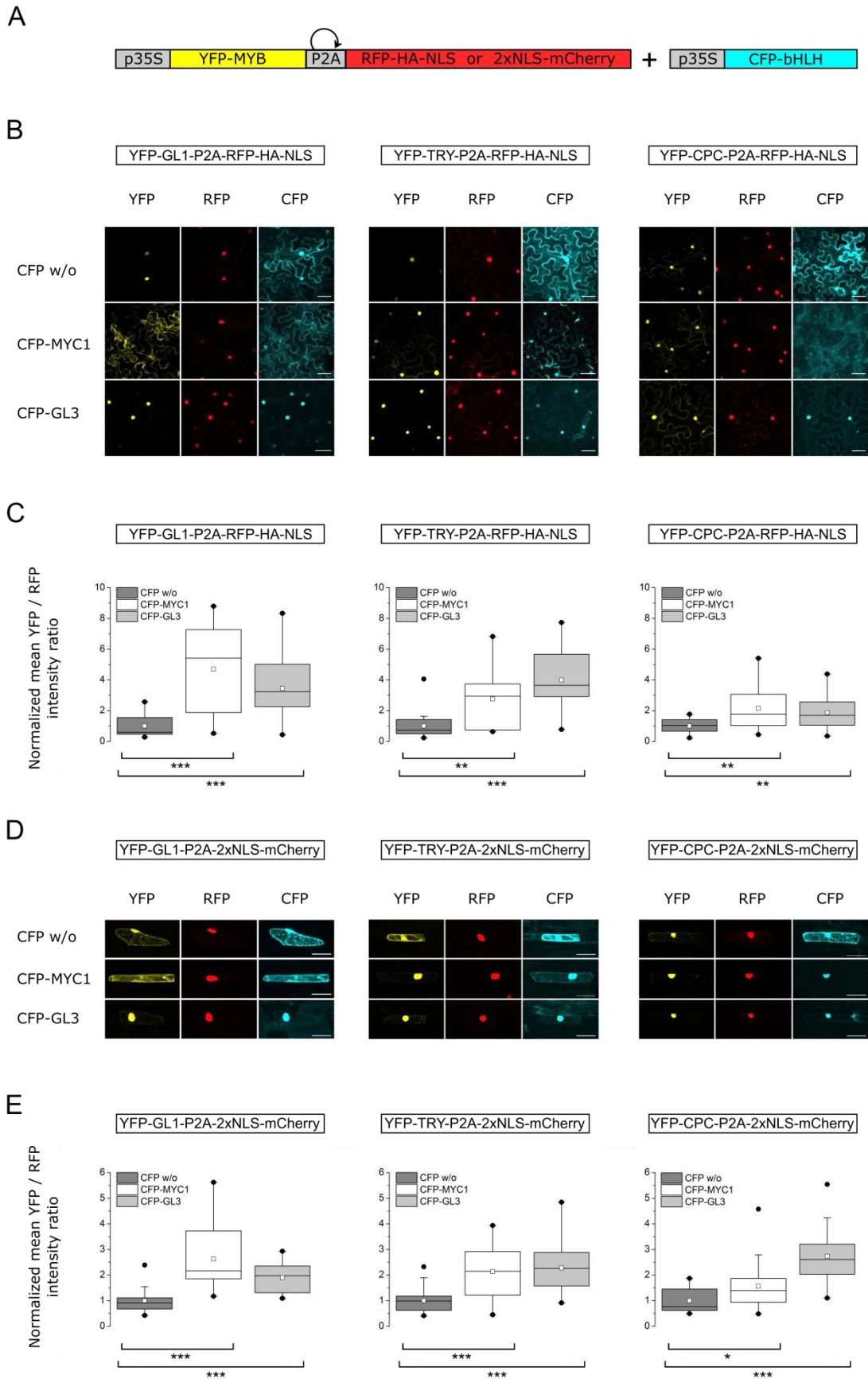


Figure S7: MYB proteins stabilized by bHLH proteins. **A)** Schematic illustration of the used P2A constructs. **B)** CLSM images of YFP-MYB-P2A-RFP-HA-NLS expression in tobacco leaves transiently transformed with CFP w/o, CFP-MYC1 or CFP-GL3. Images were taken sequentially using Leica TSC SPE with a format of 1024 x 1024 pixels. Scale bars indicate 50 μm . **C)** Box plot analyses of YFP-MYB-P2A-RFP-HA-NLS co-expressed with CFP w/o, CFP-MYC1 or CFP-GL3. YFP-GL1 was significantly stabilized when co-transformed with CFP-MYC1 ($n = 16$, median = 5.41, Mann-Whitney U test $p < 3*10^{-4}$) or CFP-GL3 ($n = 18$, median = 3.23, Mann-Whitney U test $p < 1*10^{-4}$) compared to the CFP w/o control ($n = 17$, median = 0.59). YFP-TRY was significantly stabilized when co-expressed with CFP-MYC1 ($n = 16$, median = 2.94, Mann-Whitney U test $p < 4*10^{-3}$) or CFP-GL3 ($n = 17$, median = 3.64, Mann-Whitney U test $p < 2*10^{-5}$) compared to CFP w/o ($n = 18$, median = 0.73). YFP-CPC was significantly stabilized when co-transformed with CFP-MYC1 ($n = 20$, median = 1.78, Mann-Whitney U test $p < 6*10^{-3}$) or CFP-GL3 ($n = 21$, median = 1.69, Mann-Whitney U test $p < 9*10^{-3}$) compared to the CFP w/o control ($n = 19$, median = 1.04). Mean intensity values were obtained from 366 x 366 μm^2 CLSM images comprising several cells and normalized to the mean of the CFP w/o control. Boxes show median, 0.25 and 0.75 quartiles. Dots indicate 1% and 99% percentiles, rectangles represent mean values. **D)** CLSM images of YFP-MYB-P2A-2xNLS-mCherry expression in leek epidermal cells transiently transformed with CFP w/o, CFP-MYC1 or CFP-GL3. Images were taken sequentially using Leica TSC SPE with a format of 1024 x 1024 pixels. Scale bars indicate 50 μm . **E)** Box plot analyses of YFP-MYB-P2A-2xNLS-mCherry co-expressed with CFP w/o, CFP-MYC1 or CFP-GL3. YFP-GL1 was significantly stabilized when co-transformed with CFP-MYC1 ($n = 26$, median = 2.16, Mann-Whitney U test $p < 2*10^{-7}$) or CFP-GL3 ($n = 15$, median = 1.97, Mann-Whitney U test $p < 5*10^{-5}$) compared to the CFP w/o control ($n = 22$, median = 0.91). YFP-TRY was significantly stabilized when co-expressed with CFP-MYC1 ($n = 29$, median = 2.15, Mann-Whitney U test $p < 7*10^{-6}$) or CFP-GL3 ($n = 32$, median = 2.26, Mann-Whitney U test $p < 4*10^{-8}$) compared to CFP w/o ($n = 32$, median = 0.99). YFP-CPC was significantly stabilized when co-transformed with CFP-MYC1 ($n = 31$, median = 1.39, Mann-Whitney U test $p < 0.022$) or CFP-GL3 ($n = 28$, median = 2.61, Mann-Whitney U test $p < 8*10^{-6}$) compared to the CFP w/o control ($n = 11$, median = 0.76). Mean intensity values were normalized to the mean of the CFP w/o control. Boxes show median, 0.25 and 0.75 quartiles. Dots indicate 1% and 99% percentiles, rectangles represent mean values.

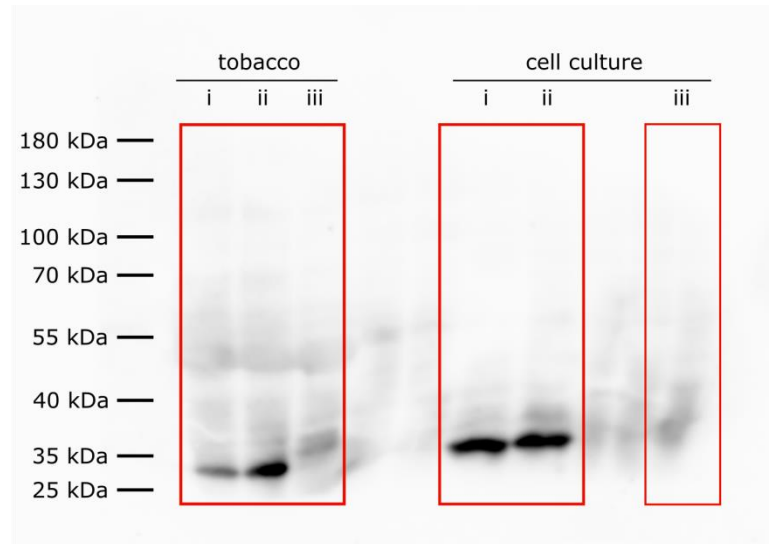


Figure S8: Cleavage efficiency of a dual P2A construct. Western blot analysis of tobacco leaves and dark grown Arabidopsis cell culture transiently transformed with either *p35S:mTurquoise2-TRY-P2A-YFP-P2A-mCherry* (i) or *p35S:mTurquoise2-TRY-P2A-YFP-P2A-mCherry-MYC1* (ii). Crude protein extract was separated by SDS-Page, blotted and analyzed using mouse α -GFP IgG (1:2000, Sigma-Aldrich) and α -mouse IgG (1:5000, Jackson ImmunoResearch). Untransformed tobacco leaves and Arabidopsis cell culture served as negative control (iii). YFP-P2A was expected to run at 30 kDa, uncleaved protein at 100 kDa or 160 kDa, respectively. The blot was exposed for 160 sec.



Figure S9: *pMYC1*_{1970 bp}:*GUS* staining in *A. thaliana*. Young rosette leaves ubiquitously expressing *pMYC1* after 24 h of incubation. (Image taken by M. Pesch.)

Appendix

Table S5: Leaf area, trichome number, and density in *A. thaliana* wildtype and various patterning mutants. Mean values and standard deviations represent the combination of leaves three and four and are given for 9-19 replicates each. [#] Not single trichomes but trichome clusters (trichome initiation sites) were measured. ^x Estimated trichome number and density. [†] These lines are entirely glabrous. ^{*} These lines show a significant difference in trichome density compared to Col-0. [▼] These trichomes are 5-branched or higher.

Background	Area [mm ²]	Trichome number	Density	4-branched trichomes [%]
Col-0	14.0 ± 2.0	66.6 ± 24.2	5.0 ± 2.1	4.5 ± 3.3
<i>cpc</i>	18.2 ± 2.4	143.2 ± 30.5	8.1 ± 2.4 *	8.6 ± 4.0
<i>cpc try</i> [#]	17.7 ± 3.0	24.5 ± 5.5	1.4 ± 0.2 *	-
<i>cpc try</i> ^x	17.7 ± 3.0	445.6 ± 109.1	25.4 ± 5.4 *	-
<i>egl3</i>	15.2 ± 3.0	71.8 ± 11.0	4.9 ± 1.4	6.8 ± 2.8
<i>etc1</i>	16.9 ± 4.1	108.1 ± 28.2	6.7 ± 2.2 *	4.8 ± 3.1
<i>etc1 etc3</i>	17.5 ± 2.4	197.6 ± 39.7	11.5 ± 2.9 *	5.5 ± 2.5
<i>etc2</i>	18.3 ± 2.0	109.5 ± 15.9	6.1 ± 1.4	7.6 ± 3.0
<i>etc3</i>	18.8 ± 2.5	135.3 ± 30.2	7.3 ± 1.8 *	1.7 ± 1.0
<i>etc3 try</i>	15.6 ± 3.3	88.4 ± 21.8	5.8 ± 1.8	83.5 ± 4.7 ▼
<i>gl2</i>	23.5 ± 3.9	9.2 ± 3.7	0.4 ± 0.2 *	-
<i>gl3</i>	17.6 ± 2.6	74.2 ± 13.8	4.3 ± 1.1	-
<i>myb23</i>	16.5 ± 3.0	64.1 ± 14.1	4.0 ± 1.1	0.2 ± 0.6
<i>myc1</i>	16.1 ± 2.8	26.7 ± 5.2	1.7 ± 0.5 *	3.6 ± 5.1
<i>myc1 egl3</i>	16.4 ± 3.2	29.8 ± 3.3	1.9 ± 0.5 *	11.4 ± 9.5
<i>tcl1</i>	18.5 ± 2.5	80.0 ± 14.8	4.4 ± 1.2	6.7 ± 4.1
<i>tcl2</i>	19.6 ± 1.9	98.5 ± 16.3	5.1 ± 1.1	3.8 ± 1.7
<i>try</i>	18.5 ± 2.2	54.9 ± 14.8	3.0 ± 1.0 *	90.3 ± 4.0 ▼
<i>ttg1</i>	25.6 ± 4.5	4.3 ± 2.2	0.2 ± 0.1 *	-
<i>ttg2</i>	18.1 ± 2.9	35.3 ± 10.1	2.1 ± 1.1 *	-
<i>gl1</i> [†]	-	-	-	-
<i>gl1 myb23</i> [†]	-	-	-	-
<i>gl3 egl3</i> [†]	-	-	-	-

Table S6: Summary of all gene expression fold changes of Arabidopsis patterning genes in various trichome mutants. Listed are the expression changes of 15 genes in 21 mutants relative to Col-0 wildtype. Upregulations are highlighted in green, downregulations in red; the darker the color, the stronger the regulation. Individual gene expressions in the corresponding mutant background were not considered and are indicated by an x. Values of unexpressed genes are bracketed.

	GL1	GL2	GL3	EGI3	TTG1	TTG2	MYC1	MYB23	CPC	TRY	ETC1	ETC2	ETC3	TC11	TC12
Col-0	1	1	1	1	1	1	1	1	1	1	1	1	1	1	1
<i>gl1</i>	x	-5.1	-1.8	1.3	1.1	-1.9	-1.1	-73.3	-2.2	-3.3	-2.3	-2.2	-1.3	-1.4	1.3
<i>gl2</i>	-3.1	x	-1.9	1.4	-1.5	-2.2	-1.3	-8.6	-2.1	-4.0	-2.6	3.7	(-282.5)	3.8	2.9
<i>gl3</i>	-2.0	-1.8	x	1.0	-1.1	-1.3	-1.9	-2.3	-1.6	-1.4	-1.7	-1.3	-2.0	-1.7	1.1
<i>egl3</i>	-1.4	-1.3	-1.0	x	-1.1	-3.5	-1.5	1.1	-1.1	1.2	-1.2	3.8	-2.0	-1.6	1.2
<i>gl3 egl3</i>	-7.2	-68.7	x	x	-1.1	(-584.8)	-2.3	-193.2	-12.9	-2.6	-193.3	5.8	-6.2	-2.9	1.3
<i>ttg1</i>	-2.8	-8.6	-3.3	1.2	x	-3.9	1.1	-29.6	-4.1	-2.8	-5.9	3.1	-2.0	1.3	2.4
<i>ttg2</i>	-1.0	1.1	1.6	1.2	-1.1	x	-1.0	2.4	-4.8	-8.9	4.9	1.8	-1.1	-2.7	-1.0
<i>myb23</i>	-1.3	-1.5	-1.4	-1.3	-1.1	-1.8	-1.6	x	-1.8	-5.5	1.1	(-17.8)	-1.5	-2.6	-1.1
<i>gl1 myb23</i>	x	-14.0	-8.2	-3.5	1.0	-4.1	-5.3	x	-4.2	1.9	-2.5	3.2	-1.2	-1.0	-1.2
<i>myc1</i>	-1.9	1.1	-2.3	-1.2	-1.1	-1.8	x	-1.2	-1.5	-1.9	-1.7	4.1	-4.5	-3.0	1.1
<i>myc1 egl3</i>	-1.2	-1.4	1.2	x	1.2	-2.3	x	-1.1	-1.5	1.0	-2.3	5.7	-1.3	-1.0	1.2
<i>cpc</i>	1.0	1.0	1.7	1.3	-1.1	-1.2	-1.3	1.3	x	1.0	1.5	1.9	-1.3	-1.6	1.0
<i>try</i>	1.6	2.9	-2.2	-1.5	-1.0	-1.1	-2.0	3.5	2.6	x	1.6	2.2	1.3	-1.6	1.3
<i>cpc try</i>	3.3	3.7	-1.7	-1.9	-2.0	1.3	-3.8	4.4	x	x	3.2	-1.4	1.0	-1.1	-1.2
<i>etc1</i>	-1.1	1.0	1.1	1.1	-1.1	-1.5	-1.7	1.1	1.6	1.8	x	(-25.0)	-1.1	-1.2	-1.0
<i>etc2</i>	-1.1	1.0	-1.1	-1.0	-1.0	-1.1	-1.3	1.4	1.1	1.0	-1.1	x	-1.3	-1.8	-1.4
<i>etc3</i>	-1.1	1.7	-3.2	-1.7	-1.1	-1.2	-1.3	2.1	1.6	-1.2	1.4	(-10.9)	x	-1.4	2.0
<i>etc1 etc3</i>	1.3	2.0	1.1	-1.1	1.0	1.2	-1.4	2.4	1.5	1.3	x	-1.3	x	-1.6	1.1
<i>etc3 try</i>	2.2	2.1	-1.3	1.1	-1.1	1.1	-1.4	2.6	2.0	x	2.0	1.2	x	-1.4	1.2
<i>tc11</i>	1.5	1.6	-1.3	-1.1	-1.0	-1.8	-1.4	1.8	2.0	2.5	1.4	(-1.9)	-1.9	x	1.4
<i>tc12</i>	1.1	3.3	-2.2	-1.1	1.1	1.2	-1.4	2.0	1.9	1.5	1.7	(-4.1)	-2.9	-3.0	x

Appendix

Table S7: Summary of 2-fold cut-off gene expressions changes of Arabidopsis patterning genes in various trichome mutants. Listed are the expression changes of 15 genes in 21 mutants relative to Col-0 wildtype applying a 2-fold threshold. Upregulations are highlighted in green, downregulations in red; the darker the color, the stronger the regulation. Individual gene expressions in the corresponding mutant background were not considered and are indicated by an x. Expression differences less than 2-fold lead to empty fields. Values of unexpressed genes are bracketed.

	GL1	GL2	GL3	EGL3	TTG1	TTG2	MYC1	MYB23	CPC	TRY	ETC1	ETC2	ETC3	TCL1	TCL2
Col-0	1	1	1	1	1	1	1	1	1	1	1	1	1	1	1
<i>gl1</i>	x	-5.1						-73.3	-2.2	-3.3	-2.3	-2.2			
<i>gl2</i>	-3.1	x				-2.2		-8.6	-2.1	-4.0	-2.6	3.7	(-282.5)	3.8	2.9
<i>gl3</i>			x					-2.3							
<i>egl3</i>				x		-3.5						3.8			
<i>gl3 egl3</i>	-7.2	-68.7	x	x		(-584.8)	-2.3	-193.2	-12.9	-2.6	-193.3	5.8	-6.2	-2.9	
<i>ttg1</i>	-2.8	-8.6	-3.3		x	-3.9		-29.6	-4.1	-2.8	-5.9	3.1			2.4
<i>ttg2</i>						x		2.4	-4.8	-8.9	4.9			-2.7	
<i>myb23</i>								x		-5.5		(-17.8)		-2.6	
<i>gl1 myb23</i>	x	-14.0	-8.2	-3.5		-4.1	-5.3	x	-4.2		-2.5	3.2			
<i>myc1</i>			-2.3				x					4.1	-4.5	-3.0	
<i>myc1 egl3</i>				x		-2.3	x				-2.3	5.7			
<i>cpc</i>									x						
<i>try</i>		2.9	-2.2				-2.0	3.5	2.6	x		2.2			
<i>cpc try</i>	3.3	3.7			-2.0		-3.8	4.4	x	x	3.2				
<i>etc1</i>											x	(-25.0)			
<i>etc2</i>												x			
<i>etc3</i>			-3.2					2.1				(-10.9)	x		
<i>etc1 etc3</i>								2.4			x		x		
<i>etc3 try</i>	2.2	2.1						2.6	2.0	x			x		
<i>tcl1</i>										2.5				x	
<i>tcl2</i>		3.3	-2.2									(-4.1)	-2.9	-3.0	x

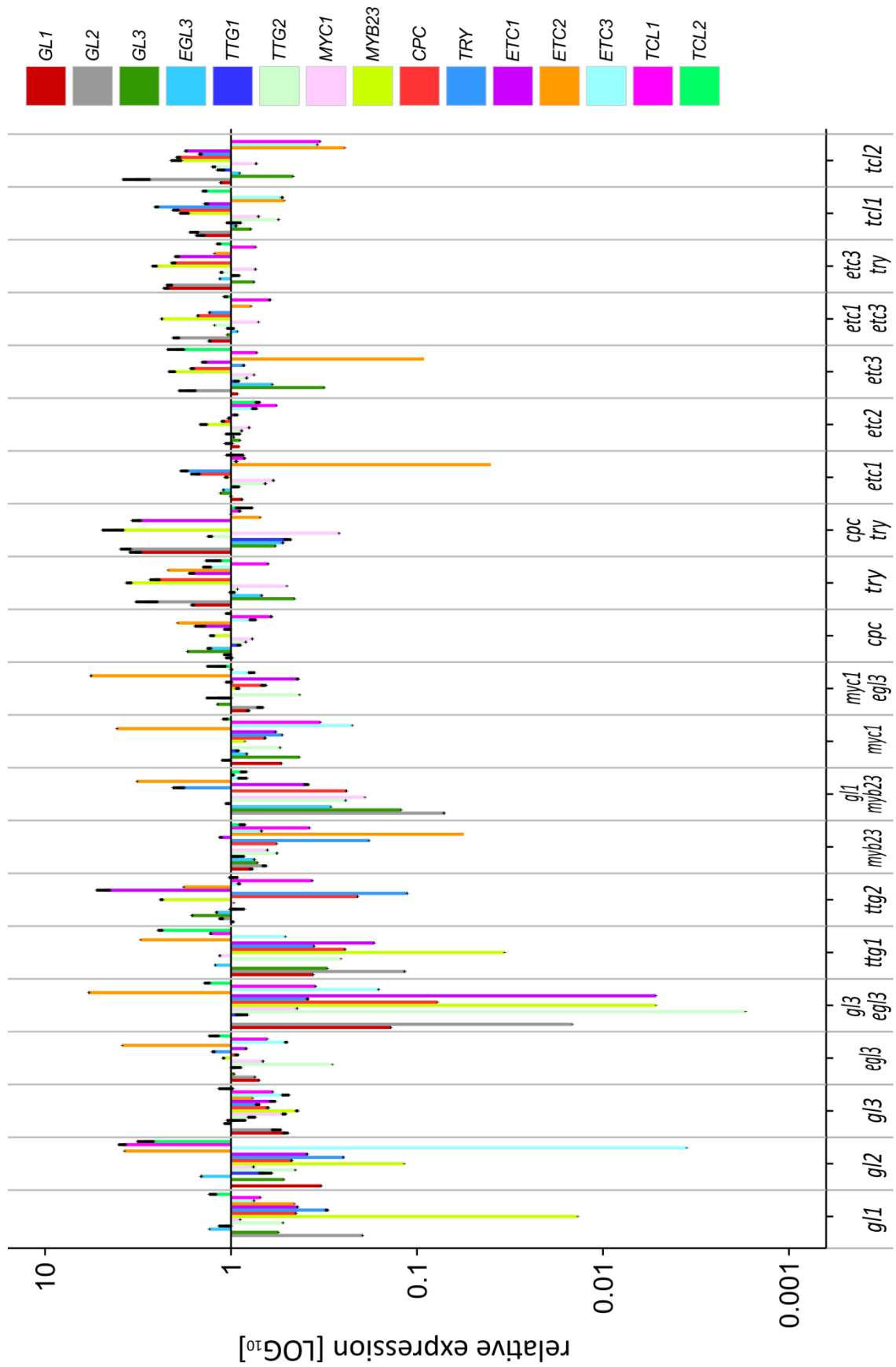


Figure S10: Summary of all relative expression values of Arabidopsis patterning genes in various trichome mutants. 15 genes were analyzed in 21 trichome mutants relative to Col-0 wildtype.

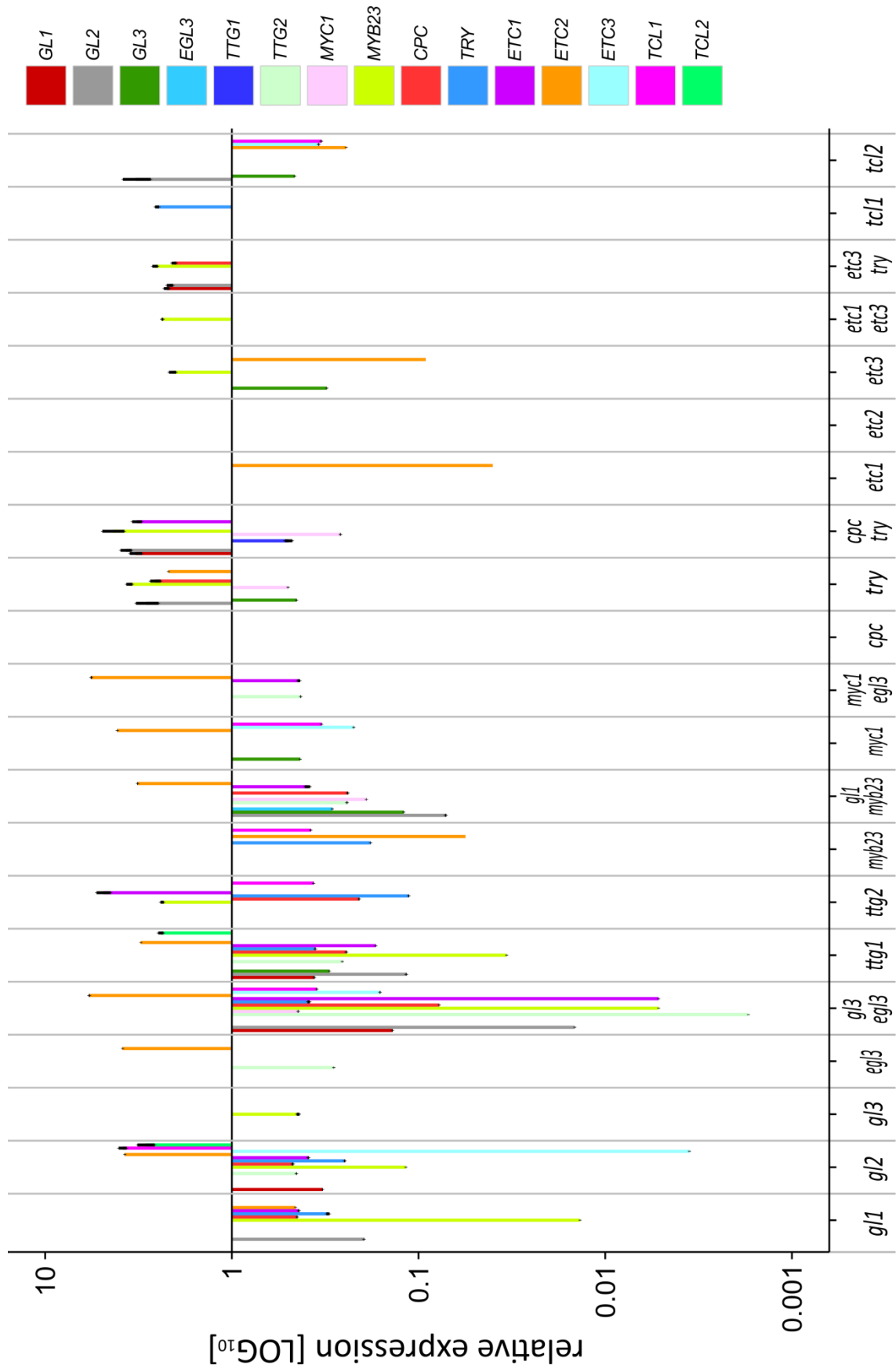


Figure S11: Summary of 2-fold cut-off relative expression values of Arabidopsis patterning genes in various trichome mutants. Bars depict 15 genes in 21 trichome mutants relative to Col-0 wildtype applying a 2-fold threshold.

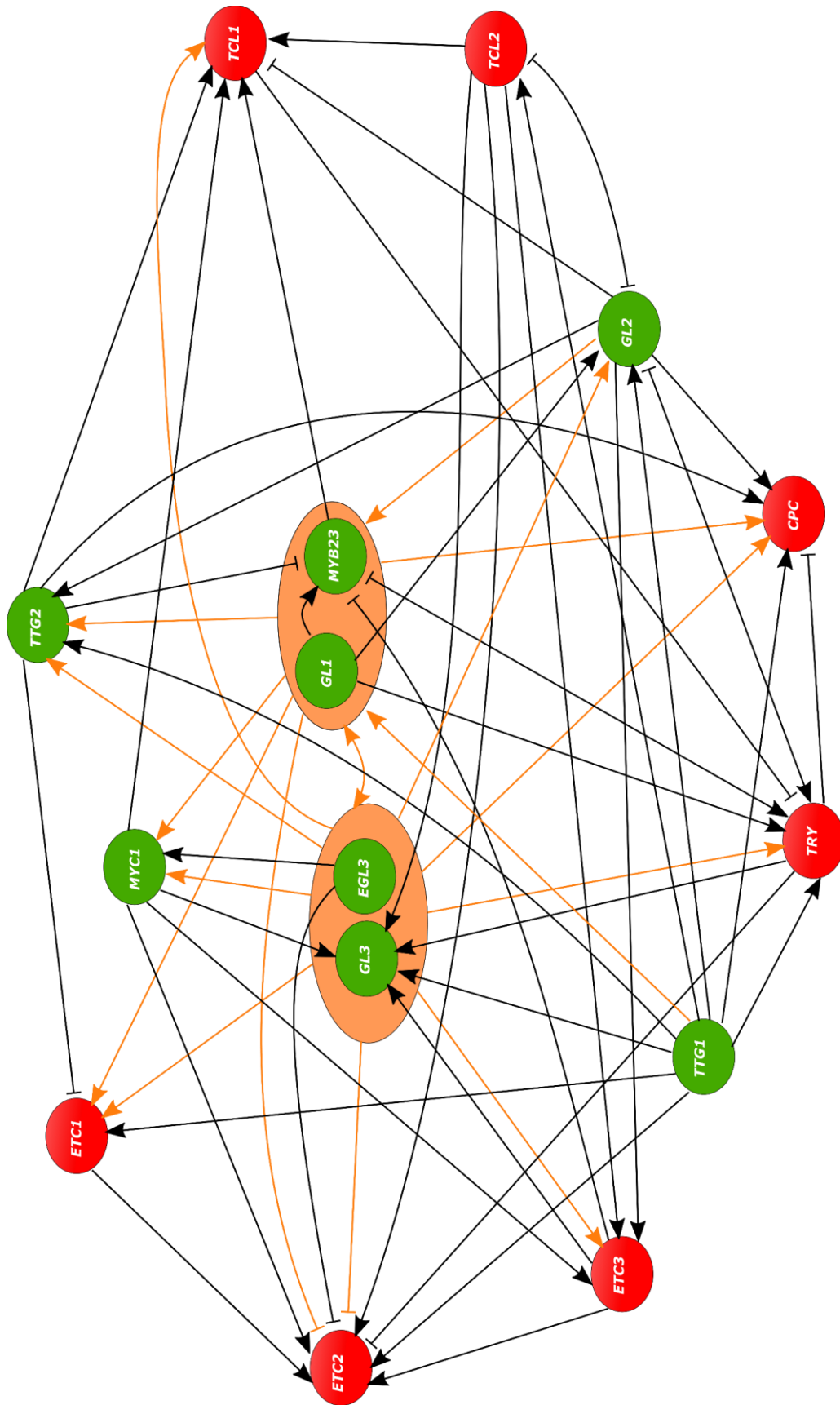


Figure S12: Cross-regulatory interaction scheme of all trichome patterning genes. Illustrated are the interaction dependencies based on the transcriptional expression profile upon a 2-fold cut-off. Activators are indicated in green, inhibitors in red. Orange ellipses contain functional units. Orange lines refer to functional units, black lines to single genes. Promoting regulations are marked by arrowheads, repressing regulations by blunt ends.

6. Bibliography

- Alonso-Blanco, C., Aarts, M. G. M., Bentsink, L., Keurentjes, J. J. B., Reymond, M., Vreugdenhil, D., & Koornneef, M. (2009). What Has Natural Variation Taught Us about Plant Development, Physiology, and Adaptation? *The Plant Cell*, *21* (7), 1877–1896. doi.org/10.1105/tpc.109.068114
- Appelhagen, I., Thiedig, K., Nordholt, N., Schmidt, N., Huep, G., Sagasser, M., & Weisshaar, B. (2014). Update on *transparent testa* mutants from *Arabidopsis thaliana*: characterisation of new alleles from an isogenic collection. *Planta*, *240* (5), 955–970. doi.org/10.1007/s00425-014-2088-0
- Balkunde, R., Deneer, A., Bechtel, H., Zhang, B., Herberth, S., Pesch, M., Jaegle, B., Fleck, C., & Hülskamp, M. (2020). Identification of the Trichome Patterning Core Network Using Data from Weak *ttg1* Alleles to Constrain the Model Space. *Cell Reports*, *33*, 1–22. doi.org/10.1016/j.celrep.2020.108497
- Balkunde, R., Pesch, M., & Hülskamp, M. (2010). Trichome Patterning in *Arabidopsis thaliana*: From Genetic to Molecular Models. In *Current Topics in Developmental Biology* (91st ed., Vol. 91, pp. 299–321). Elsevier Inc. doi.org/10.1016/S0070-2153(10)91010-7
- Beilstein, M. A., Al-Shehbaz, I. A., & Kellogg, E. A. (2006). Brassicaceae phylogeny and trichome evolution. *American Journal of Botany*, *93* (4), 607–619. doi.org/10.3732/ajb.93.4.607
- Beilstein, M. A., Al-Shehbaz, I. A., Mathews, S., & Kellogg, E. A. (2008). Brassicaceae phylogeny inferred from phytochrome A and *ndhF* sequence data: tribes and trichomes revisited. *American Journal of Botany*, *95* (10), 1307–1327. doi.org/10.3732/ajb.0800065
- Beilstein, M. A., Nagalingum, N. S., Clements, M. D., Manchester, S. R., & Mathews, S. (2010). Dated molecular phylogenies indicate a Miocene origin for *Arabidopsis thaliana*. *PNAS*, *107* (43), 18724–18728. doi.org/10.1073/pnas.0909766107
- Bernard, P., & Couturier, M. (1992). Cell Killing by the F Plasmid CcdB Protein Involves Poisoning of DNA-Topoisomerase II Complexes. *Journal of Molecular Biology*, *226* (3), 735–745. doi.org/10.1016/0022-2836(92)90629-X
- Bernhardt, C., Lee, M. M., Gonzalez, A., Zhang, F., Lloyd, A., & Schiefelbein, J. (2003). The bHLH genes *GLABRA3* (*GL3*) and *ENHANCER OF GLABRA3* (*EGL3*) specify epidermal cell fate in the *Arabidopsis* root. *Development*, *130* (26), 6431–6439. doi.org/10.1242/dev.00880

- Bouyer, D., Geier, F., Kragler, F., Schnittger, A., Pesch, M., Wester, K., Balkunde, R., Timmer, J., Fleck, C., & Hülskamp, M. (2008). Two-Dimensional Patterning by a Trapping/Depletion Mechanism: The role of TTG1 and GL3 in *Arabidopsis* Trichome Formation. *PLoS Biology*, *6* (6), 1166–1177. doi.org/10.1371/journal.pbio.0060141
- Braun, E. L., & Grotewold, E. (1999). Newly Discovered Plant *c-myb*-Like Genes Rewrite the Evolution of the Plant *myb* Gene Family. *Plant Physiology*, *121* (1), 21–24. doi.org/10.1104/pp.121.1.21
- Canales, C., & Barkoulas, M. (2010). Weeds of change: *Cardamine hirsuta* as a new model system for studying dissected leaf development. *Journal Plant Research*, *123*, 25–33. doi.org/10.1007/s10265-009-0263-3
- Cartolano, M., Pieper, B., Lempe, J., Tattersall, A., Huijser, P., Tresch, A., Darrah, P. R., Hay, A., & Tsiantis, M. (2015). Heterochrony underpins natural variation in *Cardamine hirsuta* leaf form. *PNAS*, *112* (33), 10539–10544. doi.org/10.1073/pnas.1419791112
- Chopra, D., Mapar, M., Stephan, L., Albani, M. C., Deneer, A., Coupland, G., Willing, E.-M., Schellmann, S., Schneeberger, K., Fleck, C., Schrader, A., & Hülskamp, M. (2019). Genetic and molecular analysis of trichome development in *Arabidopsis alpina*. *PNAS*, *116* (24), 12078–12083. doi.org/10.1073/pnas.1819440116
- Chopra, D., Wolff, H., Span, J., Schellmann, S., Coupland, G., Albani, M. C., Schrader, A., & Hülskamp, M. (2014). Analysis of *TTG1* function in *Arabidopsis alpina*. *BMC Plant Biology*, *14*, 2–14. doi.org/10.1186/1471-2229-14-16
- Christie, J. M., Salomon, M., Nozue, K., Wada, M., & Briggs, W. R. (1999). LOV (light, oxygen, or voltage) domains of the blue-light photoreceptor phototropin (*nph1*): Binding sites for the chromophore flavin mononucleotide. *PNAS*, *96*, 8779–8783. doi.org/10.1073/pnas.96.15.8779
- Clough, S. J., & Bent, A. F. (1998). Floral dip: a simplified method for *Agrobacterium*-mediated transformation of *Arabidopsis thaliana*. *The Plant Journal*, *16* (6), 735–743. doi.org/10.1046/j.1365-313x.1998.00343.x
- Dar, R. D., Razooky, B. S., Singh, A., Trimeloni, T. V., McCollum, J. M., Cox, C. D., Simpson, M. L., & Weinberger, L. S. (2012). Transcriptional burst frequency and burst size are equally modulated across the human genome. *PNAS*, *109* (43), 17454–17459. doi.org/10.1073/pnas.1213530109

- Deng, W., Zhang, K., Busov, V., & Wei, H. (2017). Recursive random forest algorithm for constructing multilayered hierarchical gene regulatory networks that govern biological pathways. *PLoS ONE*, *12* (2), 1–15. doi.org/10.1371/journal.pone.0171532
- Di Ruocco, G., Bertolotti, G., Pacifici, E., Polverari, L., Tsiantis, M., Sabatini, S., Costantina, P., & Dello Ioio, R. (2018). Differential spatial distribution of miR165/6 determines variability in plant root anatomy. *Development*, *145* (1), 1–21. doi.org/10.1242/dev.153858
- Digiuni, S., Schellmann, S., Geier, F., Greese, B., Pesch, M., Wester, K., Dartan, B., Mach, V., Srinivas, B. P., Timmer, J., Fleck, C., & Hülskamp, M. (2008). A competitive complex formation mechanism underlies trichome patterning on *Arabidopsis* leaves. *Molecular Systems Biology*, *4*, 1–11. doi.org/10.1038/msb.2008.54
- Dolan, L., Duckett, C. M., Grierson, C., Linstead, P., Schneider, K., Lawson, E., Dean, S., Poethig, S., & Roberts, K. (1994). Clonal relationships and cell patterning in the root epidermis of *Arabidopsis*. *Development*, *120* (9), 2465–2474. doi.org/10.1242/dev.120.9.2465
- Donnelly, M. L. L., Hughes, L. E., Luke, G., Mendoza, H., Dam, E., Gani, D., & Ryan, M. D. (2001a). The ‘cleavage’ activities of foot-and-mouth disease virus 2A site-directed mutants and naturally occurring ‘2A-like’ sequences. *Journal of General Virology*, *82*, 1027–1041. doi.org/10.1099/0022-1317-82-5-1027
- Donnelly, M. L. L., Luke, G., Mehrotra, A., Li, X., Hughes, L. E., Gani, D., & Ryan, M. D. (2001b). Analysis of the aphthovirus 2A/2B polyprotein “cleavage” mechanism indicates not a proteolytic reaction, but a novel translational effect: a putative ribosomal “skip.” *Journal of General Virology*, *82*, 1013–1025. doi.org/10.1099/0022-1317-82-5-1013
- Elowitz, M. B., Levine, A. J., Siggia, E. D., & Swain, P. S. (2002). Stochastic Gene Expression in a Single Cell. *Science*, *297*, 1183–1186. 10.1126/science.1070919
- Erwin, D. H., & Davidson, E. H. (2009). The evolution of hierarchical gene regulatory networks. *Nature Reviews Genetics*, *10*, 141–148. doi.org/10.1038/nrg2499
- Esch, J. J., Chen, M. A., Hillestad, M., & Marks, M. D. (2004). Comparison of *TRY* and the closely related *AtIg01380* gene in controlling *Arabidopsis* trichome patterning. *The Plant Journal*, *40* (6), 860–869. doi.org/10.1111/j.1365-313X.2004.02259.x

- Esch, J. J., Chen, M., Sanders, M., Hillestad, M., Ndkium, S., Idelkope, B., Neizer, J., & Marks, M. D. (2003). A contradictory *GLABRA3* allele helps define gene interactions controlling trichome development in *Arabidopsis*. *Development*, *130*, 5885–5894. doi.org/10.1242/dev.00812
- Fabiańska, I., Sosa-Lopez, E., & Bucher, M. (2019). The role of nutrient balance in shaping plant root-fungal interactions: facts and speculation. *Current Opinion in Microbiology*, *49*, 90–96. doi.org/10.1016/j.mib.2019.10.004
- Feller, A., Machemer, K., Braun, E. L., & Grotewold, E. (2011). Evolutionary and comparative analysis of MYB and bHLH plant transcription factors. *Plant Journal*, *66* (1), 94–116. doi.org/10.1111/j.1365-313X.2010.04459.x
- Feys, B. J., Wiermer, M., Bhat, R. A., Moisan, L. J., Medina-Escobar, N., Neu, C., Cabral, A., & Parker, J. E. (2005). *Arabidopsis* SENESCENCE-ASSOCIATED GENE101 Stabilizes and Signals within an ENHANCED DISEASE SUSCEPTIBILITY1 Complex in Plant Innate Immunity. *The Plant Cell*, *17*, 2601–2613. doi.org/10.1105/tpc.105.033910
- Folkers, U., Berger, J., & Hülskamp, M., (1997). Cell morphogenesis of trichomes in *Arabidopsis*: differential control of primary and secondary branching by branch initiation regulators and cell growth. *Development*, *124*, 3779–3786.
- Gan, L., Xia, K., Chen, J.-G., & Wang, S. (2011). Functional characterization of TRICHOMELESS2, a new single-repeat R3 MYB transcription factor in the regulation of trichome patterning in *Arabidopsis*. *BMC Plant Biology*, *11*, 176. doi.org/10.1186/1471-2229-11-176
- Gan, X., Hay, A., Kwantes, M., Haberer, G., Hallab, A., Ioio, R. D., Hofhuis, H., Pieper, B., Cartolana, M., Neumann, U., Nikolov, L. A., Song, B., Hajheidari, M., Briskine, R., Kougioumoutzi, E., Vlad, D., Broholm, S., Hein, J., Meksem, K., ... Tsiantis, M. (2016). The *Cardamine hirsuta* genome offers insight into the evolution of morphological diversity. *Nature Plants*, *2* (221), 1–50. doi.org/10.1038/nplants.2016.167
- Gonzalez, A., Zhao, M., Leavitt, J. M., & Lloyd, A. M. (2008). Regulation of the anthocyanin biosynthetic pathway by the TTG1/bHLH/Myb transcriptional complex in *Arabidopsis* seedlings. *The Plant Journal*, *53* (5), 814–827. doi.org/10.1111/j.1365-313X.2007.03373.x
- Greese, B., Wester, K., Bensch, R., Ronneberger, O., Timmer, J., Hülskamp, M., & Fleck, C. (2012). Influence of cell-to-cell variability on spatial pattern formation. *IET Systems Biology*, *6* (4), 143–153. doi.org/10.1049/iet-syb.2011.0050

- Greese, Bettina, Hülkamp, M., & Fleck, C. (2014). Quantification of variability in trichome patterns. *Frontiers in Plant Science*, *5*, 1–8. doi.org/10.3389/fpls.2014.00596
- Halpin, C., Barakate, A., Askari, B. M., Abbott, J. C., & Ryan, M. D. (2001). Enabling technologies for manipulating multiple genes on complex pathways. *Plant Molecular Biology*, *47* (1–2), 295–310. doi.org/10.1023/A:1010604120234
- Hanahan, D. (1983). Studies on Transformation of *Escherichia coli* with Plasmids. *Journal of Molecular Biology*, *166*, 557–580.
- Hay, A. S., Pieper, B., Cooke, E., Mandakova, T., Cartolano, M., Tattersall, A. D., Ioio, R. D., McGowan, S. J., Barkpulas, M., Galinha, C., Rast, M. I., Hofhuis, H., Then, C., Plieske, J., Ganal, M., Mott, R., Martinez-Garcia, J. F., Carine, M. A., Scotland, R. W., ... Tsiantis, M. (2014). *Cardamine hirsuta*: a versatile genetic system for comparative studies. *The Plant Journal*, *78*, 1–15. doi.org/10.1111/tpj.12447
- Hay, A., & Tsiantis, M. (2006). The genetic basis for differences in leaf form between *Arabidopsis thaliana* and its wild relative *Cardamine hirsuta*. *Nature Genetics*, *38* (8), 942–947. doi.org/10.1038/ng1835
- Hay, A., & Tsiantis, M. (2016). *Cardamine hirsuta*: a comparative view. *Current Opinion in Genetics and Development*, *39*, 1–7. doi.org/10.1016/j.gde.2016.05.005
- Hong, J., Gunasekara, C., He, C., Liu, S., Huang, J., & Wei, H. (2021). Identification of biological pathway and process regulators using sparse partial least squares and triple-gene mutual interaction. *Scientific Reports*, *11*, 1–14. doi.org/10.1038/s41598-021-92610-4
- Hong, L., Dumond, M., Tsugawa, S., Sapala, A., Routier-Kierzkowska, A.-L., Zhou, Y., Chen, c., Kiss, A., Zhu, M., Hamant, O., Smith, R. S., Komatsuzaki, T., Li, C.-B., Boudaoud, A., & Roeder, A. H. K. (2016). Variable Cell Growth Yields Reproducible Organ Development through Spatiotemporal Averaging. *Developmental Cell*, *38* (1), 15-32. doi.org/10.1016/j.devcel.2016.06.016
- Hülkamp, M. (2004). Plant trichomes: A model for cell differentiation. *Nature Reviews: Molecular Cell Biology*, *5* (6), 471–480. doi.org/10.1038/nrm1404
- Hülkamp, M., Miséra, S., & Jürgens, G. (1994). Genetic Dissection of Trichome Cell Development in *Arabidopsis*. *Cell*, *76*, 555–566. doi.org/10.1016/0092-8674(94)90118-x

- Ishida, T., Hattori, S., Sano, R., Inoue, K., Shirano, Y., Hayashi, H., Shibata, D., Sata, S., Kato, T., Tabata, S., Okada, K., & Wada, T. (2007). *Arabidopsis TRANSPARENT TESTA GLABRA2* Is Directly Regulated by R2R3 MYB Transcription Factors and Is Involved in Regulation of *GLABRA2* Transcription in Epidermal Differentiation. *The Plant Cell*, *19* (8), 2531–2543. doi.org/10.1105/tpc.107.052274
- Ishida, T., Kurata, T., Okada, K., & Wada, T. (2008). A Genetic Regulatory Network in the Development of Trichomes and Root Hairs. *Annual Review of Plant Biology*, *59*, 365–386. doi.org/10.1146/annurev.arplant.59.032607.092949
- Jaegle, B. (2014). *Natural variation of a gene network regulating trichome patterning, seed coat mucilage and proanthocyanidin production in Arabidopsis thaliana*. University of Cologne.
- Jakoby, M. J., Falkenhan, D., Mader, M. T., Brininstool, G., Wischnitzki, E., Platz, N., Hudson, A., Hülskamp, M., Larkin, J., & Schnittger, A. (2008). Transcriptional Profiling of Mature Arabidopsis Trichomes Reveals That *NOECK* Encodes the MIXTA-Like Transcriptional Regulator MYB106. *Plant Physiology*, *148*, 1583-1602. doi.org/10.1104/pp.108.126979
- Jefferson, R. A., Kavanagh, T. A., & Bevan, M. W. (1987). GUS fusions: β -glucuronidase as a sensitive and versatile gene fusion marker in higher plants. *The EMBO Journal*, *6* (13), 3901–3907. doi.org/10.1002/j.1460-2075.1987.tb02730.x
- Johnson, C. S., Kolevski, B., & Smyth, D. R. (2002). *TRANSPARENT TESTA GLABRA2*, a Trichome and Seed Coat Development Gene of Arabidopsis, Encodes a WRKY Transcription Factor. *The Plant Cell*, *14*, 1359–1375. doi.org/10.1105/tpc.001404
- Kang, Y. H., Kirik, V., Hülskamp, M., Nam, K. H., Hagely, K., Lee, M. M., & Schiefelbein, J. (2009). The *MYB23* Gene Provides a Positive Feedback Loop for Cell Fate Specification in the *Arabidopsis* Root Epidermis. *Plant Cell*, *21* (4), 1080–1094. doi.org/10.1105/tpc.108.063180
- Khosla, A., Paper, J. M., Boehler, A. P., Bradley, A. M., Neumann, T. R., & Schrick, K. (2014). HD-Zip Proteins GL2 and HDG11 Have Redundant Functions in *Arabidopsis* Trichomes, and GL2 Activates a Positive Feedback Loop via MYB23. *The Plant Cell*, *26*, 2184–2200. doi.org/10.1105/tpc.113.120360

- Kim, J. H., Lee, S.-R., Li, L.-H., Park, H.-J., Park, J.-H., Lee, K. Y., Kim, M.-K., Shin, B. A., & Choi, S.-Y. (2011). High Cleavage Efficiency of a 2A Peptide Derived from Porcine Teschovirus-1 in Human Cell Lines, Zebrafish and Mice. *PLoS ONE*, 6 (4), 1–8. doi.org/10.1371/journal.pone.0018556
- Kirik, V., Lee, M. M., Wester, K., Herrmann, U., Zheng, Z., Oppenheimer, D., Schiefelbein, D., & Hülskamp, M. (2005). Functional diversification of *MYB23* and *GLI* genes in trichome morphogenesis and initiation. *Development*, 132 (7), 1477–1485. doi.org/10.1242/dev.01708
- Kirik, V., Schnittger, A., Radchuk, V., Adler, K., Hülskamp, M., & Bäumlein, H. (2001). Ectopic Expression of the *Arabidopsis AtMYB23* Gene Induces Differentiation of Trichome Cells. *Developmental Biology*, 235 (2), 366–377. doi.org/10.1006/dbio.2001.0287
- Kirik, V., Simon, M., Huelskamp, M., & Schiefelbein, J. (2004a). The *ENHANCER OF TRY AND CPC1* gene acts redundantly with *TRIPTYCHON* and *CAPRICE* in trichome and root hair cell patterning in *Arabidopsis*. *Developmental Biology*, 268 (2), 506–513. doi.org/10.1016/j.ydbio.2003.12.037
- Kirik, V., Simon, M., Wester, K., & Schiefelbein, J. (2004b). *ENHANCER* of *TRY* and *CPC 2 (ETC2)* reveals redundancy in the region-specific control of trichome development of *Arabidopsis*. *Plant Molecular Biology*, 2(55), 389–398. doi.org/10.1007/s11103-004-0893-8
- Koch, A. J., & Meinhardt, H. (1994). Biological Pattern Formation: from Basic Mechanisms to Complex Structures. *Reviews of Modern Physics*, 66, 1481–1507. doi.org/10.1103/RevModPhys.66.1481
- Koch, M. A., Kiefer, C., Ehrich, D., Vogel, J., Brochmann, C., & Mummenhoff, K. (2006). Three times out of Asia Minor: the phylogeography of *Arabis alpina* L. (Brassicaceae). *Molecular Ecology*, 15, 825–839. doi.org/10.1111/j.1365-294X.2005.02848.x
- Koch, M., Haubold, B., & Mitchell-Olds, T. (2001). Molecular systematics of the Brassicaceae: evidence from coding plastidic *matK* and nuclear *Chs* sequences. *American Journal of Botany*, 88 (2), 534–544. doi.org/10.2307/2657117
- Koncz, C., & Schell, J. (1986). The promoter of T_L-DNA gene 5 controls the tissue-specific expression of chimaeric genes carried by a novel type of *Agrobacterium* binary vector. *Molecular and General Genetics*, 204, 383–396.

- Koornneef, M., van Eden, J., Hanhart, C. J., Stam, P., Braaksma, F. J., & Feenstra, W. J. (1983). Linkage map of *Arabidopsis thaliana*. *Journal of Heredity*, *74* (4), 265-272. doi.org/10.1093/oxfordjournals.jhered.a109781
- Koornneef, Maarten. (1981). THE COMPLEX SYNDROME OF TTG MUTANTS. In *Arabidopsis Information Server* (Vol. 18, pp. 45–51).
- Koornneef, Maarten, Dellaert, L. W. M., & van der Veen, J. H. (1982). EMS- and radiation-induced mutation frequencies at individual loci in *Arabidopsis thaliana* (L.) Heynh. *Mutation Research/Fundamental and Molecular Mechanisms of Mutagenesis*, *93*, 109–123. doi.org/10.1016/0027-5107(82)90129-4
- Kurata, T., Ishida, T., Kawabata-Awai, C., Noguchi, M., Hattori, S., Sano, R., Nagasaka, R., Tominaga, R., Koshino-Kimura, Y., Kato, T., Sata, S., Tabata, S., Okada, K., & Wada, T. (2005). Cell-to-cell movement of the CAPRICE protein in *Arabidopsis* root epidermal cell differentiation. *Development*, *132* (24), 5387-5398. doi.org/10.1242/dev.02139
- Larkin, J. C., Oppenheimer, D. G., Lloyd, A. M., Paparozzi, E. T., & Marks, M. D. (1994). Roles of the *GLABROUS1* and *TRANSPARENT TESTA GLABRA* Genes in *Arabidopsis* Trichome Development. *The Plant Cell*, *6*, 1065–1076. doi.org/10.1105/tpc.6.8.1065
- Larkin, J. C., Walker, J. D., Bolognesi-Winfield, A. C., Gray, J. C., & Walker, A. R. (1999). Allele-Specific Interactions Between *ttg* and *gll* During Trichome Development in *Arabidopsis thaliana*. *Genetics*, *151*, 1591–1604.
- Larkin, J. C., Young, N., Prigge, M., & Marks, M. D. (1996). The control of trichome spacing and number in *Arabidopsis*. *Development*, *1005*, 997–1005.
- Lee, D. W. (2002). Anthocyanins in Leaves: Distribution, Phylogeny and Development. *Advances in Botanical Research*, *37*, 1–17. doi.org/10.1016/S0065-2296(02)37042-3
- Lee, M. M., & Schiefelbein, J. (1999). WEREWOLF, a MYB-related protein in *Arabidopsis*, is a position-dependent regulator of epidermal cell patterning. *Cell*, *99* (5), 473–483. doi.org/10.1016/S0092-8674(00)81536-6
- Lee, M. M., & Schiefelbein, J. (2001). Developmentally distinct MYB genes encode functionally equivalent proteins in *Arabidopsis*. *Development*, *128*, 1539–1546. doi.org/10.1242/dev.128.9.1539

- Matsui, K., Tanaka, H., & Ohme-Takagi, M. (2004). Suppression of the biosynthesis of proanthocyanidin in *Arabidopsis* by a chimeric PAP1 repressor. *Plant Biotechnology Journal*, 2 (6), 487–493. doi.org/10.1111/j.1467-7652.2004.00094.x
- Matz, M. V., Fradkov, A. F., Labas, Y. A., Savitsky, A. P., Zaraisky, A. G., Markelov, M. L., & Lukyanov, S. A. (1999). Fluorescent proteins from nonbioluminescent Anthozoa species. *Nature Biotechnology*, 17, 969–973. doi.org/10.1038/13657
- Meinhardt, H., & Gierer, A. (1974). APPLICATIONS OF A THEORY OF BIOLOGICAL PATTERN FORMATION BASED ON LATERAL INHIBITION. *Journal of Cell Science*, 15, 321–346. doi.org/10.1242/jcs.15.2.321
- Meinhardt, Hans, & Gierer, A. (2000). Pattern formation by local self-activation and lateral inhibition. *BioEssays*, 22 (8), 753–760. https://doi.org/10.1002/1521-1878(200008)22:8<753::AID-BIES9>3.0.CO;2-Z
- Miki, T., Park, J. A., Nagao, K., Murayama, N., & Horiuchi, T. (1992). Control of segregation of chromosomal DNA by sex factor F in *Escherichia coli*: Mutants of DNA gyrase subunit A suppress *letD* (*ccdB*) product growth inhibition. *Journal of Molecular Biology*, 225 (1), 39–52. doi.org/10.1016/0022-2836(92)91024-J
- Mizuguchi, H., Xu, Z., Ishii-Watabe, A., Uchida, E., & Hayakawa, T. (2000). IRES-Dependent Second Gene Expression Is Significantly Lower Than Cap-Dependent First Gene Expression in a Bicistronic Vector. *Molecular Therapy*, 1 (4), 376–382. doi.org/10.1006/mthe.2000.0050
- Morohashi, K., & Grotewold, E. (2009). A Systems Approach Reveals Regulatory Circuitry for Arabidopsis Trichome Initiation by the GL3 and GL1 Selectors. *PLoS Genetics*, 5(2), 1–17. https://doi.org/10.1371/journal.pgen.1000396
- Morohashi, K., Zhao, M., Yang, M., Read, B., Lloyd, A., Lamb, R., & Grotewold, E. (2007). Participation of the Arabidopsis bHLH Factor GL3 in Trichome Initiation Regulatory Events. *Plant Physiology*, 145 (3), 736–746. doi.org/10.1104/pp.107.104521
- Munsky, B., Neuert, G., & van Oudenaarden, A. (2012). Using Gene Expression Noise to Understand Gene Regulation. *Science*, 336, 183–187. doi.org/10.1126/science.1216379
- Newman, J. R. S., Ghaemmaghami, S., Ihmels, J., Breslow, D. K., Noble, M., DeRisi, J. L., & Weissman, J. S. (2006). Single-cell proteomic analysis of *S. cerevisiae* reveals the architecture of biological noise. *Nature*, 441, 840–846. doi.org/10.1038/nature04785

- Nikolov, L. A., Shushkov, P., Nevado, B., Gan, X., Al-Shehbaz, I. A., Filatov, D., Bailey, C. D., & Tsiantis, M. (2019). Resolving the backbone of the Brassicaceae phylogeny for investigating trait diversity. *New Phytologist*, 222, 1638–1651. doi.org/10.1111/nph.15732
- Okamoto, S., Negishi, K., Toyama, Y., Ushijima, T., & Morohashi, K. (2020). Leaf Trichome Distribution Pattern in *Arabidopsis* Reveals Gene Expression Variation Associated with Environmental Adaptation. *Plants*, 9 (7), 1–16. doi.org/10.3390/plants9070909
- Oppenheimer, D. G., Herman, P. L., Sivakumaran, S., Esch, H., & Mark, M. D. (1991). A myb gene required for leaf trichome differentiation in *Arabidopsis* is expressed in stipules. *Cell*, 67, 483–493. doi.org/10.1016/0092-8674(91)90523-2
- Park, J.-Y., Kim, H., & Lee, I. (2017). Comparative analysis of molecular and physiological traits between perennial *Arabis alpina* Pajares and annual *Arabidopsis thaliana* Sy-0. *Scientific Reports*, 7, 1–11. doi.org/10.1038/s41598-017-13606-7
- Passardi, F., Dobias, J., Valério, L., Guimil, S., Penel, C., & Dunand, C. (2007). Morphological and physiological traits of three major *Arabidopsis thaliana* accessions. *Journal of Plant Physiology*, 164 (8), 980–992. doi.org/10.1016/j.jplph.2006.06.008
- Payne, C. T., Zhang, F., & Lloyd, A. M. (2000). *GL3* Encodes a bHLH Protein That Regulates Trichome Development in *Arabidopsis* Through Interaction With *GL1* and *TTG1*. *Genetics*, 156, 1349–1362. doi.org/10.1093/genetics/156.3.1349
- Pesch, M., Dartan, B., Birkenbihl, R., Somssich, I. E., & Hülskamp, M. (2014). *Arabidopsis* *TTG2* Regulates *TRY* Expression through Enhancement of Activator Complex-Triggered Activation. *The Plant Cell*, 26, 4067–4083. doi.org/10.1105/tpc.114.129379
- Pesch, M., & Hülskamp, M. (2004). Creating a two-dimensional pattern *de novo* during *Arabidopsis* trichome and root hair initiation. *Current Opinion in Genetics & Development*, 14 (4), 422–427. doi.org/10.1016/j.gde.2004.06.007
- Pesch, M., & Hülskamp, M. (2009). One , two , three . . . models for trichome patterning in *Arabidopsis*? *Current Opinion in Plant Biology*, 12, 587–592. doi.org/10.1016/j.pbi.2009.07.015

- Pesch, M., Schultheiß, I., Digiuni, S., Uhrig, J. F., & Hülskamp, M. (2013). Mutual control of intracellular localisation of the patterning proteins AtMYC1, GL1 and TRY/CPC in *Arabidopsis*. *Development*, *140*, 3456–3467. doi.org/10.1242/dev.094698
- Pesch, M., Schultheiß, I., Klopffleisch, K., Uhrig, J. F., Clemen, C., Simon, R., Weidtkamp-Peters, S., & Hülskamp, M. (2015). TRANSPARENT TESTA GLABRA1 and GLABRA1 compete for binding to GLABRA3 in *Arabidopsis thaliana*. *Plant Physiology*, *168*, 584–597. doi.org/10.1104/pp.15.00328
- Pieper, B., Monniaux, M., & Hay, A. (2016). The genetic architecture of petal number in *Cardamine hirsuta*. *New Phytologist*, *209* (1), 395–406. doi.org/10.1111/nph.13586
- Rabinowicz, P. D., Braun, E. L., Wolfe, A. D., Bowen, B., & Grotewold, E. (1999). Maize R2R3 Myb Genes: Sequence Analysis Reveals Amplification in the Higher Plants. *Genetics*, *153* (1), 427–444. doi.org/10.1093/genetics/153.1.427
- Raj, A., & van Oudenaarden, A. (2008). Stochastic gene expression and its consequences. *Cell*, *135* (2), 1–21. doi.org/10.1016/j.cell.2008.09.050
- Ramsay, N. A., & Glover, B. J. (2005). MYB-bHLH-WD40 protein complex and the evolution of cellular diversity. *Trends in Plant Science*, *10* (2), 63–70. doi.org/10.1016/j.tplants.2004.12.011
- Raser, J. M., & O’Shea, E. K. (2005). Noise in Gene Expression: Origins, Consequences, and Control. *Science*, *309*, 1–11. doi.org/10.1126/science.1105891
- Renicke, C., Schuster, D., Usherenko, S., Essen, L., & Taxis, C. (2013). Resource A LOV2 Domain-Based Optogenetic Tool to Control Protein Degradation and Cellular Function. *Chemistry & Biology*, *20* (4), 619–626. doi.org/10.1016/j.chembiol.2013.03.005
- Rerie, W. G., Feldmann, K. A., & Marks, M. D. (1994). The GLABRA2 gene encodes a homeo domain protein required for normal trichome development in *Arabidopsis*. *Genes & Development*, *8*, 1388–1399. doi.org/10.1101/gad.8.12.1388
- Ryan, M. D., King, A. M. Q., & Thomas, G. P. (1991). Cleavage of foot-and-mouth disease virus polyprotein is mediated by residues located within a 19 amino acid sequence. *Journal of General Virology*, *72*, 2727–2732. doi.org/10.1099/0022-1317-72-11-2727

- Samalova, M., Fricker, M., & Moore, I. (2006). Ratiometric Fluorescence-Imaging Assays of Plant Membrane Traffic Using Polyproteins. *Traffic*, 7 (12), 1701–1723. doi.org/10.1111/j.1600-0854.2006.00502.x
- Schellmann, S., Schnittger, A., Kirik, V., Wada, T., Okada, K., Beermann, A., Thumfahrt, J., Jürgens, G., & Hülskamp, M. (2002). *TRIPTYCHON* and *CAPRICE* mediate lateral inhibition during trichome and root hair patterning in *Arabidopsis*. *The EMBO Journal*, 21 (19), 5036–5046. doi.org/10.1093/emboj/cdf524
- Schellmann, Swen, & Hülskamp, M. (2005). Epidermal differentiation: trichomes in *Arabidopsis* as a model system. *International Journal of Developmental Biology*, 49, 579–584. doi.org/10.1387/ijdb.051983ss
- Schnittger, A., Folkers, U., Schwab, B., Jürgens, G., & Hülskamp, M. (1999). Generation of a Spacing Pattern: The Role of *TRIPTYCHON* in Trichome Patterning in *Arabidopsis*. *The Plant Cell*, 11, 1105–1116. doi.org/10.1105/tpc.11.6.1105
- Schultheiß Araújo, I., Pietsch, J. M., Keizer, E. M., Greese, B., Balkunde, R., Fleck, C., & Hülskamp, M. (2017). Stochastic gene expression in *Arabidopsis thaliana*. *Nature Communications*, 8, 1–9. doi.org/10.1038/s41467-017-02285-7
- Schultheiß, I. (2015). *Analysis of trichome patterning in Arabidopsis thaliana - From noisy gene expression to trichome pattern formation*. University of Cologne.
- Seo, E., Yu, J., Ryu, K. H., Lee, M. M., & Lee, I. (2011). *WEREWOLF*, a Regulator of Root Hair Pattern Formation, Controls Flowering Time through the Regulation of *FT* mRNA Stability. *Plant Physiology*, 156 (4), 1867–1877. doi.org/10.1104/pp.111.176685
- Sessa, G., Borello, U., Morelli, G., & Ruberti, I. (1998). A Transient Assay for Rapid Functional Analysis of Transcription Factors in *Arabidopsis*. *Plant Molecular Biology Reporter*, 16, 191–197. doi.org/10.1023/A:1007442607645
- Simon, M., Bruex, A., Kainkaryam, R. M., Zheng, X., Huang, L., Woolf, P. J., & Schiefelbein, J. (2013). Tissue-Specific Profiling Reveals Transcriptome Alterations in *Arabidopsis* Mutants Lacking Morphological Phenotype. *Plant Cell*, 25 (9), 3175–3185. doi.org/10.1105/tpc.113.115121
- Simon, M., Lee, M. M., Lin, Y., Gish, L., & Schiefelbein, J. (2007). Distinct and overlapping roles of single-repeat MYB genes in root epidermal patterning. *Developmental Biology*, 311 (2), 566–578. doi.org/10.1016/j.ydbio.2007.09.001

- Stracke, R., Werber, M., & Weisshaar, B. (2001). The *R2R3-MYB* gene family in *Arabidopsis thaliana*. *Current Opinion in Plant Biology*, 4 (5), 447–456. doi.org/10.1016/s1369-5266(00)00199-0
- Symonds, V. V., Hatlestad, G., & Lloyd, A. M. (2011). Natural Allelic Variation Defines a Role for *ATMYC1*: Trichome Cell Fate Determination. *PLoS Genetics*, 7 (6), 1–9. doi.org/10.1371/journal.pgen.1002069
- Szymanski, D. B., Lloyd, A. M., & Marks, M. D. (2000). Progress in the molecular genetic analysis of trichome initiation and morphogenesis in *Arabidopsis*. *Trends in Plant Science*, 5 (5), 214–219. doi.org/10.1016/s1360-1385(00)01597-1
- Szymczak, A. L., & Vignali, D. A. A. (2005). Development of 2A peptide-based strategies in the design of multicistronic vectors. *Expert Opinion on Biological Therapy*, 5 (5), 627–638. doi.org/10.1517/14712598.5.5.627
- Szymczak, A. L., Workman, C. J., Wang, Y., Vignali, K. M., Dilioglou, S., Vanin, E. F., & Vignali, D. A. A. (2004). Correction of multi-gene deficiency in vivo using a single “self-cleaving” 2A peptide-based retroviral vector. *Nature Biotechnology*, 22 (5), 589–594. doi.org/10.1038/nbt957
- Taniguchi, Y., Choi, P. J., Li, G.-W., Chen, H., Babu, M., Hearn, J., Emili, A., & Xie, X. S. (2010). Quantifying *E. coli* proteome and transcriptome with single-molecule sensitivity in single cells. *Science*, 329, 533–539. doi.org/10.1126/science.1188308
- Telfer, A., Bollman, K. M., & Poethig, R. S. (1997). Phase change and the regulation of trichome distribution in *Arabidopsis thaliana*. *Development*, 124, 645–654. doi.org/10.1242/dev.124.3.645
- Tominaga-Wada, R., Nukumizu, Y., Sato, S., Kato, T., Tabata, S., & Wada, T. (2012). Functional Divergence of MYB-Related Genes, *WEREWOLF* and *AtMYB23* in *Arabidopsis*. *Bioscience, Biotechnology and Biochemistry*, 76 (5), 883–887. doi.org/10.1271/bbb.110811
- Tominaga-Wada, R., & Wada, T. (2017). Extended C termini of CPC-LIKE MYB proteins confer functional diversity in *Arabidopsis* epidermal cell differentiation. *Development*, 144, 2375–2380. doi.org/10.1242/dev.149542
- Tominaga, R., Iwata, M., Sano, R., Inoue, K., Okada, K., & Wada, T. (2008). *Arabidopsis CAPRICE-LIKE MYB 3 (CPL3)* controls endoreduplication and flowering development in addition to trichome and root hair formation. *Development*, 135 (7), 1335–1345. doi.org/10.1242/dev.017947

- Tsutsui, H., Karasawa, S., Shimizu, H., Nukina, N., & Miyawaki, A. (2005). Semi-rational engineering of a coral fluorescent protein into an efficient highlighter. *EMBO Reports*, 6 (3), 233–238. doi.org/10.1038/sj.embor.7400361
- Turing, A. M. (1952). The Chemical Basis of Morphogenesis. *Philosophical Transactions of the Royal Society of London*, 237 (641), 37–72. doi.org/10.1098/rstb.1952.0012
- Ueki, S., Lacroix, B., Krichevsky, A., Lazarowitz, S. G., & Citovsky, V. (2009). Functional transient genetic transformation of *Arabidopsis* leaves by biolistic bombardment. *Nature Protocols*, 4 (1), 71–77. doi.org/10.1038/nprot.2008.217
- Urao, T., Yamaguchi-Shinozaki, K., Mitsukawa, N., Shibata, D., & Shinozaki, K. (1996). Molecular cloning and characterization of a gene that encodes a MYC-related protein in *Arabidopsis*. *Plant Molecular Biology*, 32, 571–576.
- Voinnet, O., Pinto, Y. M., & Baulcombe, D. C. (1999). Suppression of gene silencing: A general strategy used by diverse DNA and RNA viruses of plants. *PNAS*, 96(24), 14147–14152. doi.org/10.1073/pnas.96.24.14147
- Wada, T., Tachibana, T., & Shimura, Y. (1997). Epidermal Cell Differentiation in *Arabidopsis* Determined by a *Myb* Homolog, *CPC*. *Nature*, 277, 1113–1117. doi.org/10.1126/science.277.5329.1113
- Wagner, G. J., Wang, E., & Shepherd, R. W. (2004). New Approaches for Studying and Exploiting an Old Protuberance, the Plant Trichome. *Annals of Botany*, 93, 3–11. doi.org/10.1093/aob/mch011
- Walker, A. R., Davison, P. A., Bolognesi-Winfield, A. C., James, C. M., Srinivasan, N., Blundell, T. L., Esch, J. J., Marks, M. D., & Gray, J. C. (1999). The *TRANSPARENT TESTA GLABRA1* Locus, Which Regulates Trichome Differentiation and Anthocyanin Biosynthesis in *Arabidopsis*, Encodes a WD40 Repeat Protein. *The Plant Cell*, 11, 1337–1349. doi.org/10.1105/tpc.11.7.1337
- Wang, R., Albani, M. C., Vincent, C., Bergonzi, S., Luan, M., Bai, Y., Kiefer, C., Castillo, R., & Coupland, G. (2011). Aa *TFL1* Confers an Age-Dependent Response to Vernalization in Perennial *Arabis alpina*. *The Plant Cell*, 23 (4), 1307–1321. doi.org/10.1105/tpc.111.083451
- Wang, R., Farrona, S., Vincent, C., Joecker, A., Schoof, H., Turck, F., Alonso-Blanco, C., Coupland, G., & Albani, M. C. (2009). *PEP1* regulates perennial flowering in *Arabis alpina*. *Nature*, 459, 423–427. doi.org/10.1038/nature07988

- Wang, S., & Chen, J.-G. (2014). Regulation of cell fate determination by single-repeat R3 MYB transcription factors in *Arabidopsis*. *Frontiers in Plant Science*, *5*, 1–11. doi.org/10.3389/fpls.2014.00133
- Wang, S., Kwak, S.-H., Zeng, Q., Ellis, B. E., Chen, X.-Y., Schiefelbein, J., & Chen, J.-G. (2007). TRICHOMELESS1 regulates trichome patterning by suppressing *GLABRA1* in *Arabidopsis*. *Development*, *134* (21), 3873–3882. doi.org/10.1242/dev.009597
- Wester, K., Digiuni, S., Geier, F., Timmer, J., Fleck, C., & Hülskamp, M. (2009). Functional diversity of R3 single-repeat genes in trichome development. *Development*, *136* (9), 1487–1496. doi.org/10.1242/dev.021733
- Willing, E.-M., Rawat, V., Mandáková, T., Maumus, F., James, G. V., Nordström, K. J. V., Becker, C., Warthmann, N., Chica, C., Szarzynska, B., Zytnicki, M., Albaini, M. C., Kiefer, C., Bergonzi, S., Castaings, L., Mateos, J. L., Berns, M. C., Bujdoso, N., Piofczyk, T., ... Schneeberger, K. (2015). Genome expansion of *Arabis alpina* linked with retrotransposition and reduced symmetric DNA methylation. *Nature Plants*, *1*, 1–7. doi.org/10.1038/nplants.2014.23
- Xu, W., Dubos, C., & Lepiniec, L. (2015). Transcriptional control of flavonoid biosynthesis by MYB-bHLH-WDR complexes. *Trends in Plant Science*, *20* (3), 176–185. doi.org/10.1016/j.tplants.2014.12.001
- Yen, H.-C. S., Xu, Q., Chou, D. M., Zhao, Z., & Elledge, S. J. (2008). Global Protein Stability Profiling in Mammalian Cells. *Science*, *322*, 918–924. doi.org/10.1126/science.1160489
- Yewdell, J. W., Lacsina, J. R., Rechsteiner, M. C., & Niccitta, C. V. (2011). Out with the Old, In with the New? Comparing Methods for Measuring Protein Degradation. *Cell Biology International*, *35* (5), 457–462. doi.org/10.1042/CBI20110055
- Zhang, B. (2018). *Evolutionary Analysis of MYBs-bHLH-WD40 Protein Complexes Formation and Their Functional Relationship in Planta*. University of Cologne.
- Zhang, B., & Hülskamp, M. (2019). Evolutionary Analysis of MBW Function by Phenotypic Rescue in *Arabidopsis thaliana*. *Frontiers in Plant Science*, *10*, 1–10. doi.org/10.3389/fpls.2019.00375
- Zhang, B., & Schrader, A. (2017). TRANSPARENT TESTA GLABRA 1-Dependent Regulation of Flavonoid Biosynthesis. *Plants*, *6* (65), 1–30. doi.org/10.3390/plants6040065

- Zhang, F., Gonzalez, A., Zhao, M., Payne, C. T., & Lloyd, A. (2003). A network of redundant bHLH proteins functions in all TTG1-dependent pathways of *Arabidopsis*. *Development*, *130* (20), 4859–4869. doi.org/10.1242/dev.00681
- Zhang, X., & Oppenheimer, D. G. (2004). A Simple and Efficient Method for Isolating Trichomes for Downstream Analyses. *Plant and Cell Physiology*, *45* (2), 221–224. doi.org/10.1093/pcp/pch016
- Zhao, H., Wang, X., Zhu, D., Cui, S., Li, X., Cao, Y., & Ma, L. (2012). A Single Amino Acid Substitution in IIIf Subfamily of Basic Helix-Loop-Helix Transcription Factor AtMYC1 Leads to Trichome and Root Hair Patterning Defects by Abolishing Its Interaction with Partner Proteins in *Arabidopsis*. *The Journal of Biological Chemistry*, *287* (17), 14109–14121. doi.org/10.1074/jbc.M111.280735
- Zhao, M., Morohashi, K., Hatlestad, G., Grotewold, E., & Lloyd, A. (2008). The TTG1-bHLH-MYB complex controls trichome cell fate and patterning through direct targeting of regulatory loci. *Development*, *135* (11), 1991–1999. doi.org/10.1242/dev.016873
- Zimmermann, I. M., Heim, M. a, Weisshaar, B., & Uhrig, J. F. (2004). Comprehensive identification of *Arabidopsis thaliana* MYB transcription factors interacting with R/B-like BHLH proteins. *The Plant Journal*, *40* (1), 22–34. doi.org/10.1111/j.1365-313X.2004.02183.x

Danksagung

Mein größter Dank gilt Herrn **Prof. Dr. Martin Hülskamp**. Vielen herzlichen Dank für die uneingeschränkte Unterstützung in den letzten Jahren. All die Ideen, Diskussionen und Ratschläge haben mir enorm geholfen. Es hat mir sehr viel Freude bereitet dieses packende Thema zu bearbeiten und ich bin gespannt welche Ergebnisse folgen werden.

Vielen lieben Dank Frau **Prof. Dr. Ute Höcker**, dass Sie sich die Zeit für das Zweitgutachten nehmen und Teil meiner Prüfungskommission sind.

Nachdem ich meine wissenschaftliche Laufbahn in Ihrer Arbeitsgruppe begonnen habe, freue ich mich ganz besonders, dass Sie, Herr **Prof. Dr. Siegfried Roth**, den Vorsitz für meine Disputation übernommen haben. Vielen Dank!

Liebe **AG Hülskamp**, vielen Dank für die wunderbar angenehme Arbeitsatmosphäre. Ich bin jeden Morgen mit Freude ins Labor gekommen und möchte all die gemeinsamen Stunden, Gespräche und Lacher nicht missen wollen. Ihr seid ein tolles Team!

Meine gute und so fleißige **Sabine**, ohne dich wären die experimentellen Versuche in dem Umfang und der Zeit nicht zu schaffen gewesen. Ich danke dir so sehr für die unzählbaren Pipettierschritte, ausgelegten Samen und immer unterhaltsamen Telefonate.

Lisa, tausend Dank, dass du mir bei all meinen Fragen rund um die Welt der qPCR immer zur Seite gestanden und dir so viel Zeit genommen hast als ich diese Dissertation geschrieben habe. Dein Wissen, deine Erfahrungen und deine Kreativität haben so viel aus diesem Projekt herausgeholt. An dieser Stelle ebenfalls meinen herzlichen Dank an **Arijit**, der für jedes Problem die passende Formel gefunden hat.

Ein ganz herzlicher Dank an **Hanna** und **Eva** für euer kritisches Lesen meiner Doktorarbeit. Eure Anmerkungen haben mir sehr geholfen und mich manchmal zum Schmunzeln gebracht.

Liebe **Barbara**, es ist schön dich in unserer Truppe zu haben und ich möchte mich bei dir für all unsere gemeinsamen Stunden im Labor und Büro bedanken.

Ebenfalls möchte ich **Anna Deneer** für ihr mathematisches Modell danken, mit dem sie uns aufgezeigt hat worauf es beim trichome patterning so wirklich ankommt.

Vielen Dank **Ilka**, dass du mich zu Beginn meiner Zeit in der AG umfassend betreut und auch nach Jahren wieder alte Ordner durchsucht hast um der noisy gene expression auf die Spur zu kommen.

Meine liebe **Lena, Steffi & Anna**, so viele gemeinsame Erlebnisse verbinden uns seit der Schulzeit und ich freue mich riesig auf all unsere Wiedersehen bis wir alt und grau sind. Vielen Dank, dass der Kontakt niemals abgebrochen ist.

Meinen **Eltern** und meiner **Familie** kann ich nicht genug danken. Ihr habt mich immer unterstützt und gefördert, mir dabei aber meine Freiheiten gelassen. Es ist ein beruhigendes Gefühl euch auch aus der Distanz an meiner Seite zu wissen.

Tobi, ob über oder unter Wasser, du bist immer vertrauensvoll an meiner Seite und hast mir während der heißen Phase stets den Rücken freigehalten. Meinen allerherzlichsten Dank! Gespannt warten wir auf **Leonie**, die bereits bei jedem dieser Worte dabei gewesen ist.

Declaration of academic integrity

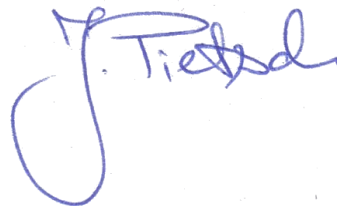
Ich versichere, dass ich die von mir vorgelegte Dissertation selbständig angefertigt, die benutzten Quellen und Hilfsmittel vollständig angegeben und die Stellen der Arbeit – einschließlich Tabellen, Karten und Abbildungen –, die anderen Werken im Wortlaut oder dem Sinn nach entnommen sind, in jedem Einzelfall als Entlehnung kenntlich gemacht habe; dass diese Dissertation noch keiner anderen Fakultät oder Universität zur Prüfung vorgelegen hat; dass sie – abgesehen von unten angegebenen Teilpublikationen – noch nicht veröffentlicht worden ist, sowie, dass ich eine solche Veröffentlichung vor Abschluss des Promotionsverfahrens nicht vornehmen werde.

Die Bestimmungen der Promotionsordnung sind mir bekannt. Die von mir vorgelegte Dissertation ist von Prof. Dr. Martin Hülskamp betreut worden.

Teilpublikationen:

Schultheiß Araújo, I., Pietsch, J. M., Keizer, E. M., Greese, B., Balkunde, R., Fleck, C., & Hülskamp, M. (2017). Stochastic gene expression in *Arabidopsis thaliana*. Nature Communications, 8, 1–9. <https://doi.org/10.1038/s41467-017-02285-7>

Brühl, den 18.05.2022

A handwritten signature in blue ink, appearing to read 'J. Pietsch', is written over a faint, circular stamp.